

Novel Methods and Algorithms for Fitting and Equivalent Circuit Synthesis of Multi-port  
Systems' Frequency Response for Time-Domain Simulation

A Thesis

Presented in Partial Fulfilment of the Requirements for the

Degree of Master of Science

with a

Major in Electrical Engineering

in the

College of Graduate Studies

University of Idaho

by

Venkatesh Avula

Major Professor: Ata Zadehgol, Ph.D.

Committee Members: Herbert Hess, Ph.D.; Feng Li, Ph.D.

Department Administrator: Mohsen Guizani, Ph. D.

December 2016

## Authorization to Submit Thesis

This thesis of Venkatesh Avula, submitted for the degree of Master of Science with a major in Electrical Engineering and titled “Novel Methods and Algorithms for Fitting and Equivalent Circuit Synthesis of Multi-port Systems’ Frequency Response for Time-Domain Simulation,” has been reviewed in final form. Permission, as indicated by the signatures and dates given below, is now granted to submit final copies to the College of Graduate Studies for approval.

Major Professor: \_\_\_\_\_ Date \_\_\_\_\_  
Ata Zadehgol, Ph.D.

Committee  
Members: \_\_\_\_\_ Date \_\_\_\_\_  
Herbert Hess, Ph.D.

\_\_\_\_\_ Date \_\_\_\_\_  
Feng Li, Ph.D.

Department  
Administrator: \_\_\_\_\_ Date \_\_\_\_\_  
Mohsen Guizani, Ph.D.

## **Abstract**

Interconnects in electrical/electronic systems are commonly modeled in frequency-domain. However, system level transient simulation typically needs its macromodel in circuit level representation. In this thesis, a novel iterative fitting method, Pole Residue Equivalent System Solver (PRESS), that approximates a multi-port frequency response to a set of poles and residues which can then be synthesized as an equivalent circuit netlist is proposed. The fitting method iteratively picks a few consecutive points from the frequency response and identifies a local transfer function matching their response; however, it tends to generate large number of poles/residues. To optimize the model order, improvements to the original PRESS algorithm are proposed. Experiments on multitude of test cases show that the performance of the resultant equivalent circuit matches closely to the given frequency-domain model, demonstrating the potential in the method for wide applications in signal and power integrity modeling and simulation of interconnect networks.

## **Acknowledgements**

I would like to thank my adviser Dr. Ata Zadehgol for the guidance and support, without which this work would not have been possible.

We'd like to acknowledge Brent Keeth, Ph.D., Sr. Fellow at Micron Technology, Inc., for supporting this work.

## **Dedication**

To my family, especially parents, Madhu Kumari and Sambasiva Rao, and  
grand father, Ramamohana Rao Avula, for perseverance,  
and to Keerthi and Ruthvik Avula, for forbearance.

## Table of Contents

Authorization to Submit Thesis .....	ii
Abstract.....	iii
Acknowledgements .....	iv
Dedication .....	v
Table of Contents .....	vi
List of Tables .....	ix
List of Figures .....	x
<b>1 Introduction .....</b>	<b>1</b>
1.1 Problem: mixed-domain simulation .....	2
1.2 Current state of the art.....	2
1.3 Contribution.....	4
<b>2 Fitting of frequency response .....</b>	<b>6</b>
2.1 Pole Residue Equivalent System Solver (PRESS).....	6
2.1.1 Formulation: choosing and fitting a subset $\Psi$ .....	7
2.1.2 Algorithm .....	10
2.2 Coarse-to-fine Malleable Pole/Residue Equivalent System Solver (COMPRESS) .....	10
2.2.1 Formulation: iteratively adapting and fitting a subset.....	11
2.2.2 Algorithm .....	12
2.3 Error Maxima-agnostic Pole Residue Equivalent System Solver (EMPRESS) ...	13
2.3.1 Algorithm .....	13
2.4 Optimized Pole/Residue Equivalent System Solver (OPPRESS) .....	14

2.4.1	Formulation: iteratively fitting a subset.....	15
2.4.2	Algorithm .....	16
<b>3</b>	<b>Model order reduction .....</b>	<b>18</b>
3.1	Formulation.....	18
3.1.1	PRESS: iteratively choosing and fitting a subset .....	18
3.1.2	SPA: identify and residualize weaker states.....	19
3.2	Algorithm.....	21
<b>4</b>	<b>Synthesis .....</b>	<b>23</b>
4.1	Formulation.....	23
4.1.1	Synthesizing an equivalent circuit block.....	23
4.1.2	Building equivalent multi-port network from the circuit blocks.....	26
4.1.3	Passivity verification of the multi-port network .....	27
4.2	Algorithm.....	27
<b>5</b>	<b>Results.....</b>	<b>29</b>
5.1	Experiment 1: Stripline .....	29
5.1.1	Setup .....	29
5.1.2	Validation of PRESS .....	29
5.2	Experiment 2: Package .....	34
5.2.1	Setup .....	34
5.2.2	Validation of PRESS .....	34
5.3	Experiment 3: Microstrip.....	39
5.3.1	Setup .....	39
5.3.2	Validation of PRESS .....	40
5.4	Experiment 4: Power planes .....	45
5.4.1	Setup .....	45
5.4.2	Validation of PRESS .....	45

5.5	Experiment 5: Package .....	48
5.5.1	Setup .....	48
5.5.2	Validation of COMPRESS.....	48
5.5.3	Validation of EMPRESS.....	48
5.5.4	Validation of OPPRESS .....	48
5.5.5	MOR by SPA.....	55
5.5.6	Validation of Indirect synthesis .....	55
5.6	Experiment 6: Broadband antenna.....	61
5.6.1	Setup .....	61
5.6.2	Validation of Synthesis .....	61
5.7	Experiment 7: Power planes with 3 ports.....	64
5.7.1	Setup .....	64
5.7.2	Validation of Direct Synthesis .....	64
<b>6</b>	<b>Discussion .....</b>	<b>76</b>
6.1	Performance .....	76
6.1.1	Fitting .....	76
6.1.2	Model order reduction .....	79
6.1.3	Synthesis.....	79
6.2	Computational complexity .....	81
<b>7</b>	<b>Conclusion .....</b>	<b>82</b>
	<b>References .....</b>	<b>84</b>

## List of Tables

5.1	Comparison of fitting algorithms' computation time for 10 iterations. . . . .	55
5.2	Comparison [1] of PRESS and Vector Fitting algorithms' computation time. . .	55

## List of Figures

1.1	Typical serial link transient co-simulation of nonlinear active circuits and linear passive interconnects . . . . .	2
1.2	Macromodeling process, as per the current dominant methodology . . . . .	3
1.3	Macromodeling process as covered and contributed in the thesis . . . . .	5
4.1	Pole/residues to circuit branch synthesis: (a) Type 1 (b) Type 2 (c) Type 3. Permission from [2], ©2016 IEEE . . . . .	25
4.2	Multi-port network synthesis using admittance parameters. Permission from [2], ©2016 IEEE . . . . .	27
5.1	strip lines 2'' long. Permission from [3], ©2016 IEEE . . . . .	29
5.2	Fitting of strip-line return loss after 100 <sup>th</sup> iteration: (a) <i>Magnitude</i> (b) <i>Phase</i> . Permission from [3], ©2016 IEEE . . . . .	30
5.3	Fitting on strip-line insertion loss $S_{21}$ magnitude after iterations: (a) 1 <sup>st</sup> (b) 5 <sup>th</sup> (c) 100 <sup>th</sup> . Permission from [3], ©2016 IEEE . . . . .	31
5.4	Fitting on strip-line insertion loss $S_{21}$ phase after iterations: (a) 1 <sup>st</sup> (b) 5 <sup>th</sup> (c) 100 <sup>th</sup> . Permission from [3], ©2016 IEEE . . . . .	32
5.5	Error convergence of fitting the strip-line over 100 iterations. . . . .	33
5.6	Response at output port of strip-line equivalent circuit excited by step: (a) Voltage & (b) Current. Permission from [3], ©2016 IEEE . . . . .	33
5.7	Package [4] 0.2'' × 0.6'' with 4 ports size. Permission from [3], ©2016 IEEE . . . . .	34
5.8	Fitting of Package near-end crosstalk after 50 <sup>th</sup> iteration: (a) <i>Magnitude</i> & (b) <i>Phase</i> . Permission from [3], ©2016 IEEE . . . . .	35
5.9	Fitting of Package far-end crosstalk after 50 <sup>th</sup> iteration: (a) <i>Magnitude</i> & (b) <i>Phase</i> . Permission from [3], ©2016 IEEE . . . . .	36
5.10	Fitting of Package return loss after 50 <sup>th</sup> iteration: (a) <i>Magnitude</i> & (b) <i>Phase</i> . . . . .	37

5.11 Fitting of Package insertion loss after 50 <sup>th</sup> iteration: (a) <i>Magnitude</i> & (b) <i>Phase</i> . Permission from [3], ©2016 IEEE . . . . .	38
5.12 Error convergence of fitting the package over 50 iterations. Permission from [3], ©2016 IEEE . . . . .	39
5.13 microstrip 2" long. Permission from [5], ©2016 IEEE . . . . .	39
5.14 Fitting of microstrip insertion loss after 100 <sup>th</sup> iteration: (a) <i>Magnitude</i> & (b) <i>Phase</i> . Permission from [5], ©2016 IEEE . . . . .	40
5.15 Fitting of microstrip near-end crosstalk after 100 <sup>th</sup> iteration: (a) 1st (b) 10th & (c) 100th. Permission from [5], ©2016 IEEE . . . . .	41
5.16 Fitting of microstrip near-end crosstalk after 100 <sup>th</sup> iteration: (a) <i>Magnitude</i> & (b) <i>Phase</i> . Permission from [5], ©2016 IEEE . . . . .	42
5.17 Fitting of microstrip far-end crosstalk after 100 <sup>th</sup> iteration: (a) <i>Magnitude</i> & (b) <i>Phase</i> . Permission from [5], ©2016 IEEE . . . . .	43
5.18 Fitting of microstrip return loss after 100 <sup>th</sup> iteration: (a) <i>Magnitude</i> & (b) <i>Phase</i> . Permission from [5], ©2016 IEEE . . . . .	44
5.19 square power planes 1" × 1" with a port. Permission from [5], ©2016 IEEE . . . . .	45
5.20 Fitting power plane self-impedance after 80 <sup>th</sup> iteration: (a) <i>Magnitude</i> & (b) <i>Phase</i> . Permission from [5], ©2016 IEEE . . . . .	46
5.21 Current at the input port of power planes equivalent circuit excited by step. PRESS after 20 iterations is compared with 10 <sup>th</sup> order VF. Permission from [5], ©2016 IEEE . . . . .	47
5.22 Setup: package [6] (a) cross-section (b) planes 1.36" × 1.36" size (c) signal trans- mission lines. Permission from [7], ©2016 IEEE . . . . .	49
5.23 COMPRESS fitting of power planes admittance after 30 <sup>th</sup> iteration: (a) <i>Magnitude</i> & (b) <i>Phase</i> . Permission from [7], ©2016 IEEE . . . . .	50
5.24 COMPRESS fitting of signal insertion loss $S_{24}$ after 30 <sup>th</sup> iteration: (a) <i>Magnitude</i> & (b) <i>Phase</i> . Permission from [7], ©2016 IEEE . . . . .	51

5.25	COMPRESS fitting of signal insertion loss $S_{13}$ after 30 <sup>th</sup> iteration: (a) <i>Magnitude</i> & (b) <i>Phase</i> . Permission from [7], ©2016 IEEE . . . . .	52
5.26	Error convergence of PRESS vs COMPRESS over 30 iterations: (a) self-admittance $Y_{11}$ , insertion losses (b) $S_{24}$ & (c) $S_{13}$ . Permission from [7], ©2016 IEEE . . . . .	53
5.27	Error convergence of PRESS vs EMPRESS over 30 iterations: (a) self-admittance $Y_{11}$ , insertion losses (b) $S_{24}$ & (c) $S_{13}$ . . . . .	54
5.28	Error convergence of PRESS vs OPPRESS over 30 iterations: (a) self-admittance $Y_{11}$ , insertion losses (b) $S_{24}$ & (c) $S_{13}$ . . . . .	56
5.29	Fitting of power planes admittance after 30 <sup>th</sup> iteration: (a) <i>Magnitude</i> & (b) <i>Phase</i> . . . . .	57
5.30	Error convergence of fit of the admittance over 30 iterations. . . . .	58
5.31	Hankel singular values of fit of the admittance over 30 iterations. . . . .	58
5.32	Model order reduction of fit of admittance: (a) <i>Magnitude</i> & (b) <i>Phase</i> . . . . .	59
5.33	Comparison of the Package power plane's return loss with that of the synthesized circuit: (a) <i>Magnitude</i> & (b) <i>Phase</i> . . . . .	60
5.34	Setup - coax fed patch antenna [8] 40 × 30mm size with feed position of 10.8 mm : (a) top view (b) side view, port placement at feed . . . . .	61
5.35	Fitting on the patch antenna $Y'_{11}$ after iterations: (a) 1 <sup>st</sup> & (b) 10 <sup>th</sup> . . . . .	62
5.36	Fitting on the patch antenna $Y'_{11}$ after iterations: (a) 1 <sup>st</sup> & (b) 10 <sup>th</sup> . . . . .	63
5.37	Convergence of magnitude of fitting error over 10 iterations. . . . .	64
5.38	Comparison of the antenna's return loss with that of the synthesized circuit: (a) <i>Magnitude</i> & (b) <i>Phase</i> . . . . .	65
5.39	Setup - power planes 0.5" × 0.5" size with three vias : (a) top view, vias at .25" and .125" (b) side view, port placement for each via. Permission from [2], ©2016 IEEE . . . . .	66
5.40	Fitting of power planes $Y'_{31}$ after 20 <sup>th</sup> iteration: (a) <i>Magnitude</i> & (b) <i>Phase</i> . Permission from [2], ©2016 IEEE . . . . .	67

5.41 Fitting on power planes $Y'_{32}$ after iterations: (a) 1 <sup>st</sup> , (b) 5 <sup>th</sup> , & (c) 20 <sup>th</sup> . Permission from [2], ©2016 IEEE . . . . .	68
5.42 Fitting on power planes $Y'_{32}$ after iterations: (a) 1 <sup>st</sup> , (b) 5 <sup>th</sup> , & (c) 20 <sup>th</sup> . Permission from [2], ©2016 IEEE . . . . .	69
5.43 Fitting of power planes $Y'_{21}$ after 20 <sup>th</sup> iteration: (a) <i>Magnitude</i> & (b) <i>Phase</i> . Permission from [2], ©2016 IEEE . . . . .	70
5.44 Fitting of power planes $Y'_{33}$ after 20 <sup>th</sup> iteration: (a) <i>Magnitude</i> & (b) <i>Phase</i> . Permission from [2], ©2016 IEEE . . . . .	71
5.45 Fitting of power planes $Y'_{22}$ after 5 <sup>th</sup> iteration: (a) <i>Magnitude</i> & (b) <i>Phase</i> . Permission from [2], ©2016 IEEE . . . . .	72
5.46 Fitting of power planes $Y'_{11}$ after 5 <sup>th</sup> iteration: (a) <i>Magnitude</i> & (b) <i>Phase</i> . Permission from [2], ©2016 IEEE . . . . .	73
5.47 Convergence of magnitude of fitting error of admittance over 20 iterations: (a) transfer admittance $Y_{32}$ and self admittance $Y_{33}$ & (b) transfer admittance $Y_{21}$ and self admittance $Y_{11}$ . Permission from [2], ©2016 IEEE . . . . .	74
5.48 Comparison of power planes frequency-domain model with the synthesized circuit: (a) <i>Magnitude</i> & (b) <i>Phase</i> . Permission from [2], ©2016 IEEE . . . . .	75

# CHAPTER 1

## Introduction

Frequency domain network parameters such as scattering (S), admittance (Y), and impedance (Z) parameters containing a systems frequency response at discrete samples over a frequency range are ubiquitous, especially in the area of signal and power integrity for high speed interconnects and power delivery networks. In some applications, models are directly utilized; for example, self-impedance  $Z_{11}$  of power delivery planes are analyzed and optimized to push resonant frequencies beyond load operating frequencies and below target impedance [9]. In other applications where time domain SPICE based simulation is necessary, the frequency domain models are processed further [10]; for example, performance of package interconnects [11] can be assessed only in time domain by running a long sequence of 1s and 0s to evaluate the actual degradation caused to eye diagrams [12]. In such cases of mixed time-frequency domain simulations, many approaches exists to reconcile the usage of frequency-domain models for time-domain simulations: inverse Fourier transform based convolution method [13], moment matching based complex frequency hopping ( CFH ) method [14] [15] and rational function approximation based macromodeling method [16] [17] [18] [19] [20].

Macromodeling of the frequency domain model is an efficient approach for mixed time-frequency system simulation involving non-linear circuits such as active transceivers. The macromodel is obtained rational function approximation and contains the equivalent pole/residue of the given frequency domain model. Then the macromodel can either be used in recursive convolution [10] based transient analysis or converted to equivalent lumped circuits [12] to simulate along with nonlinear devices in time-domain simulators like SPICE.

This thesis focuses on macromodeling and the consequent equivalent circuit synthesis of systems' frequency domain models.

## 1.1 Problem: mixed-domain simulation

With wide usage of frequency domain models [21], the problem of mixed-domain transient simulation, as in Figure 1.1, exists in many areas of electrical engineering, including computational electromagnetics [22] [23] [24] [25] [26] [27] [28], power systems [29], RF design [30] and signal/power integrity [31] applications. Antenna based wireless communication systems, for instance, are traditionally characterized, modeled and analyzed in frequency-domain; antenna performance is analyzed mainly with antenna gain and VSWR, especially return-loss  $S_{11}$  and self-impedance  $Z_{11}$ , which are used to determine [32] the radiation efficiency and to match impedance. But as the available bandwidth increases, as in the case of Ultra-wideband (UWB) [33] for example, the system design becomes challenging, especially the co-design of antenna/circuit interface. This requires co-simulation of antennas along with the transceivers; such time-domain analysis involves interfacing frequency-domain models of antennas with the SPICE models of non-linear [34] transceivers. This calls for circuit-level [35] representation of the sampled frequency responses of antennas, which typically requires macromodeling: rational function approximation [36] of the sampled frequency response and synthesis of partial fractions as equivalent lumped circuits.

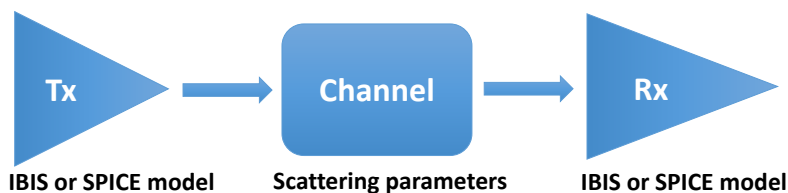


Figure 1.1: Typical serial link transient co-simulation of nonlinear active circuits and linear passive interconnects

## 1.2 Current state of the art

A critical step in the current established macromodeling process [37] [38], shown below in the Figure 1.2, for converting sampled frequency response to circuit netlist is rational function

approximation with partial fractions by Vector Fitting [39] [40] [41] [42]. Before performing the fitting, however, the given frequency response model first need to be verified [43] [44] [45] [46] for Causality by checking for Hilbert transform [47] based violations since any non-causal behaviour in the model can cause failure in the VF based pole-residue fitting. If the model fails the causality test, it is either causality enforced or the model is discarded. After the causality sanctity confirmation, vector fitting with stability enforcement by either throwing away the unstable poles or flipping them is performed. The resultant stable poles/residues are subsequently converted to state-space [48] [12]. In the state-space form, model order reduction [49] [50] [51] is performed before synthesis using controlled sources. Passivity, then, is verified by the Eigen values of Hamiltonian matrices [52] [53] [54] [55] [52] [56] and enforced by either perturbing the poles [57] or residue pairs [58] .

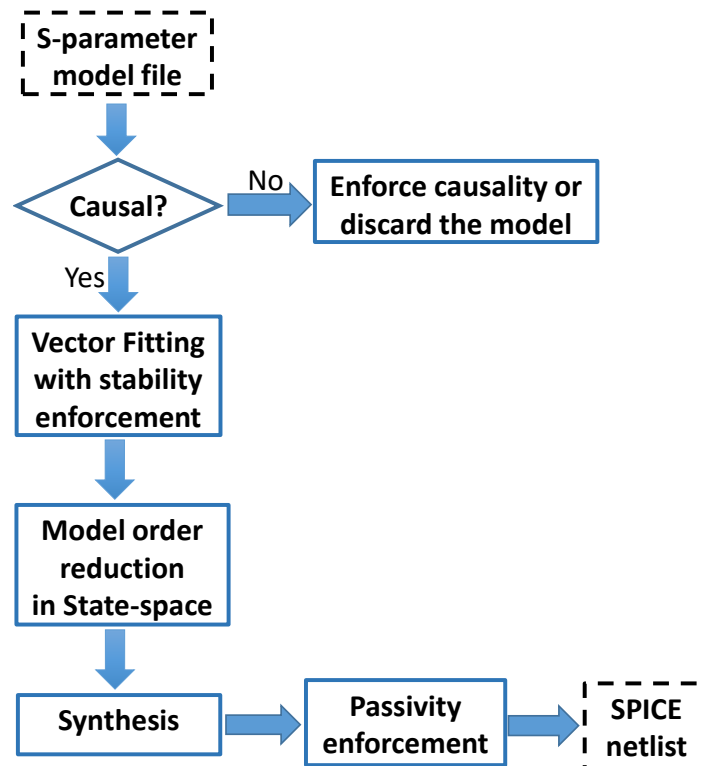


Figure 1.2: Macromodeling process, as per the current dominant methodology

### 1.3 Contribution

Macromodeling converts frequency response to a pole/residue representation before being synthesized [59] as lumped element network. Many pole-zero fitting methods exist; for example, the well-known method of vector fitting (VF) [39]. The VF method requires formulating all sampled frequency response data into matrices and solving least squares; however, this approach can quickly lead to very large matrices for increasing number of system ports, thereby increasing computational complexity and cost. On the otherhand, the proposed method, PRESS, may be regarded as a simpler, yet powerful, alternative that can address very large systems because it formulates the problem in terms of at most 3 sample data points in each iteration. In this thesis an alternate macromodeling flow based on the PRESS fitting, shown below in the Figure 1.3, is demonstrated to work successfully in converting multi-port networks to SPICE netlists. Passivity verification and enforcement can then be performed [60] on the synthesized circuits.

Fitting by PRESS and the subsequent improvements to its algorithm in terms of performance and computational complexity are covered in the Chapter 2. The order of fitted poles residues can be high and is proposed to be reduced by using the Singular perturbation approximation (SPA), which is covered in Chapter 3. Once we have the optimized pole/residue or reduced state-space representation, multi-port network synthesis is performed, as covered in the Chapter 4. The results and discussion are in Chapters 5 and 6.

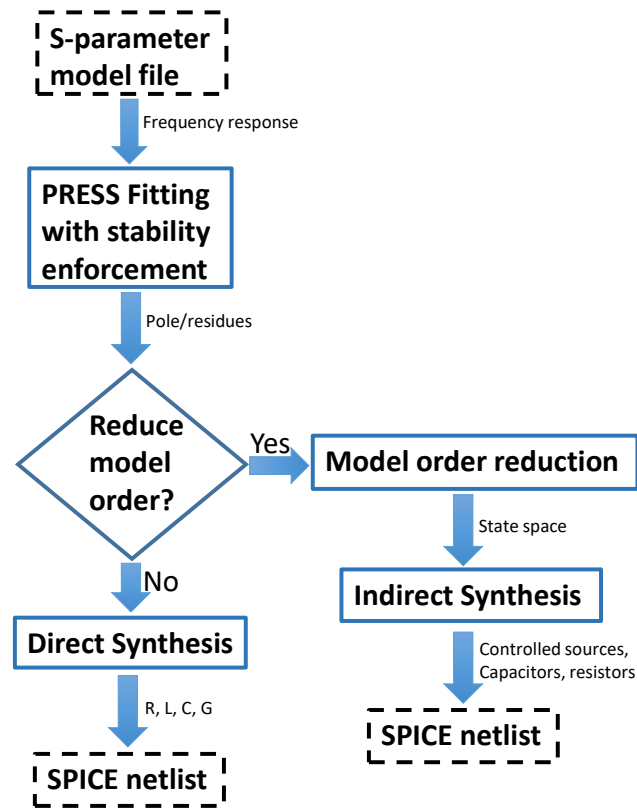


Figure 1.3: Macromodeling process as covered and contributed in the thesis

## CHAPTER 2

### Fitting of frequency response

The proposed fitting methods are based on bottom-up approach. They start with naught and generates approximant recursively by building one block at a time. The building blocks are individual local transfer functions matching at local subsets; the blocks are then combined to approximate or fit the given model's frequency response. This chapter details the original PRESS algorithm and its improvements.

#### 2.1 Pole Residue Equivalent System Solver (PRESS)

Before delving deeper, some notations follow. The given frequency domain transfer function  $H_{given}$  consists of  $N$  samples,  $H_{given} = \{[\omega_1, h_1], [\omega_2, h_2], \dots, [\omega_N, h_N]\}$  defined over discrete angular frequency samples  $\Omega = \{\omega_1, \omega_2, \dots, \omega_N\}$ . The subset  $\Psi$  is defined a collection of selected consecutive points from the frequency response around the peak or maxima position  $M \in \text{Integers}$  where  $1 \leq M \leq N$ . For example,  $\Psi = \{[\omega_L, h_L], [\omega_M, h_M], [\omega_R, h_R]\}$  is a three point subset, where left sample  $\omega_L = \omega_{M-1}$ , middle sample  $\omega_M$ , and right sample  $\omega_R = \omega_{M+1}$ .

The frequency domain model of a system contains its responses at multiple discrete frequencies; all frequency responses together describe the system behavior. The proposed PRESS method, relies on the premise that combination of individual local transfer functions matching at multiple local  $\Psi$  subsets can be effective in approximating the given model's frequency response. The method starts with the given frequency response and sets it equal to the error that is minimized repeatedly by performing local fits at  $\Psi$  which are centered at peak or maxima position of error magnitude. After fitting at  $\Psi$ , the remnant error response is designated as the new response from which yet another  $\Psi$  subset is obtained for local fitting; this process of local fitting continues iteratively until the sum of all local fits produces an approximate global fit within desired accuracy. Stability is enforced at each local fit stage by discarding [39] the unstable local fit poles and traversing the peaks of error until a stable

local fit is found.

### 2.1.1 Formulation: choosing and fitting a subset $\Psi$

For each iteration,  $\Psi$  is centered at position of peak of magnitude of error. If an unstable transfer function results from matching a particular subset  $\Psi$ , then the next error peak is chosen for fitting. Once position of  $\Psi$  is determined, local fit is found over the selected points. There are three types of local fit transfer functions, as described below.

#### Type 1 Local Fit

A low pass real single-pole filter is used to fit  $\Psi$  at one data point.

$$H_{fit1}(s) = \frac{c}{s - p} \quad (2.1)$$

where  $c, p \in \text{Reals}$ ,  $s = j\omega$ ,  $j^2 = -1$ ,  $\omega = 2\pi f$ , and  $f$  is frequency in (Hz). Using the  $\Psi$  frequency point and response  $\{[\omega_M, h_M]\}$  in (2.1), yields

$$H_{fit1}(j\omega_M) = h_M$$

Writing the response in terms of a complex number, and expanding both sides produces

$$\frac{c}{j\omega_M - p} = a_M + jb_M$$

Taking the real and imaginary parts of above, we obtain 2 equations and 2 unknowns

$$\Re\left[\frac{c}{j\omega_M - p}\right] = a_M; \quad \Im\left[\frac{c}{j\omega_M - p}\right] = b_M \quad (2.2)$$

where  $\Re$  is real part and  $\Im$  is imaginary part of a complex number. From the above two equations, the two unknowns  $c$  and  $p$  can be solved numerically.

## Type 2 Local Fit

A band-pass complex-conjugate 2-pole filter is used to fit  $\Psi$  at two data points.

$$H_{fit2}(s) = \frac{C}{s - P} + \frac{C^*}{s - P^*} \quad (2.3)$$

where  $C, P \in \text{Complexes}$ ,  $C = c_r + jc_i$ ,  $P = p_r + jp_i$  and  $*$  is complex conjugate operator.

Using  $\Psi = \{[\omega_L, h_L], [\omega_M, h_M]\}$  in (2.3), we obtain

$$H_{fit2}(j\omega_L) = h_L;$$

$$H_{fit2}(j\omega_M) = h_M$$

Expanding both sides,

$$\frac{C}{j\omega_L - P} + \frac{C^*}{j\omega_L - P^*} = a_L + jb_L$$

$$\frac{C}{j\omega_M - P} + \frac{C^*}{j\omega_M - P^*} = a_M + jb_M$$

Separating to real and imaginary components,

$$\Re\left[\frac{c_r + jc_i}{j\omega_L - (p_r + jp_i)} + \frac{c_r - jc_i}{j\omega_L - (p_r - jp_i)}\right] = a_L \quad (2.4)$$

$$\Im\left[\frac{c_r + jc_i}{j\omega_L - (p_r + jp_i)} + \frac{c_r - jc_i}{j\omega_L - (p_r - jp_i)}\right] = b_L \quad (2.5)$$

$$\Re\left[\frac{c_r + jc_i}{j\omega_M - (p_r + jp_i)} + \frac{c_r - jc_i}{j\omega_M - (p_r - jp_i)}\right] = a_M \quad (2.6)$$

$$\Im\left[\frac{c_r + jc_i}{j\omega_M - (p_r + jp_i)} + \frac{c_r - jc_i}{j\omega_M - (p_r - jp_i)}\right] = b_M \quad (2.7)$$

From the above four equations, the four unknowns  $c_r, c_i, p_r$  and  $p_i$  can be solved numerically.

### Type 3 Local Fit

Equation (2.3) may be modified to add a high frequency term and a DC term, as follows

$$H_{fit3}(s) = \frac{C}{s - P} + \frac{C^*}{s - P^*} + \frac{s - f}{k} \quad (2.8)$$

where  $C, P \in \text{Complexes}$  and  $f, d \in \text{Reals}$ . Using  $\Psi = \{[\omega_L, h_L], [\omega_M, h_M], [\omega_R, h_R]\}$  in (2.8) yields

$$H_{fit3}(j\omega_L) = h_L;$$

$$H_{fit3}(j\omega_M) = h_M;$$

$$H_{fit3}(j\omega_R) = h_R$$

Expanding both sides,

$$\frac{C}{j\omega_L - P} + \frac{C^*}{j\omega_L - P^*} + \frac{j\omega_L - f}{k} = a_L + jb_L$$

$$\frac{C}{j\omega_M - P} + \frac{C^*}{j\omega_M - P^*} + \frac{j\omega_M - f}{k} = a_M + jb_M$$

$$\frac{C}{j\omega_R - P} + \frac{C^*}{j\omega_R - P^*} + \frac{j\omega_R - f}{k} = a_R + jb_R$$

Separating to real and imaginary components,

$$\Re\left[\frac{c_r + jc_i}{j\omega_L - (p_r + jp_i)} + \frac{c_r - jc_i}{j\omega_L - (p_r - jp_i)} + \frac{j\omega_L - f}{k}\right] = a_L \quad (2.9)$$

$$\Im\left[\frac{c_r + jc_i}{j\omega_L - (p_r + jp_i)} + \frac{c_r - jc_i}{j\omega_L - (p_r - jp_i)} + \frac{j\omega_L - f}{k}\right] = b_L \quad (2.10)$$

$$\Re\left[\frac{c_r + jc_i}{j\omega_M - (p_r + jp_i)} + \frac{c_r - jc_i}{j\omega_M - (p_r - jp_i)} + \frac{j\omega_M - f}{k}\right] = a_M \quad (2.11)$$

$$\Im\left[\frac{c_r + j c_i}{j \omega_M - (p_r + j p_i)} + \frac{c_r - j c_i}{j \omega_M - (p_r - j p_i)} + \frac{j \omega_M - f}{k}\right] = b_M \quad (2.12)$$

$$\Re\left[\frac{c_r + j c_i}{j \omega_R - (p_r + j p_i)} + \frac{c_r - j c_i}{j \omega_R - (p_r - j p_i)} + \frac{j \omega_R - f}{k}\right] = a_R \quad (2.13)$$

$$\Im\left[\frac{c_r + j c_i}{j \omega_R - (p_r + j p_i)} + \frac{c_r - j c_i}{j \omega_R - (p_r - j p_i)} + \frac{j \omega_R - f}{k}\right] = b_R \quad (2.14)$$

From the above six equations, the six unknowns  $c_r, c_i, p_r, p_i, k$  and  $f$  can be solved numerically.

### 2.1.2 Algorithm

The given sampled response is  $H_{given}$ , the approximant to be obtained is  $H_{sum}$ , the error is defined as  $H_{err} = H_{given} - H_{sum}$ , and  $H_{fit}$  is the local fit at each iteration. The method tries to reduce magnitude of  $H_{err}$  at its peak by finding stable transfer function  $H_{fit}$  that fits  $\Psi$  and subtracting  $H_{fit}$  from  $H_{err}$ . If unstable fit occurs,  $\Psi$  is chosen at position of the next peak error, and so on. Such Iterations are repeated until  $H_{sum}$  reaches to desired error. Total error level is computed by summing up the magnitude of  $H_{err}$  across all available samples. Desired target error is  $E \in \text{Real}$ . The method is summarized in Algorithm 1 below.

## 2.2 Coarse-to-fine Malleable Pole/Residue Equivalent System Solver (COMPRESS)

PRESS [5] [3] is a simple fitting method, relying on processing at most 3 consecutive sample data points in each iteration. But the fit results in large model with high number of pole/residues. In this section, to lower fitting error and improve the model order, non-consecutive sample subset based local fitting is proposed, allowing local fits with variable bandwidth, adapting to the peaks and valleys of the given response.

---

**Algorithm 1:** PRESS algorithm
 

---

**Input:**  $H_{given}$  is the given frequency response.

**Output:**  $H_{sum}$  is the approximated frequency response.

```

1 begin
2    $H_{sum} = 0, H_{err} = H_{given} - H_{sum}$ 
3   while  $\sum_{i=1}^N |H_{err}(i)| > E$  do
4     Find index  $M$  at maxima of  $|H_{err}|$ .
5     Identify  $H_{fit}(j\omega_M)$  type with lowest error.
6     if  $\Re[p] > 0$  then
7       Set  $\Psi$  to the next peak position in  $|H_{err}|$ , go to step 5.
8      $H_{sum} = H_{sum} + H_{fit}$ .
9      $H_{err} = H_{given} - H_{sum}$ .

```

---

Unlike PRESS [5] that chooses atmost three consecutive sample points, non-consecutive [7] sample points based local fitting is proposed in this section to build approximant with local fit transfer function as building-block. At each iteration, the center point of subset is fixed at a peak while the other two points are varied to get the lowest error yielding local fit, thereby adapting to the complexities of the frequency response. Stability is enforced at each local fit stage by discarding [39] the unstable local fit poles and traversing to the other peaks of frequency response until a stable local fit is found.

### 2.2.1 Formulation: iteratively adapting and fitting a subset

From the given frequency domain transfer function,  $H_{given} = \{[\omega_1, h_1], [\omega_2, h_2], \dots, [\omega_N, h_N]\}$  consisting responses over  $N$  discrete frequency samples  $\Omega = \{\omega_1, \omega_2, \dots, \omega_N\}$ , a three point adaptive subset  $\Psi$  is defined as a collection of points from  $H_{given}$  around position  $M \in$  Integers where  $1 \leq M \leq N$ ,  $\Psi = \{[\omega_L, h_L], [\omega_M, h_M], [\omega_R, h_R]\}$ , where left sample  $\omega_L = \omega_{M-d_L}$ , middle sample  $\omega_M$ , and right sample  $\omega_R = \omega_{M+d_R}$ , at offsets  $d_L$  and  $d_R \in$  Integers, where  $1 \leq d_L \leq M - 1$  and  $1 \leq d_R \leq N - M$ , from the middle point  $M$ .

At each iteration, to adapt to the frequency response, disparate subsets, formed by all the possible combination of offsets  $d_L$  and  $d_R$ , are locally fitted before choosing the best fit among them, resulting in the lowest possible fitting error. Note that the subset offsets are

fixed, as 1, in the original PRESS [5] algorithm.

For local fitting of each adaptive subset, one of the three local fit transfer function types below is used.

## 2.2.2 Algorithm

The method starts with initializing error  $H_{error}$  with the given input frequency response,  $H_{given}$  and output approximant,  $H_{sum}$  as zero. It reduces the error and builds approximant by recursively performing local fits  $H_{fit}$  to  $H_{error}$  with stable transfer functions: each iteration picks the best non-consecutive point subset  $\Psi$  from  $H_{error}$ , identifies a stable transfer function that matches their response,  $H_{fit}$ , thereby reducing error,  $H_{error} = H_{given} - H_{sum}$  and building approximant,  $H_{sum} = H_{sum} + H_{fit}$ . Once the total error level, computed by summing up the magnitude of  $H_{error}$  across all available samples, reaches below the desired target error,  $E \in \text{Real}$ , it stops.

Total error level is computed by summing up the magnitude of  $H_{err}$  across all available samples. Desired target error is  $E \in \text{Real}$ . The method is summarized in Algorithm 2 below.

---

### Algorithm 2: COMPRESS algorithm

---

**Input:**  $H_{given}$  is the given frequency response.

**Output:**  $H_{sum}$  is the approximated frequency response.

1 **begin**

2      $H_{sum} = 0, H_{err} = H_{given} - H_{sum}$

3     **while**  $\sum_{i=1}^N |H_{err}(i)| > E$  **do**

4         Find index M at maxima of  $|H_{err}|$ .

5         Identify subset  $\Psi$  width and  $H_{fit}(j\omega_M)$  type with the lowest error.

6         **if**  $\Re[p] > 0$  **then**

7             Set  $\Psi$  to the next peak position in  $|H_{err}|$ , go to step 5.

8          $H_{sum} = H_{sum} + H_{fit}$ .

9          $H_{err} = H_{given} - H_{sum}$ .

---

## 2.3 Error Maxima-agnostic Pole Residue Equivalent System Solver (EMPRESS)

PRESS [5] is a simple fitting method, relying on processing at most 3 consecutive sample data points in each iteration. But the fit results in large model with high number of pole/residues. In this section, to lower fitting error and improve the model order, instead of fitting at the error peak, local fitting anywhere with the best fit performance is proposed, allowing to widen the net of possible local fit locations, thereby reducing the error quickly in lesser number of iterations when compared to the original PRESS algorithm

Unlike PRESS [5] that chooses atmost three consecutive sample points at the error peak, sweeping all the points by fitting at all the points and choosing the best fit interms of lowest error, basically maxima or peak agnostic, is proposed [1] to build approximant with local fit transfer function as building-block. At each iteration, the center point of subset is swept across the frequency range to get the lowest error yielding local fit, thereby adapting to the complexities of the frequency response. Stability is enforced at each local fit stage by discarding [39] the unstable local fit poles and traversing to the next best subset of frequency response until a stable local fit is found.

### 2.3.1 Algorithm

The method starts with initializing error  $H_{error}$  with the given input frequency response,  $H_{given}$  and output approximant,  $H_{sum}$  as zero. It reduces the error and builds approximant by recursively performing local fits  $H_{fit}$  to  $H_{error}$  with stable transfer functions: across the frequency range, each iteration picks the best consecutive point subset  $\Psi$  from  $H_{error}$ , identifies a stable transfer function that matches their response,  $H_{fit}$ , thereby reducing error,  $H_{error} = H_{given} - H_{sum}$  and building approximant,  $H_{sum} = H_{sum} + H_{fit}$ . Once the total error level, computed by summing up the magnitude of  $H_{error}$  across all available samples, reaches below the desired target error,  $E \in \text{Real}$ , it stops.

Total error level is computed by summing up the magnitude of  $H_{err}$  across all available samples. Desired target error is  $E \in \text{Real}$ . The method is summarized in Algorithm 3 below.

---

**Algorithm 3:** EMPRESS algorithm

---

**Input:**  $H_{given}$  is the given frequency response.

**Output:**  $H_{sum}$  is the approximated frequency response.

```

1 begin
2    $H_{sum} = 0, H_{err} = H_{given} - H_{sum}$ 
3   while  $\sum_{i=1}^N |H_{err}(i)| > E$  do
4     forall elements of  $H_{err}$  do
5       Identify  $H_{fit}(j\omega_M)$  type with the lowest error.
6       if  $\Re[p] > 0$  then
7         Discard and set  $\Psi$  to the next element position in  $|H_{err}|$ , go to step 5.
8     Find index M that has the minima or lowest  $|H_{err}|$ .
9     Identify subset  $\Psi$  width and  $H_{fit}(j\omega_M)$  type with the lowest error.
10     $H_{sum} = H_{sum} + H_{fit}$ .
11     $H_{err} = H_{given} - H_{sum}$ .

```

---

## 2.4 Optimized Pole/Residue Equivalent System Solver (OPPRESS)

PRESS [5] [3] is a simple fitting method, relying on processing at most 3 consecutive sample data points in each iteration. But each iteration's local fitting needs solving six non-linear equations for type-3 fit type; also, the approximant results in a large model with high number of pole/residues. In this section, to lower both the computational complexity of type-3 fit and improve the model order, simplified type-3 local fit type with flexible improper term is proposed, allowing local fits with variable bandwidth, adapting to the peaks and valleys of the given response.

Unlike PRESS [5] that chooses atmost three consecutive sample points, non-consecutive [7] sample points based and simplified type-3 local fitting is proposed in this section to build approximant with local fit transfer function as building-block. At each iteration, the center point of subset is fixed at a peak for type-1 and type-2 fits; but for type-3's the other point

is swept to get the lowest error yielding local fit, thereby adapting to the complexities of the frequency response. Stability is enforced at each local fit stage by discarding [39] the unstable local fit poles and traversing to the other peaks of frequency response until a stable local fit is found.

### 2.4.1 Formulation: iteratively fitting a subset

From the given frequency domain transfer function,  $H_{given} = \{[\omega_1, h_1], [\omega_2, h_2], \dots, [\omega_N, h_N]\}$  consisting responses over  $N$  discrete frequency samples  $\Omega = \{\omega_1, \omega_2, \dots, \omega_N\}$ , a three point adaptive subset  $\Psi$  is defined as a collection of points from  $H_{given}$  around position  $M \in$  Integers where  $1 \leq M \leq N$ ,  $\Psi = \{[\omega_L, h_L], [\omega_M, h_M], [\omega_R, h_R]\}$ , where left sample  $\omega_L = \omega_{M-1}$ , middle sample  $\omega_M$ , and right sample  $\omega_R = \omega_{M+1}$ .

At each iteration, the three types of fits are sequentially fitted at the error peak before choosing the best fit among them. After the Type-2 fit, it is reused and a simple improper system is adaptively fitted to the remnant frequency response, reducing the computational complexity of type-3 type.

For local fitting of each subset, one of the three local fit transfer function types below is used.

#### Type 1 Local Fit

A low-pass, single real-pole filter is used to fit  $\Psi$  at one data point.

$$H_{fit1}(s) = \frac{c}{s - p} \quad (2.15)$$

where  $c, p \in$  Reals,  $s = j\omega$ ,  $j^2 = -1$ , and  $\omega$  is angular frequency in (radians/second). The two unknowns  $k$  and  $p$  can be solved numerically from (2.1) after substituting  $\Psi = \{[\omega_M, h_M]\}$ .

## Type 2 Local Fit

A band-pass, complex-conjugate 2-pole filter is used to fit  $\Psi$  at two data points.

$$H_{fit2}(s) = \frac{C}{s - P} + \frac{C^*}{s - P^*} \quad (2.16)$$

where  $C, P \in \text{Complexes}$  and  $*$  is complex conjugate operator. The unknowns  $C$  and  $P$  can be solved numerically from (2.3) after substituting  $\Psi = \{[\omega_L, h_L], [\omega_M, h_M]\}$ .

## Type 3 Local Fit

A high frequency term and a DC term are added to Equation (2.3) and  $\Psi$  is fit at one data point.

$$H_{fit3}(s) = H_{fit2}(s) + \frac{s - f}{k} \quad (2.17)$$

where  $f, k \in \text{Reals}$  and can be solved numerically from (2.8) after substituting  $\Psi = \{[\omega_{M+d}, h_{M+d}]\}$ . where the middle sample  $\omega_{M+d}$ , at an offset  $d \in \text{Integers}$ , where  $1 - M \leq d \leq N - M$ , from the middle point  $M$ . Note that this type-3 fit involves type-2 local fit at  $M$  and the improper fit at  $M + d$  at an offset,  $d$ , from the maxima.

### 2.4.2 Algorithm

The OPPRESS algorithm is essentially the PRESS algorithm with a modified, simplified Type-3 fit type: only one equation is solved instead of six equations in PRESS and the given frequency range is swept to identify the best location for the new Type-3 fit. The method starts with initializing error  $H_{error}$  with the given input frequency response,  $H_{given}$  and output approximant,  $H_{sum}$  as zero. It reduces the error and builds approximant by recursively performing local fits  $H_{fit}$  to  $H_{error}$  with stable transfer functions: each iteration picks the consecutive point subset  $\Psi$  from  $H_{error}$  at its peak, identifies a stable transfer function that matches their response,  $H_{fit}$ , thereby reducing error,  $H_{error} = H_{given} - H_{sum}$

and building approximant,  $H_{sum} = H_{sum} + H_{fit}$ . Once the total error level, computed by summing up the magnitude of  $H_{error}$  across all available samples, reaches below the desired target error,  $E \in \text{Real}$ , it stops.

Total error level is computed by summing up the magnitude of  $H_{err}$  across all available samples. Desired target error is  $E \in \text{Real}$ . The method is summarized in Algorithm 4 below.

---

**Algorithm 4:** OPPRESS algorithm

---

**Input:**  $H_{given}$  is the given frequency response.

**Output:**  $H_{sum}$  is the approximated frequency response.

```

1 begin
2    $H_{sum} = 0, H_{err} = H_{given} - H_{sum}$ 
3   while  $\sum_{i=1}^N |H_{err}(i)| > E$  do
4     Find index M at maxima of  $|H_{err}|$ .
5     Identify  $H_{fit}(j\omega_M)$  types-1, 2 and  $H_{fit}(j\omega_{M_d})$  type-3 with lowest error.
6     if  $\Re[p] > 0$  then
7       Set  $\Psi$  to the next peak position in  $|H_{err}|$ , go to step 5.
8      $H_{sum} = H_{sum} + H_{fit}$ .
9      $H_{err} = H_{given} - H_{sum}$ .

```

---

## CHAPTER 3

### Model order reduction

PRESS [5] is a simple fitting method, relying on processing at most 3 sample data points in each iteration. But the fit results in large model with high number of pole/residues. In this thesis, singular perturbation approximation (SPA) [61] technique is proposed to reduce and optimize the model order. Unlike other truncation based model order reduction (MOR) methods, SPA method residualizes the weaker states; so the reduced model contain more information about the original system and maintains performance. This chapter covers the formulation of the problem and algorithm .

### 3.1 Formulation

PRESS [5] iteratively builds approximant with local fit transfer function as building-block. Stability is enforced at each local fit stage by discarding [39] the unstable local fit poles and traversing to the other peaks of frequency response until a stable local fit is found. The approximate global fit is then converted to balanced state-space form. Based on Hankel singular values of the state-space, the energy contribution of the states is assessed. Instead of truncating the low-energy states, singular perturbation approximation method [61] residualizes them by setting their derivatives to zero and then solves for the reduced state-space model, which can be synthesized [12] as broadband circuits [59].

#### 3.1.1 PRESS: iteratively choosing and fitting a subset

For each iteration, a subset of utmost three points centered at a peak position of frequency response is chosen and one of the three types of local fit transfer functions is fitted.

After certain iterations, a combination of local fit types gives the global fit, having proper,

improper and constant terms,  $H_{sum}^F(s) = H_p^F(s) + H_c(s) + H_i(s)$ .

$$H_p^F(s) = \sum_{i=1}^{n_1} \frac{c_i}{s - p_i} + \sum_{i=1}^{n_2+n_3} \left( \frac{C_i}{s - P_i} + \frac{C_i^*}{s - P_i^*} \right) \quad (3.1)$$

$$H_i(s) = s \sum_{i=1}^{n_3} \frac{1}{k_i} \quad (3.2)$$

$$H_c(s) = \sum_{i=1}^{n_3} \frac{-f_i}{k_i} \quad (3.3)$$

where  $n_1$ ,  $n_2$ , and  $n_3$  are the number of local fit types-1, 2 and 3 respectively; subscript  $i$  corresponds to  $i^{th}$  iteration and superscript like  $F$  is the order of proper terms, equaling  $F = n_1 + 2 * (n_2 + n_3)$ .

### 3.1.2 SPA: identify and residualize weaker states

The fitted system admittance transfer function's proper part,  $H_p(s)$ , in the poles and residues form in (3.1) is converted [12] to a set of first-order differential equations in the state-space domain.

$$\dot{X} = AX + BU;$$

$$Y = CX + DU$$

where  $A \in \mathbb{R}^{F \times F}$ ,  $B \in \mathbb{R}^{F \times 1}$ ,  $C \in \mathbb{R}^{1 \times F}$ ,  $D \in \mathbb{R}^{1 \times 1}$  are state-matrices, X is the state vector of length F, U and Y are the input voltage and output current vectors of length 1.

Considering a generic case of multiple complex conjugate pairs based PRESS fit of  $t$  iterations,

$\sum_{i=1}^t \left( \frac{C_i}{s-P_i} + \frac{C_i^*}{s-P_i^*} \right)$  where  $C_i = v_i + jw_i$  and  $P_i = h_i + jg_i$ , its state-space matrices are-

$$A = \begin{bmatrix} h_1 & g_1 & 0 & \dots & \dots & \dots & 0 \\ -g_1 & h_1 & 0 & \dots & \dots & \dots & 0 \\ 0 & 0 & h_2 & g_2 & 0 & \dots & 0 \\ 0 & 0 & -g_2 & h_2 & 0 & \ddots & \vdots \\ \vdots & \vdots & 0 & 0 & \ddots & 0 & 0 \\ 0 & \dots & \dots & \ddots & 0 & h_t & g_t \\ 0 & \dots & \dots & \dots & 0 & -g_t & h_t \end{bmatrix},$$

$$B = \begin{bmatrix} 2 \\ 0 \\ 2 \\ 0 \\ \vdots \\ 2 \\ 0 \end{bmatrix},$$

$$C = \begin{bmatrix} v_1 & w_1 & v_2 & w_2 & \dots & v_t & w_t \end{bmatrix},$$

$$D = \begin{bmatrix} 0 \end{bmatrix}$$

Transformation [62] matrix  $T$  is then used to balance the state-space.

$$\tilde{A} = T^{-1}AT,$$

$$\tilde{B} = T^{-1}B,$$

$$\tilde{C} = CT,$$

$$\tilde{D} = D.$$

Based on Hankel singular values of the balanced state-matrix, the number of strongly contributing states,  $r$ , is determined and the state-space is partitioned as-

$$\tilde{A} = \begin{bmatrix} \tilde{A}_{11} & \tilde{A}_{12} \\ \tilde{A}_{21} & \tilde{A}_{22} \end{bmatrix},$$

$$\begin{aligned}\tilde{B} &= \begin{bmatrix} \tilde{B}_1 \\ \tilde{B}_2 \end{bmatrix}, \\ \tilde{C} &= \begin{bmatrix} \tilde{C}_1 \\ \tilde{C}_2 \end{bmatrix}, \\ \Sigma &= \begin{bmatrix} \Sigma_1 & 0 \\ 0 & \Sigma_2 \end{bmatrix}, \\ X &= \begin{bmatrix} X_1 \\ X_2 \end{bmatrix}\end{aligned}$$

where  $\Sigma$  is gramian,  $\sigma_i$  is ordered Hankel singular values of the system  $\Sigma_1 = \text{diag}(\sigma_1, \sigma_2, \dots, \sigma_r)$ ,  $\Sigma_2 = \text{diag}(\sigma_{r+1}, \sigma_{r+2}, \dots, \sigma_N)$  and  $\sigma_r > \sigma_{r+1}$ . Instead of discarding  $X_2$ , it is residualized by setting its derivative to zero and solving [63] for  $X_2$  in terms of  $X_1$  and input  $U$  gives the singular perturbation approximation-

$$\begin{aligned}H_{spa}^r(s) &= C_r(sI - A_r)^{-1}B_r + D_r, \text{ where} \\ A_r &= \tilde{A}_{11} - \tilde{A}_{12}\tilde{A}_{22}^{-1}\tilde{A}_{21}, \\ B_r &= \tilde{B}_1 - \tilde{A}_{12}\tilde{A}_{22}^{-1}\tilde{B}_2, \\ C_r &= \tilde{C}_1 - \tilde{C}_2\tilde{A}_{22}^{-1}\tilde{A}_{21}, \\ D_r &= \tilde{D} - \tilde{C}_2\tilde{A}_{22}^{-1}\tilde{B}_2\end{aligned}$$

The model order reduced system is  $H_{mor}^r(s) = H_{spa}^r(s) + H_c(s) + H_i(s)$ .

## 3.2 Algorithm

The method starts with initializing error  $H_{error}$  with the given input frequency response,  $H_{given}$  and output approximant,  $H_{sum}$  as zero. It reduces the error and builds approximant by recursively performing local fits  $H_{fit}$  to  $H_{error}$  with stable transfer functions: each iteration picks a consecutive point subset  $\Psi$  from  $H_{error}$ , identifies a stable transfer function that matches their response,  $H_{fit}$ , thereby reducing error,  $H_{error} = H_{given} - H_{sum}$  and building approximant,  $H_{sum} = H_{sum} + H_{fit}$ . Once the total error level, computed by summing up

the magnitude of  $H_{error}$  across all available samples, reaches below the desired target error,  $E \in \text{Real}$ , it stops. The algorithm is tabulated in [5]. The proper terms of the  $H_{sum}$  are converted to a balanced state-space of order  $F$ ; based on its Hankel singular values, the reduced model order,  $r$ , is determined. Then the original state space is partitioned at  $r$  and residualized [61].

## CHAPTER 4

### Synthesis

Traditional synthesis techniques rely on state-space approaches [12], resulting in controlled source elements such as voltage-controlled current sources (VCCS). However, along with this indirect synthesis method, this chapter includes admittance parameters based direct synthesis [2], resulting in equivalent circuits that consists of basic circuit elements - resistor, capacitor and inductor and extends the branch level cellular synthesis [59] to multi-port level network synthesis. Also, the admittance based direct synthesis approach allows for simpler passivity assessment [64] of the equivalent circuits.

#### 4.1 Formulation

##### 4.1.1 Synthesizing an equivalent circuit block

##### Direct method: synthesis from the set of poles-residues

From the earlier Chapter 2 on fitting, we get approximation to a given sampled frequency response in pole-residue form as sum of partial fractions.

$$H(s) = G + sC + \sum_{i=1}^t \frac{C_k}{s - P_k}$$

where  $t$  is the number of iterations;  $C_i$  and  $P_i$  are residue and pole of the  $i^{th}$  iteration respectively, which can be real or complex conjugate pairs depending on the fit type; and  $G$  and  $C$  are real numbers and are the sum of all the corresponding constant and improper terms that resulted from the Type 3 fits.

Among the 't' number of iterations, there can be a mix of the three types of local fit - real pole, complex conjugate pair and complex conjugate pair improper transfer function. Since the admittance (Y) parameters are directly implementable, each partial fractional term

becomes a branch: the real pole transfer function is realized as RL branch, while the complex conjugate pair function is realized as RLCG branch. The values of resistor, capacitor and inductor elements are calculated from the equations [59] as shown in the Figure 4.1. So fitting a sampled frequency response data with  $t$  iterations results in a single block consisting of  $t$  branches connected in parallel.

### Indirect method: synthesis from the state space

From the previous Section 3.1.2 on model reduction, we get optimized approximation to a given sampled frequency response in state-space form as a set of complete matrices. Such state-space form of admittance matrix can be synthesized [12] as a network of controlled sources. As an example, a state space form with three states is considered for synthesis below.

$$A_r = \begin{bmatrix} a_{11} & a_{12} & a_{13} \\ a_{21} & a_{22} & a_{23} \\ a_{31} & a_{32} & a_{33} \end{bmatrix}$$

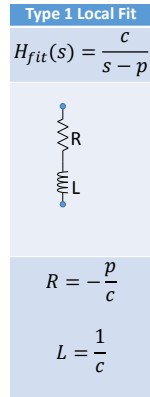
$$B_r = \begin{bmatrix} b_{11} \\ b_{21} \\ b_{31} \end{bmatrix}$$

$$C_r = \begin{bmatrix} c_{11} & c_{12} & c_{13} \end{bmatrix}$$

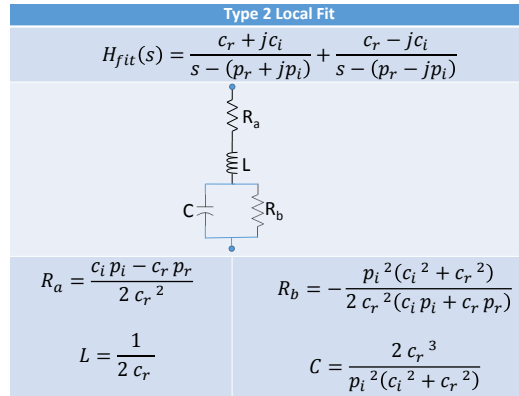
$$D_r = \begin{bmatrix} d_{11} \end{bmatrix}$$

where the matrices  $A_r, B_r, C_r, D_r$  are real matrices.

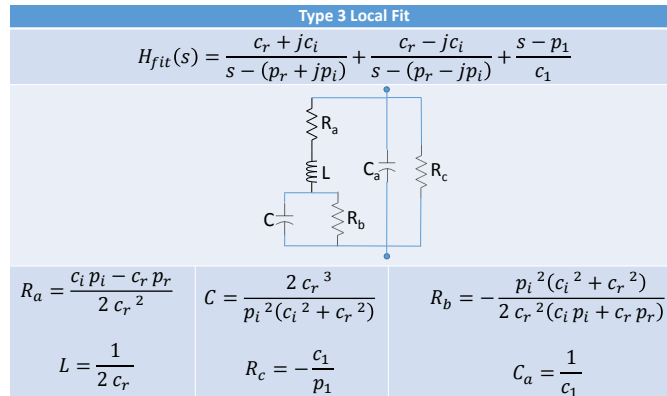
Since the admittance (Y) parameters are directly implementable, each of the non-diagonal element of matrix  $A_r$  and all the elements of matrices  $B_r, C_r$  becomes controlled current



(a)



(b)



(c)

Figure 4.1: Pole/residues to circuit branch synthesis: (a) Type 1 (b) Type 2 (c) Type 3. Permission from [2], ©2016 IEEE

source branch, while the diagonal elements of matrix  $A_r$  and  $D_r$  becomes a resistor branch.

### 4.1.2 Building equivalent multi-port network from the circuit blocks

Admittance parameters based direct synthesis of multi-port networks [65] is used in this thesis.

$$Y = \begin{bmatrix} Y_{11} & Y_{12} & \dots & Y_{1n} \\ Y_{21} & Y_{22} & \dots & Y_{2n} \\ \vdots & \vdots & \ddots & \vdots \\ Y_{n1} & Y_{n2} & \dots & Y_{nn} \end{bmatrix}$$

where  $n$  is number of ports in the given frequency-domain model.

An  $n$ -port network model contains  $n^2$  frequency responses. But, by assuming reciprocity and common reference among the ports, we can represent and realize the given admittance multi-port model as a topology of  $n$  nodes with  $n + \frac{n(n-1)}{2}$  blocks:  $n$  transformed self admittance blocks interconnected by  $\frac{n(n-1)}{2}$  transformed transfer admittance blocks, as shown in Figure 4.2.

The blocks of the topology are calculated from the given admittance parameters by transforming them using the equations below.

$$Y'_{ii} = \sum_{j=1}^n Y_{ij} \tag{4.1}$$

$$Y'_{ij} = -Y_{ij}, i \neq j$$

So for fitting, the given diagonal self-admittance terms are transformed by adding with transfer admittance terms, while the transfer admittance parameters gets sign reversed.

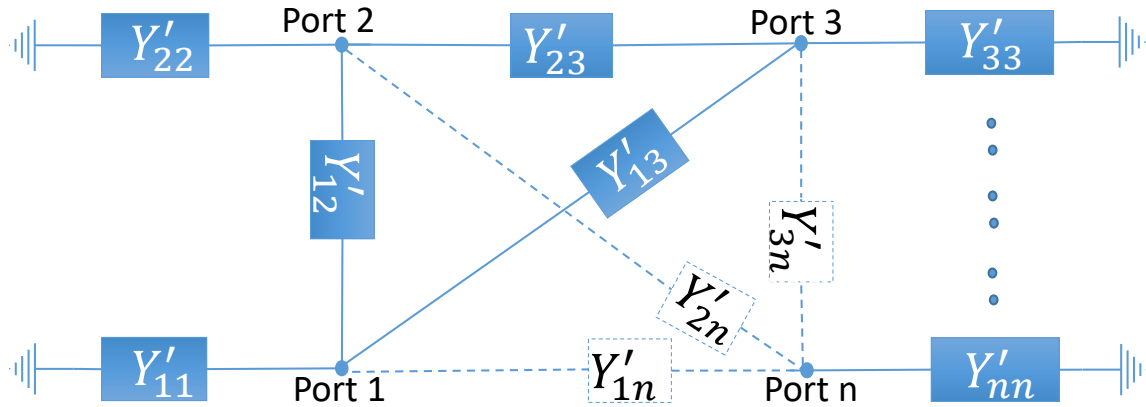


Figure 4.2: Multi-port network synthesis using admittance parameters. Permission from [2], ©2016 IEEE

### 4.1.3 Passivity verification of the multi-port network

Passivity of the realized circuits is an important property for running stable simulations. Since synthesis is based on direct implementation [59] of admittance parameters as resistor, capacitor and inductor based circuits, passivity checking and enforcement [60] is simplified by first calculating the admittance of equivalent circuit at each frequency and checking whether the eigen values of the real part of the admittance [64] is less than 0.

$$\text{eig}(\Re[Y_c]) > 0 \quad (4.2)$$

where  $\text{eig}()$  is eigen values of a matrix and  $Y_c$  is admittance parameters of the equivalent circuit at a frequency.

## 4.2 Algorithm

The multi-port admittance parameters are first transformed using the equations 4.1. For each of the transformed admittance parameters, fitting and synthesis of corresponding block of branches is performed. It start with initializing error  $H_{err}$  with the input frequency response,  $H_{given}$  and output approximant,  $H_{sum}$  as zero. It reduces the error and builds approximant by recursively performing local fits  $H_{fit}$  to  $H_{err}$  with stable transfer functions:

each iteration picks a consecutive point subset  $\Psi$  from  $H_{err}$ , identifies a stable transfer function that matches their response,  $H_{fit}$ , thereby reducing error,  $H_{err} = H_{given} - H_{sum}$  and building approximant,  $H_{sum} = H_{sum} + H_{fit}$ . The resultant  $H_{fit}$  of each iteration is synthesized as equivalent circuit branch. Once the total error level, computed by summing up the magnitude of  $H_{err}$  across all available samples, reaches below the desired target error,  $E \in \text{Real}$ , it stops after certain number of iterations 't', simultaneously making a block of 't' branches. All such blocks of the transformed admittance parameters form the equivalent network, on which Passivity is assessed.

## CHAPTER 5

### Results

This chapter shows various experiments, involving disparate interconnect structures ranging from wire-line to power delivery planes to antennas, that validate the proposed methods and algorithms.

#### 5.1 Experiment 1: Stripline

The proposed algorithm is applied on a test case, commonly found in signal integrity applications, a single-ended strip-line.

##### 5.1.1 Setup

A strip-line transmission line of length 2" long and width 0.007" with reference planes separated by 0.02", as shown in the Figure 5.1, is considered for this experiment.

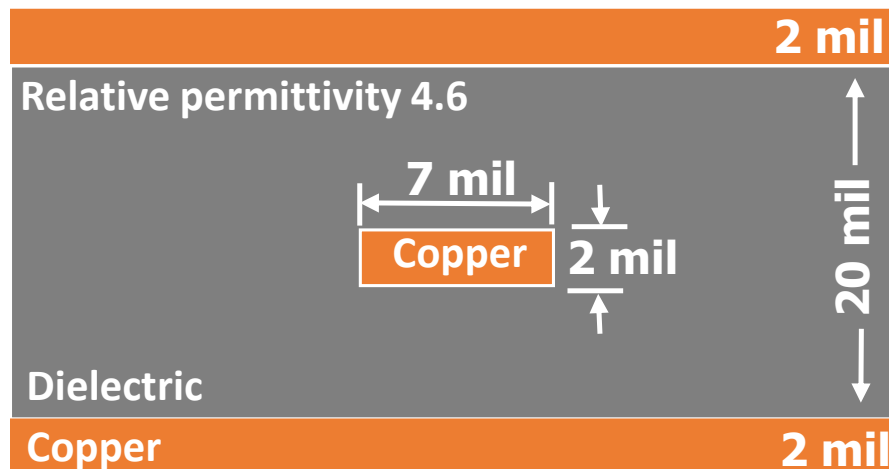
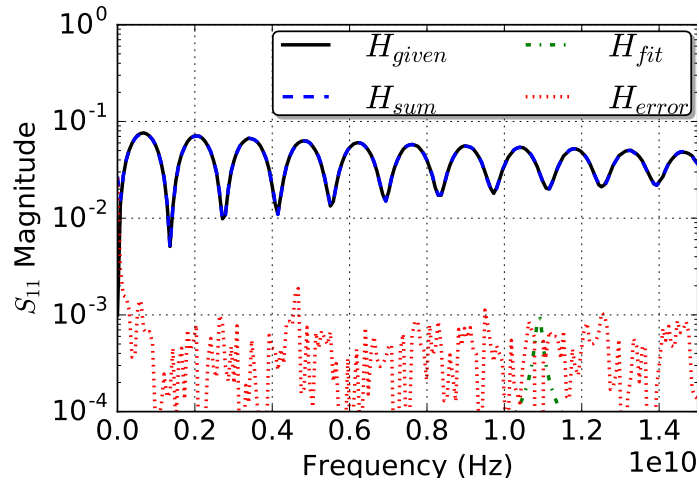


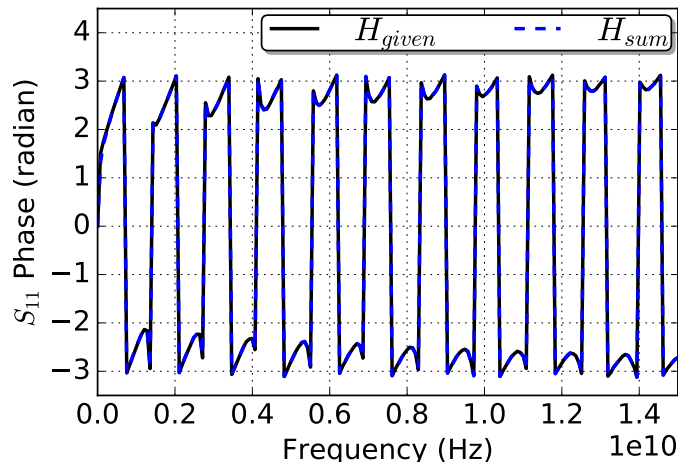
Figure 5.1: strip lines 2" long. Permission from [3], ©2016 IEEE

##### 5.1.2 Validation of PRESS

The results of fitting on return loss  $S_{11}$  and insertion loss  $S_{21}$  of the strip-line are shown Figures 5.2-5.4. Also, comparison with VF method [66] is done on a one inch two-port strip-



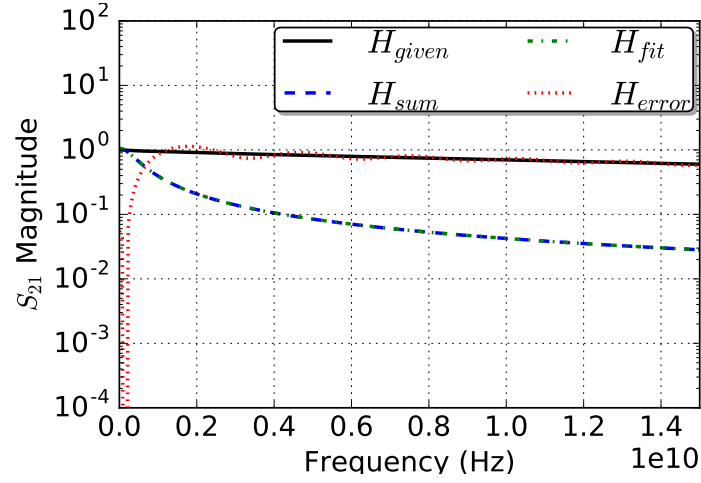
(a)



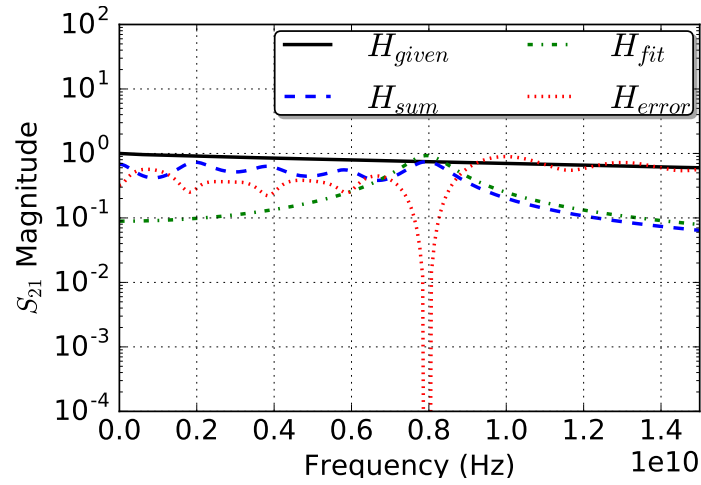
(b)

Figure 5.2: Fitting of strip-line return loss after 100<sup>th</sup> iteration: (a) *Magnitude* (b) *Phase*. Permission from [3], ©2016 IEEE

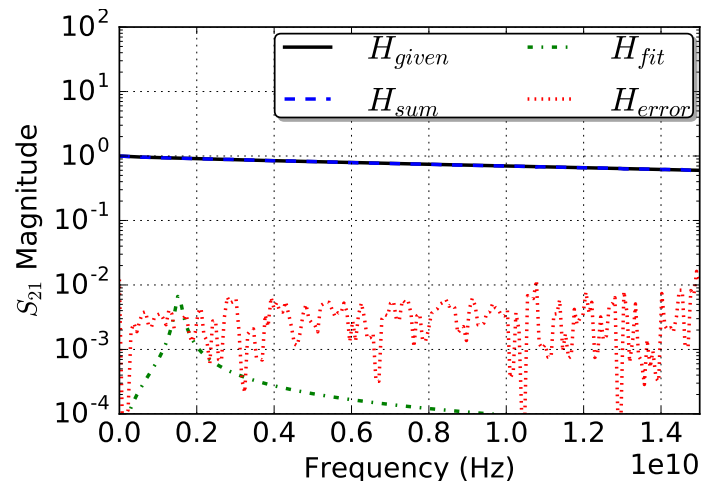
line testcase structure shown in Figure 5.1 where equivalent circuits are synthesized [65] [59] from the poles-residues fitted by both the VF method [39] and proposed method. The synthesized equivalent circuits are excited by a 1 V step voltage of rise time 1 ns and the current and voltage at input port and output port respectively are simulated in ADS tool [67]. The comparison results are shown Figures 5.6a-5.6b.



(a)



(b)



(c)

Figure 5.3: Fitting on strip-line insertion loss  $S_{21}$  magnitude after iterations: (a) 1<sup>st</sup> (b) 5<sup>th</sup> (c) 100<sup>th</sup>. Permission from [3], ©2016 IEEE

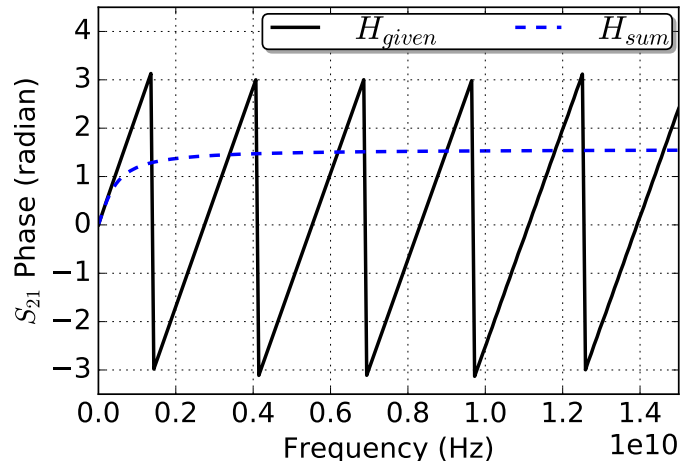
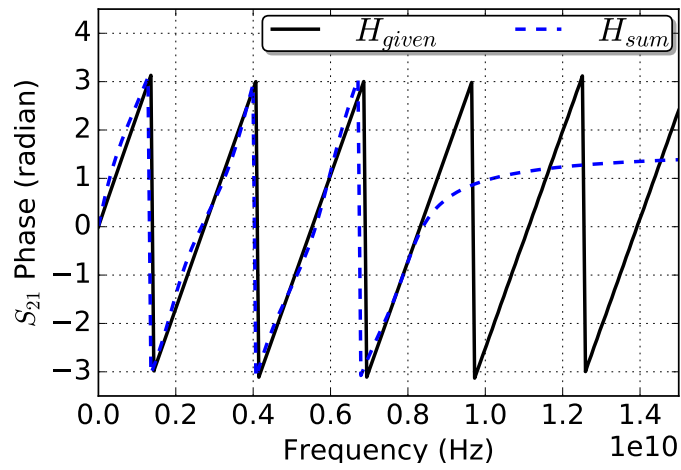
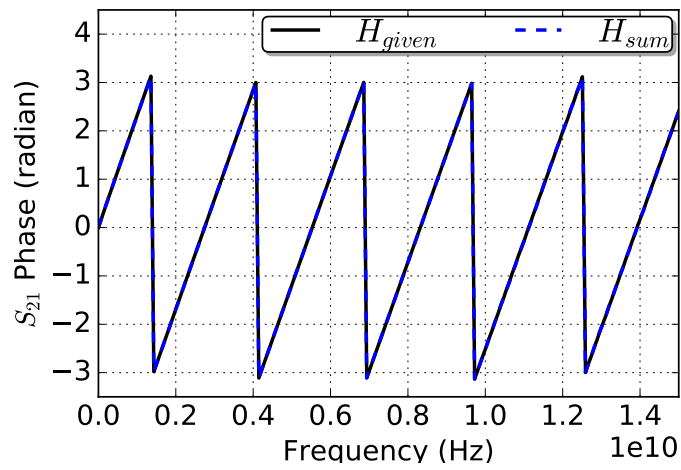
(a) 1<sup>st</sup>(b) 5<sup>th</sup>(c) 100<sup>th</sup>

Figure 5.4: Fitting on strip-line insertion loss  $S_{21}$  phase after iterations: (a) 1<sup>st</sup> (b) 5<sup>th</sup> (c) 100<sup>th</sup>. Permission from [3], ©2016 IEEE

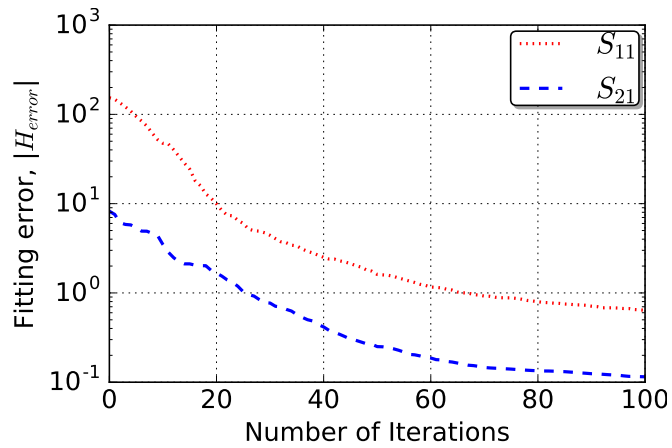
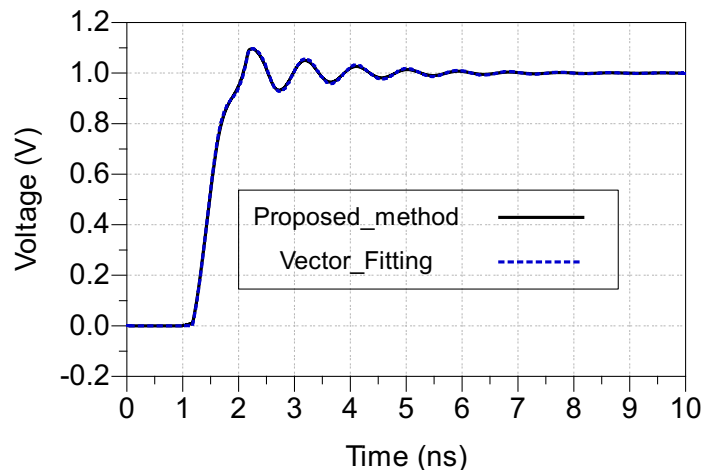
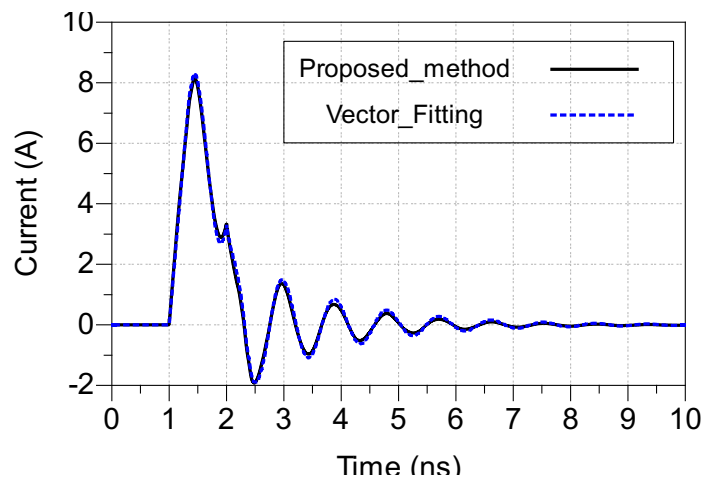


Figure 5.5: Error convergence of fitting the strip-line over 100 iterations.



(a)



(b)

Figure 5.6: Response at output port of strip-line equivalent circuit excited by step: (a) Voltage & (b) Current. Permission from [3], ©2016 IEEE

## 5.2 Experiment 2: Package

The proposed algorithm is applied on an interconnect test case, commonly found in signal and power integrity applications, package.

### 5.2.1 Setup

The size of package [4] is  $0.2'' \times 0.6''$ . It has two signal transmission interconnects with four ports, as shown in Figure 5.7. Signal path includes the wire bonds and on-package interconnect and solder balls.

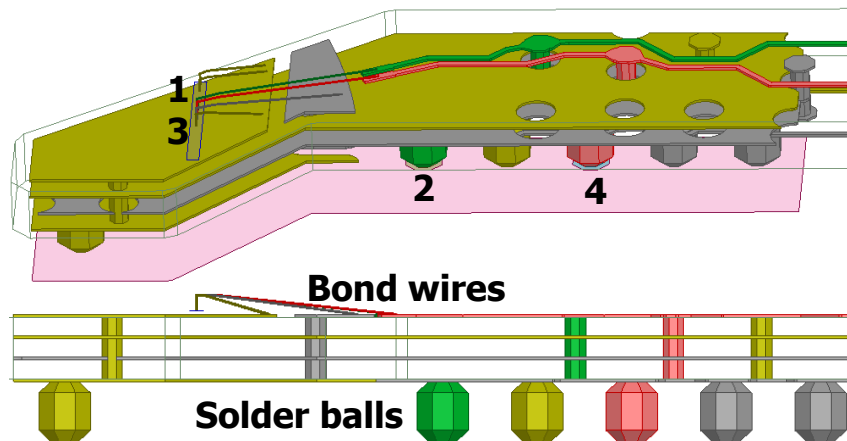
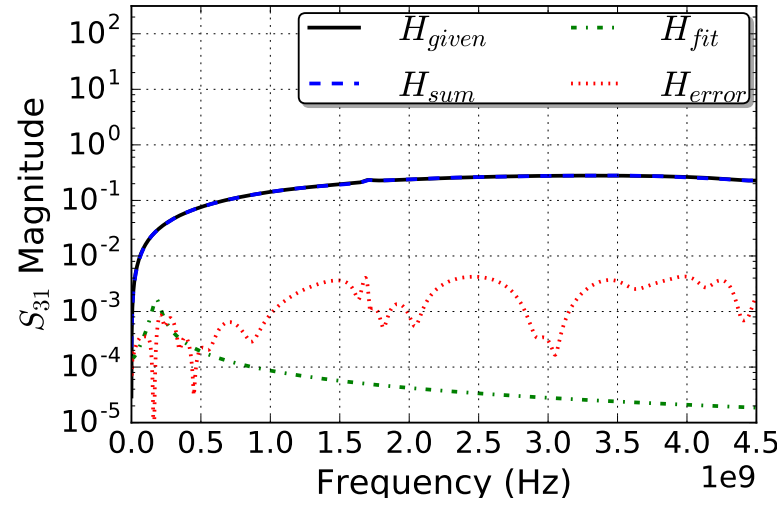


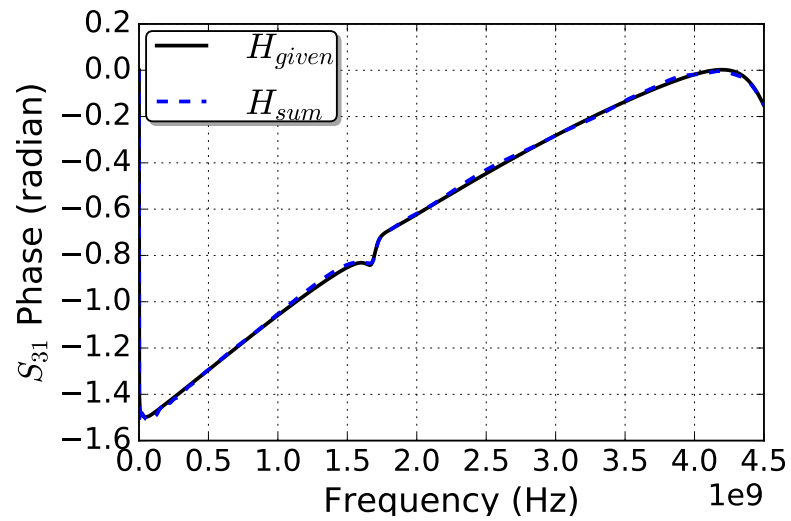
Figure 5.7: Package [4]  $0.2'' \times 0.6''$  with 4 ports size. Permission from [3], ©2016 IEEE

### 5.2.2 Validation of PRESS

The results of fitting on insertion loss  $S_{21}$ , crosstalk  $S_{31}$ ,  $S_{41}$  and return loss  $S_{11}$  of the package respectively are shown Figures 5.8-5.11.

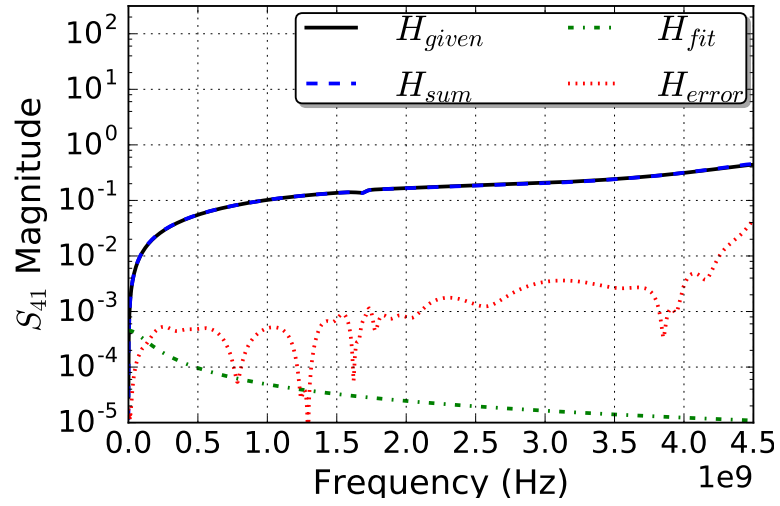


(a)

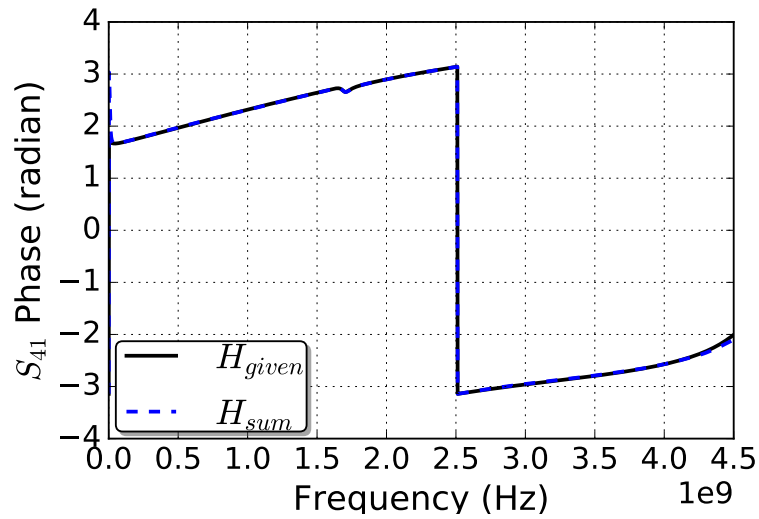


(b)

Figure 5.8: Fitting of Package near-end crosstalk after 50<sup>th</sup> iteration: (a) *Magnitude* & (b) *Phase*. Permission from [3], ©2016 IEEE

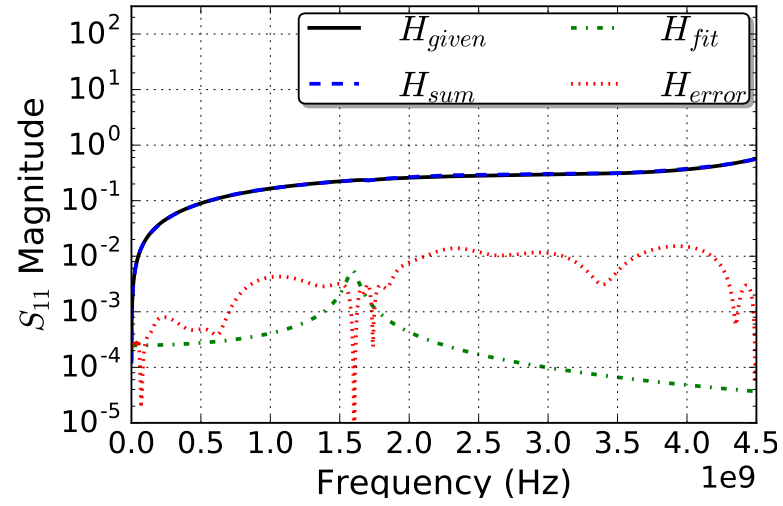


(a)

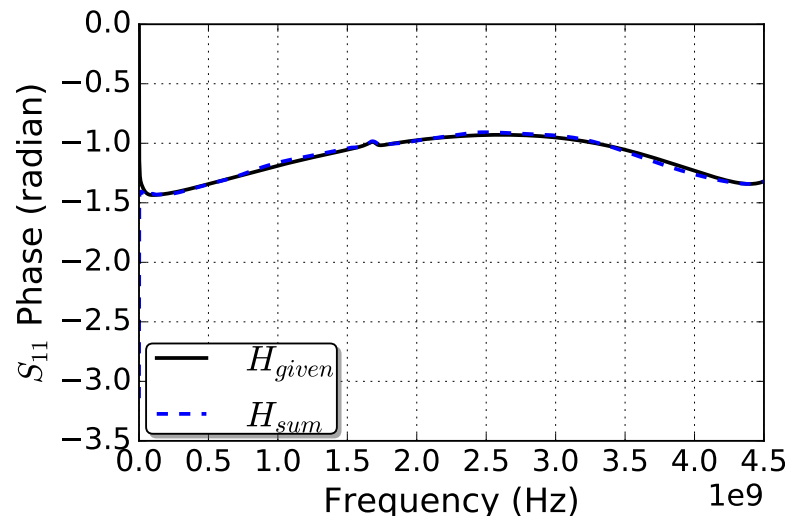


(b)

Figure 5.9: Fitting of Package far-end crosstalk after 50<sup>th</sup> iteration: (a) *Magnitude* & (b) *Phase*. Permission from [3], ©2016 IEEE

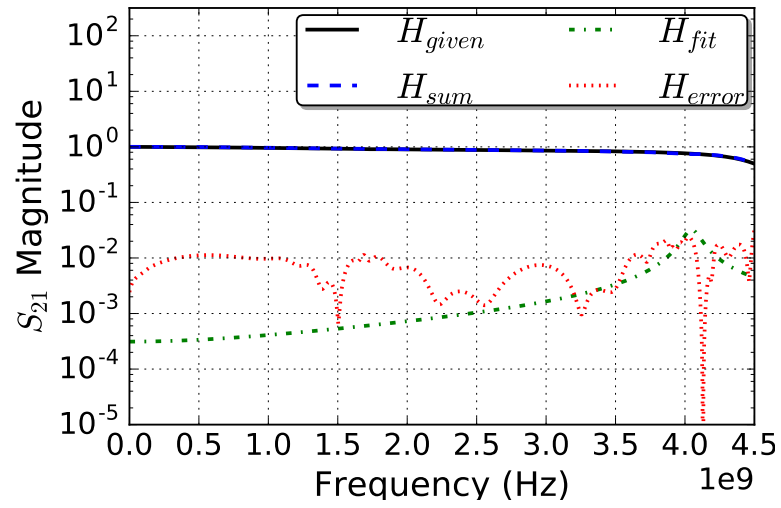


(a)

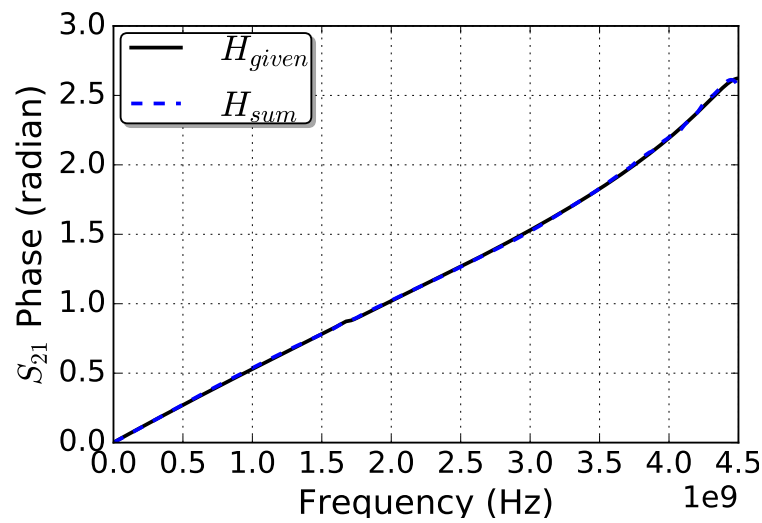


(b)

Figure 5.10: Fitting of Package return loss after 50<sup>th</sup> iteration: (a) *Magnitude* & (b) *Phase*.



(a)



(b)

Figure 5.11: Fitting of Package insertion loss after 50<sup>th</sup> iteration: (a) *Magnitude* & (b) *Phase*. Permission from [3], ©2016 IEEE

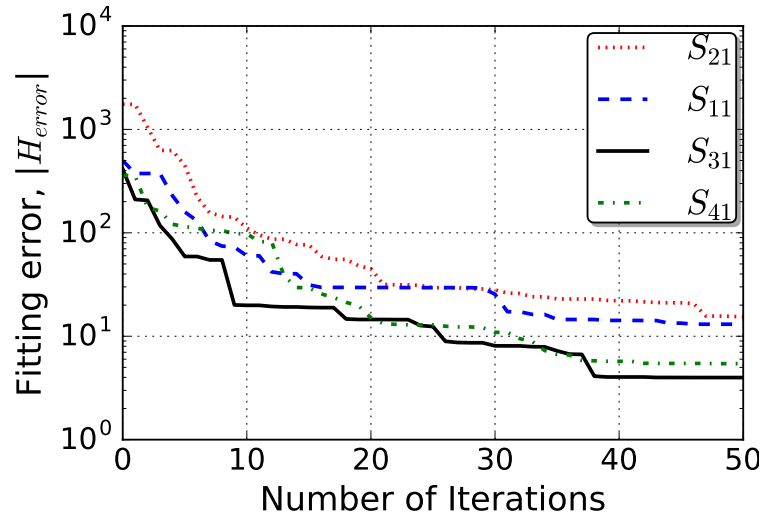


Figure 5.12: Error convergence of fitting the package over 50 iterations. Permission from [3], ©2016 IEEE

### 5.3 Experiment 3: Microstrip

The proposed algorithm is applied to interconnect structures widely used in RF and signal integrity applications: pair of microstrip transmission lines.

#### 5.3.1 Setup

A pair of microstrip transmission lines of length 2" long is considered for this experiment as shown in Figure 5.13.

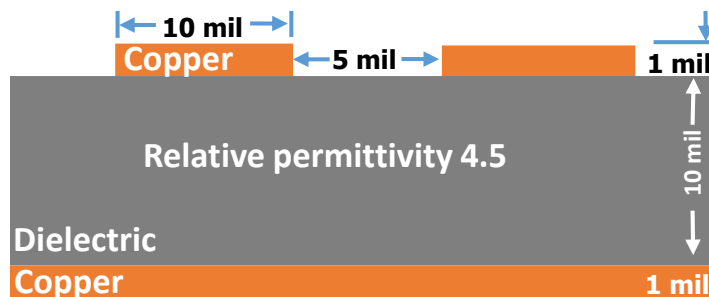
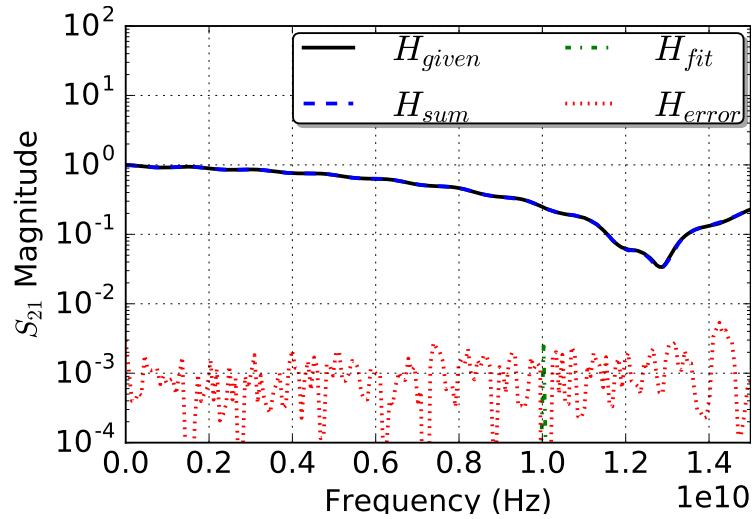


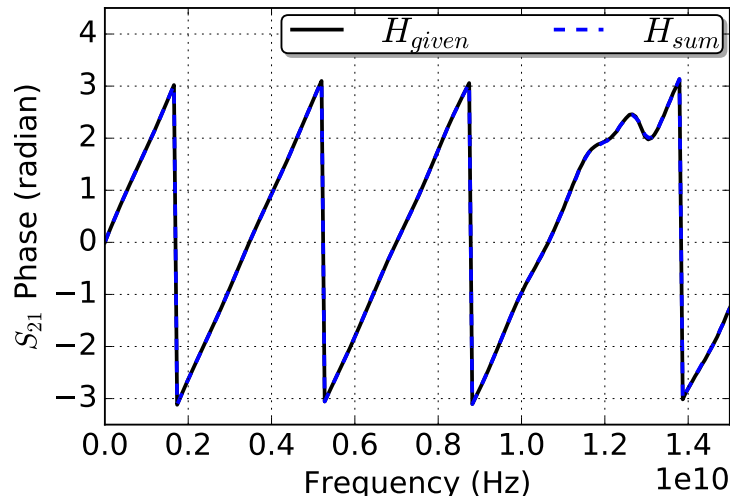
Figure 5.13: microstrip 2" long. Permission from [5], ©2016 IEEE

### 5.3.2 Validation of PRESS

Our proposed method is applied to the insertion loss  $S_{21}$ , crosstalk  $S_{31}$ ,  $S_{41}$  and return loss  $S_{11}$  of the microstrip; results are shown Figures 5.14-5.18.

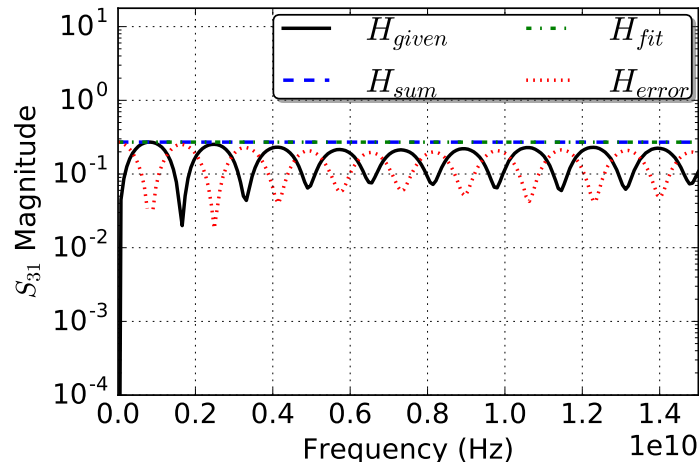


(a)

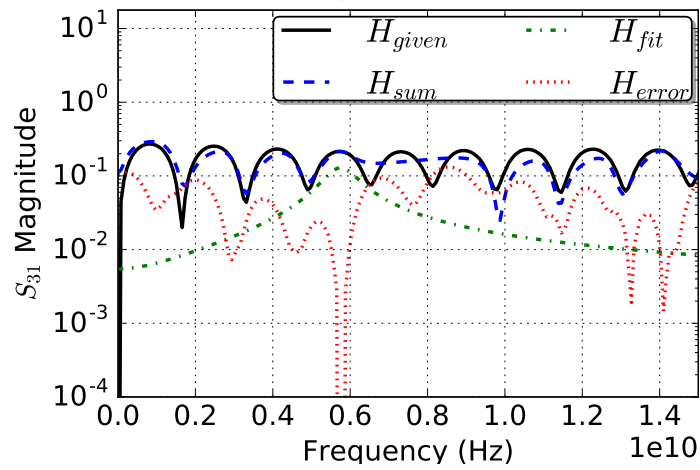


(b)

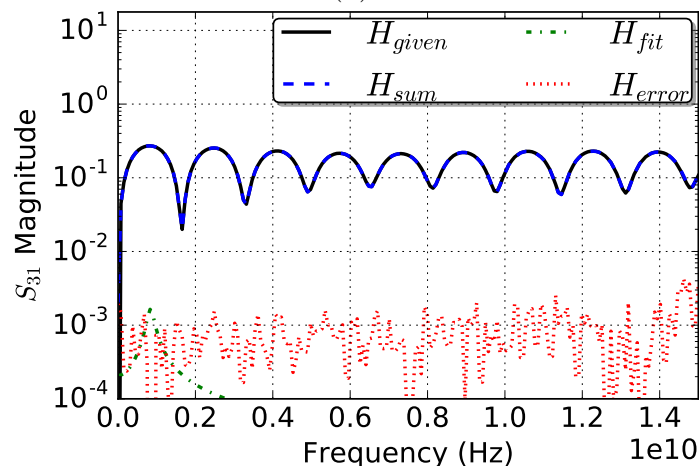
Figure 5.14: Fitting of microstrip insertion loss after 100<sup>th</sup> iteration: (a) *Magnitude* & (b) *Phase*. Permission from [5], ©2016 IEEE



(a)

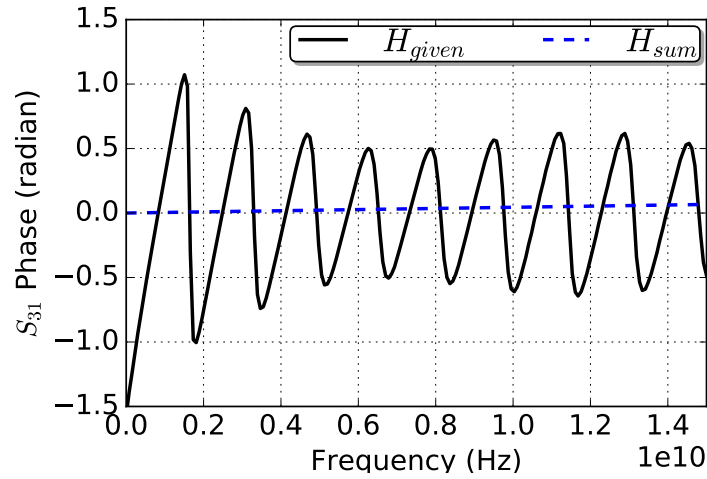


(b)

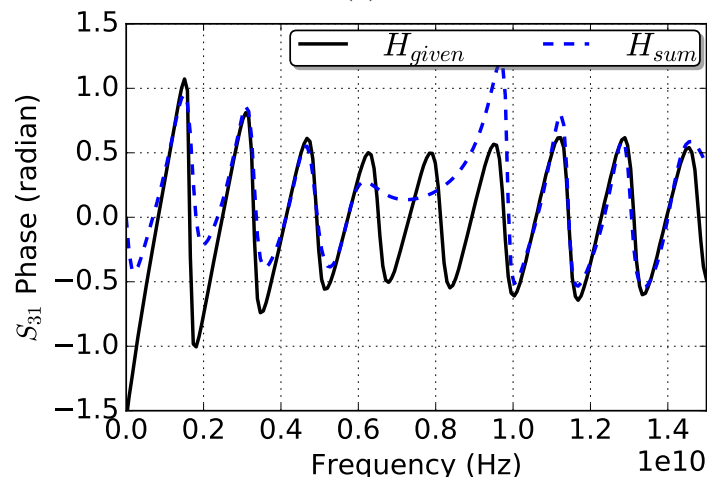


(c)

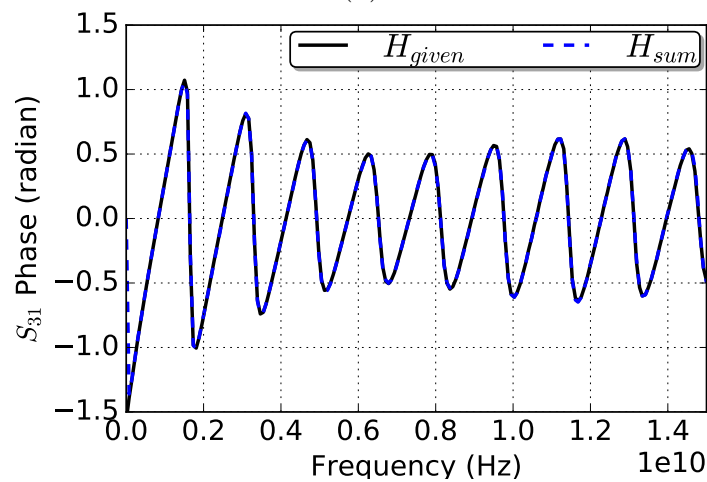
Figure 5.15: Fitting of microstrip near-end crosstalk after 100<sup>th</sup> iteration: (a) 1<sup>st</sup> (b) 10<sup>th</sup> & (c) 100<sup>th</sup>. Permission from [5], ©2016 IEEE



(a)

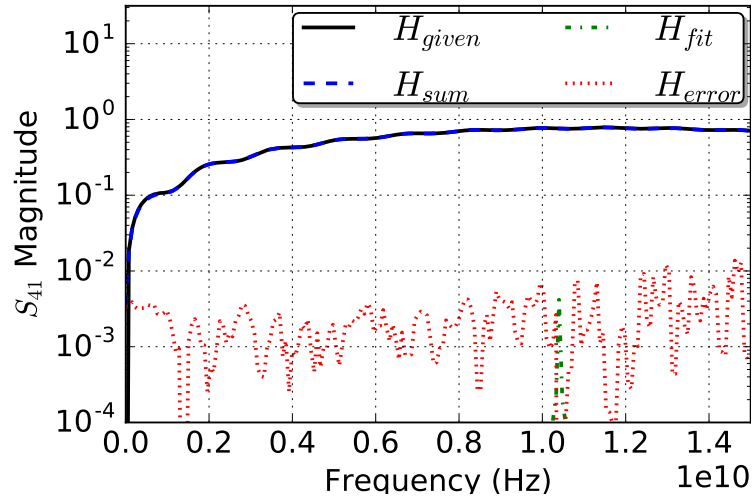


(b)

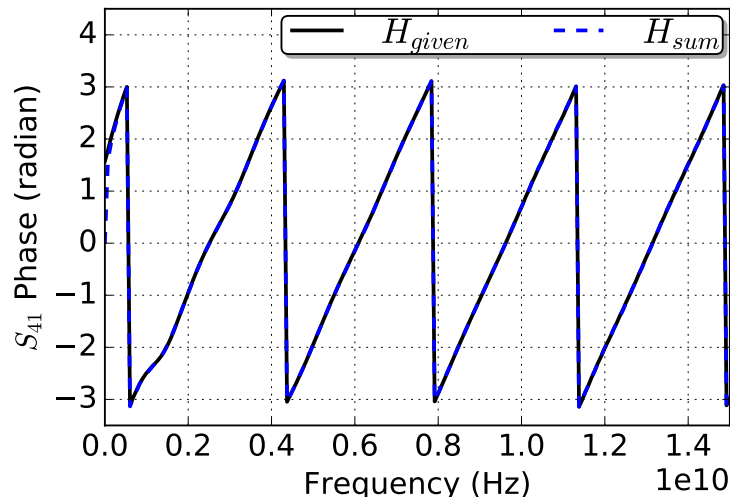


(c)

Figure 5.16: Fitting of microstrip near-end crosstalk after 100<sup>th</sup> iteration: (a) *Magnitude* & (b) *Phase*. Permission from [5], ©2016 IEEE

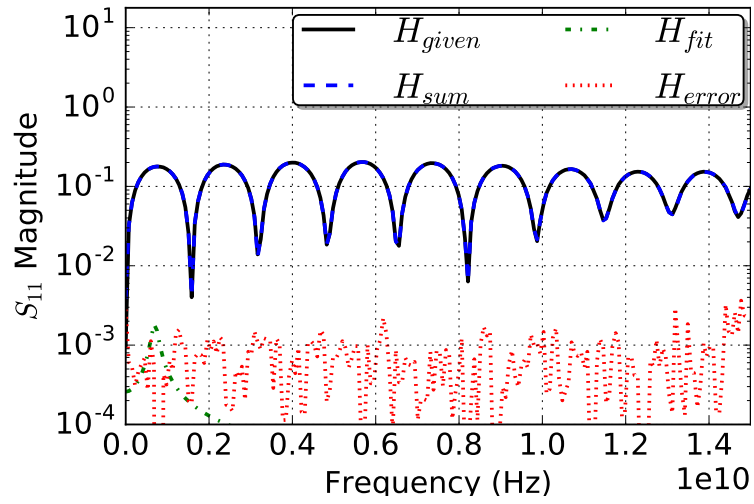


(a)

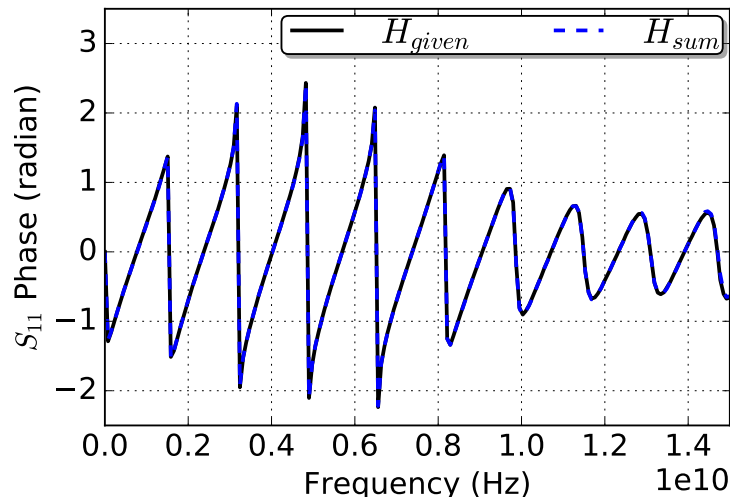


(b)

Figure 5.17: Fitting of microstrip far-end crosstalk after 100<sup>th</sup> iteration: (a) *Magnitude* & (b) *Phase*. Permission from [5], ©2016 IEEE



(a)



(b)

Figure 5.18: Fitting of microstrip return loss after 100<sup>th</sup> iteration: (a) *Magnitude* & (b) *Phase*. Permission from [5], ©2016 IEEE

## 5.4 Experiment 4: Power planes

Power planes are commonly found as power delivery networks in electronics products and analyzed by transient co-simulation [68] of signal and power interconnects for signal and power interactions or coupling.

### 5.4.1 Setup

Power planes are of size 1 inch square planes separated by dielectric. Port is placed at the via located at the center of the planes as shown in Figure 5.19.

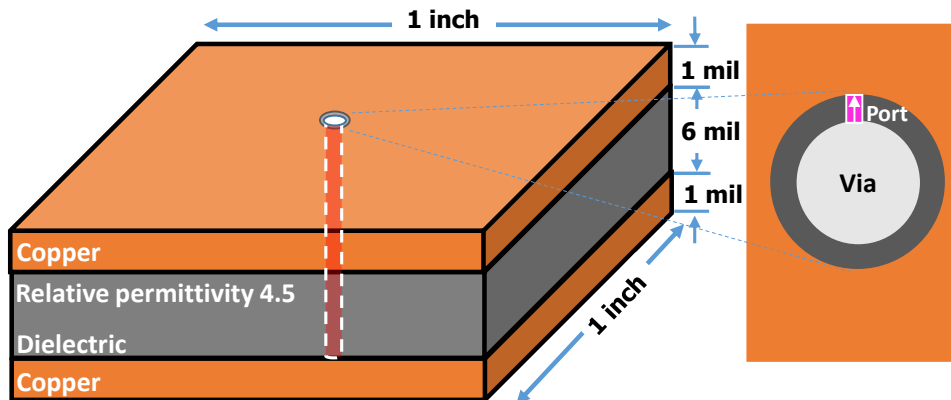
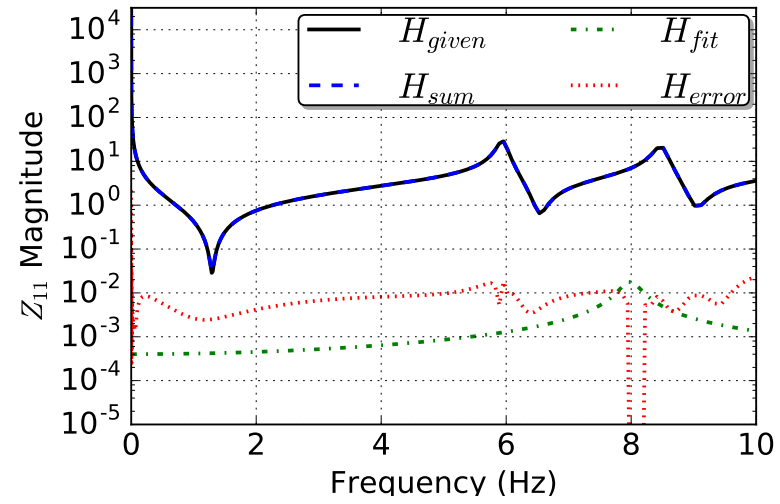


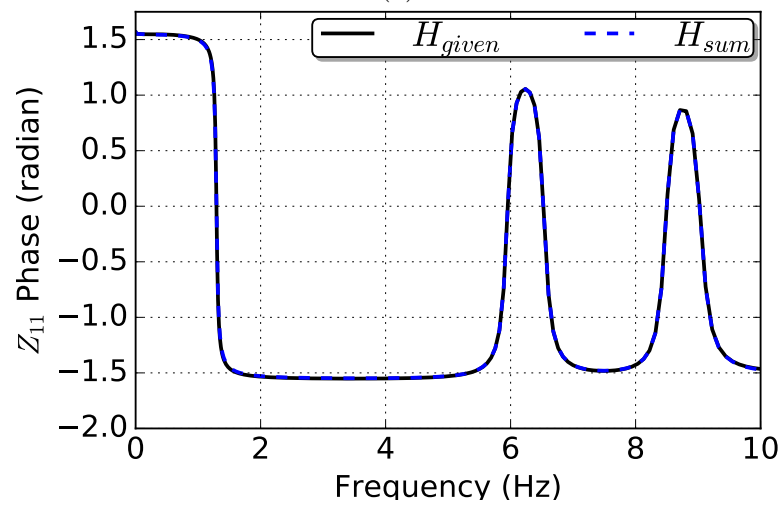
Figure 5.19: square power planes 1"  $\times$  1" with a port. Permission from [5], ©2016 IEEE

### 5.4.2 Validation of PRESS

Our proposed method is applied to the self impedance  $Z_{11}$  of power planes; results are shown Figure 5.20. Also, performance of the fitted self impedance  $Z_{11}$  profile is compared against VF method by synthesizing [65] [59] the equivalent circuits and exciting it with a 1 V step voltage of rise time 10 ns in ADS tool [67], as shown in the Figure 5.21.



(a)



(b)

Figure 5.20: Fitting power plane self-impedance after 80<sup>th</sup> iteration: (a) *Magnitude* & (b) *Phase*. Permission from [5], ©2016 IEEE

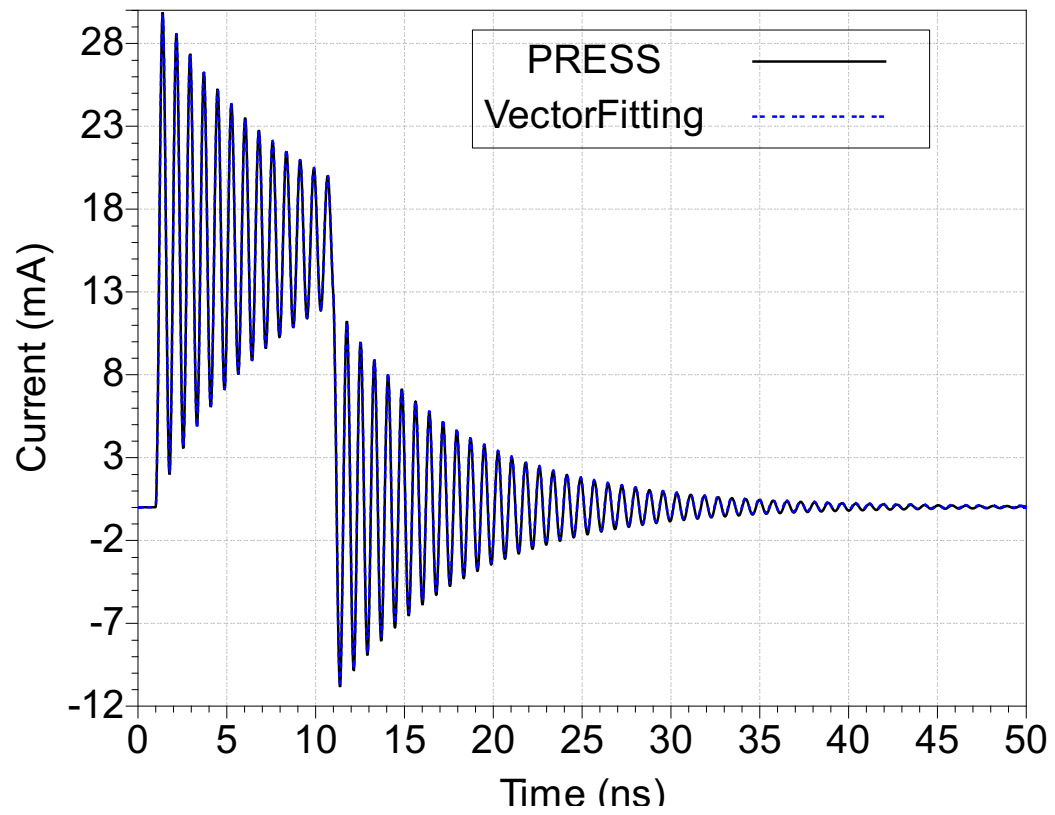


Figure 5.21: Current at the input port of power planes equivalent circuit excited by step. PRESS after 20 iterations is compared with 10<sup>th</sup> order VF. Permission from [5], ©2016 IEEE

## 5.5 Experiment 5: Package

The proposed fitting and multi-port synthesis algorithm is applied on a test case - package, a critical interconnect in high speed serial applications.

### 5.5.1 Setup

Package [6] of size  $1.36'' \times 1.36''$  with power planes and signal transmission lines with port placements is shown in Figure 5.22. Using this interconnects' frequency response, multitude of fitting algorithms proposed in the Chapter 2 are compared.

### 5.5.2 Validation of COMPRESS

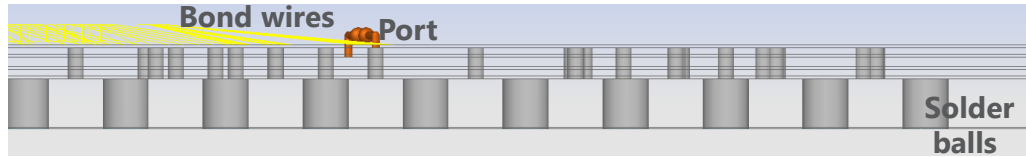
The proposed adaptive subset width based local fitting technique is applied on the package power planes and signal lines as shown in Figures 5.23 - 5.25. Also, the performance of proposed method, COMPRESS, is compared against the original PRESS [5] fitted model in Figures 5.26a, 5.26b and 5.26c.

### 5.5.3 Validation of EMPRESS

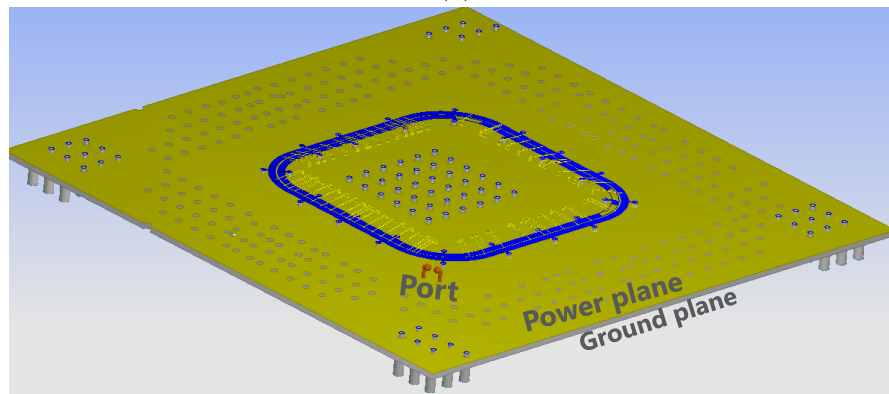
The performance of proposed method is compared against the original PRESS [5] fitted model for self-admittance  $Y_{11}$ , insertion losses-  $S_{13}$  and  $S_{24}$  in Figures 5.27a, 5.27b and 5.27c respectively.

### 5.5.4 Validation of OPPRESS

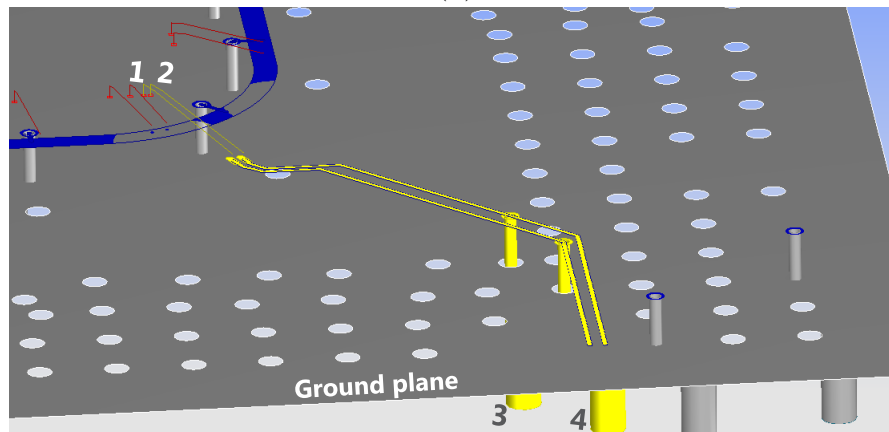
The performance of proposed improved fitting method, OPPRESS, is compared against the original PRESS [5] fitted model for self-admittance  $Y_{11}$ , insertion losses-  $S_{13}$  and  $S_{24}$  in Figures 5.28a, 5.28b and 5.28c respectively. Also, the computational complexity comparison in terms of computation time, taken on a computer with Intel Core i7 5600U CPU @ 2.6GHz



(a)

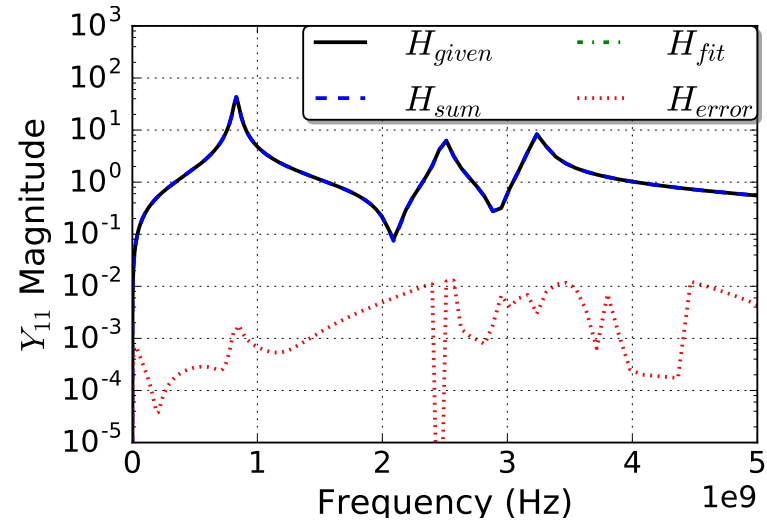


(b)

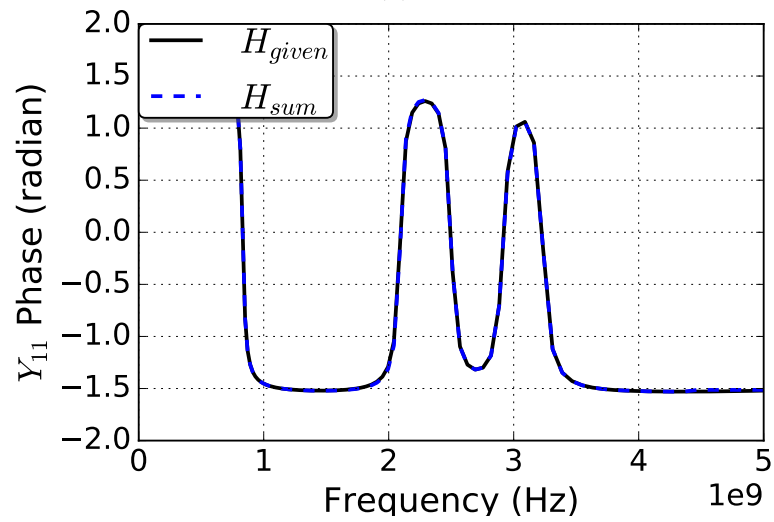


(c)

Figure 5.22: Setup: package [6] (a) cross-section (b) planes 1.36''  $\times$  1.36'' size (c) signal transmission lines. Permission from [7], ©2016 IEEE

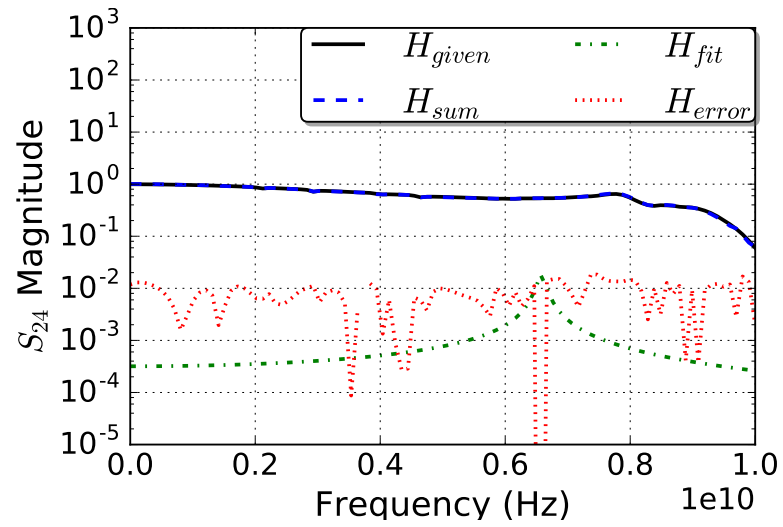


(a)

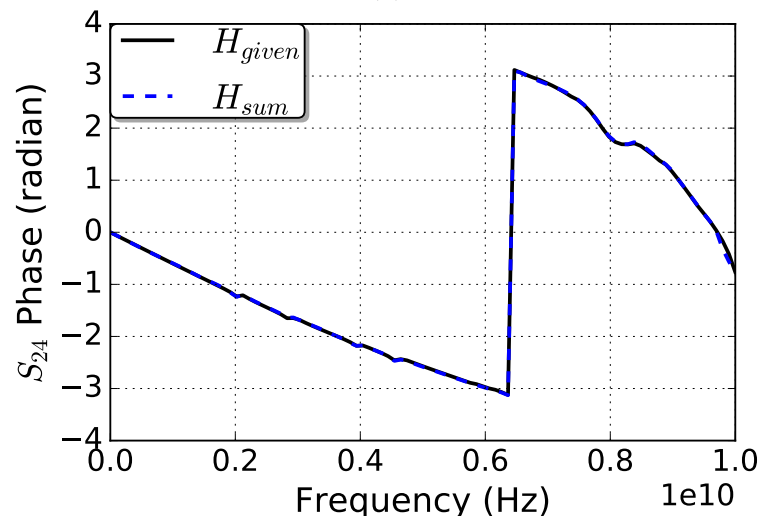


(b)

Figure 5.23: COMPRESS fitting of power planes admittance after 30<sup>th</sup> iteration: (a) Magnitude & (b) Phase. Permission from [7], ©2016 IEEE

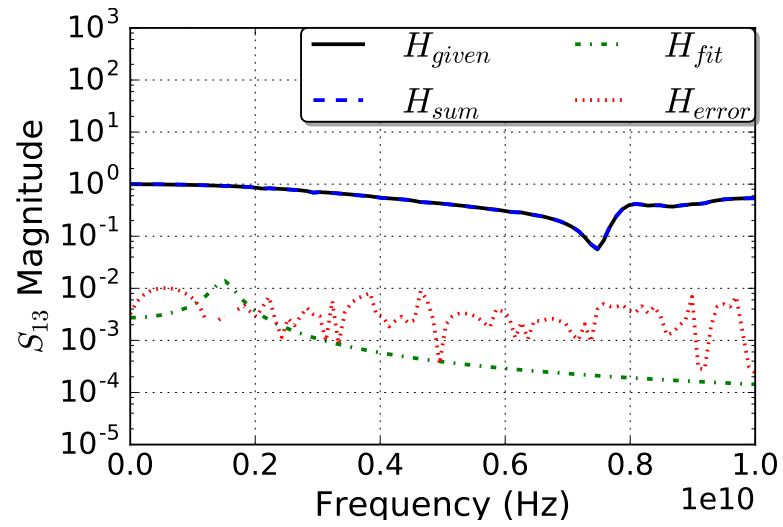


(a)

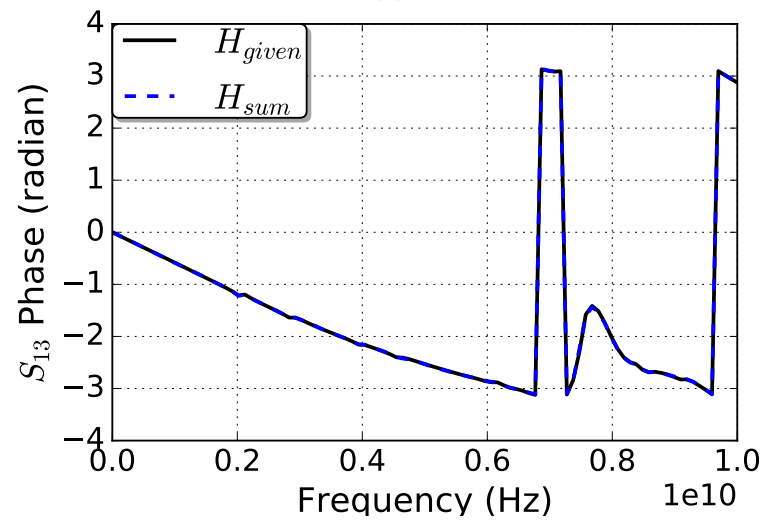


(b)

Figure 5.24: COMPRESS fitting of signal insertion loss  $S_{24}$  after 30<sup>th</sup> iteration: (a) Magnitude & (b) Phase. Permission from [7], ©2016 IEEE

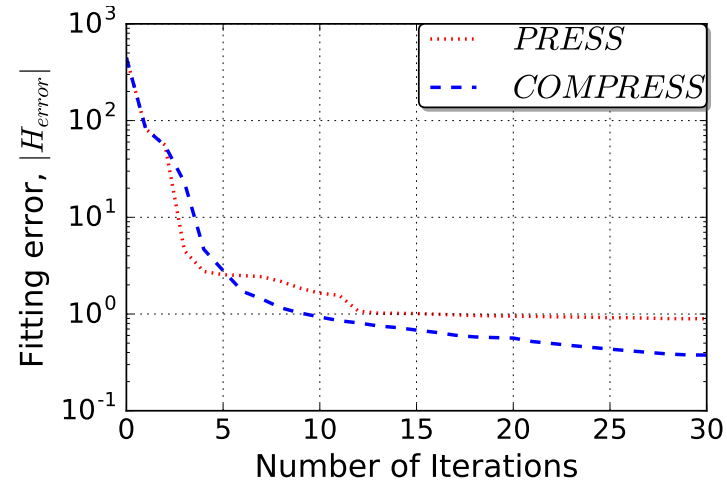


(a)

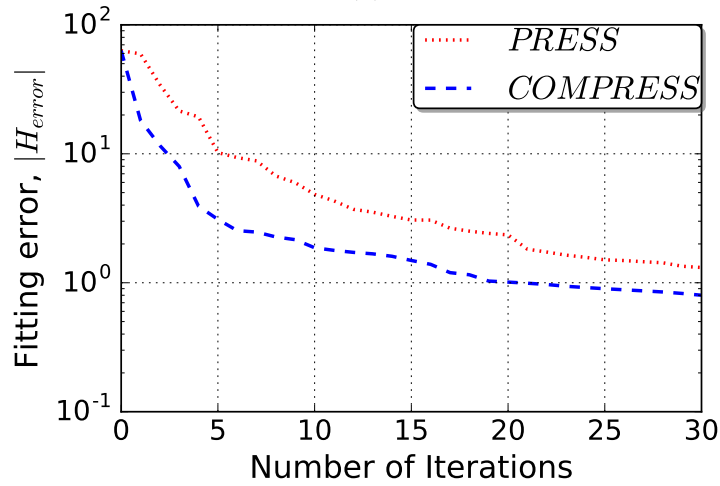


(b)

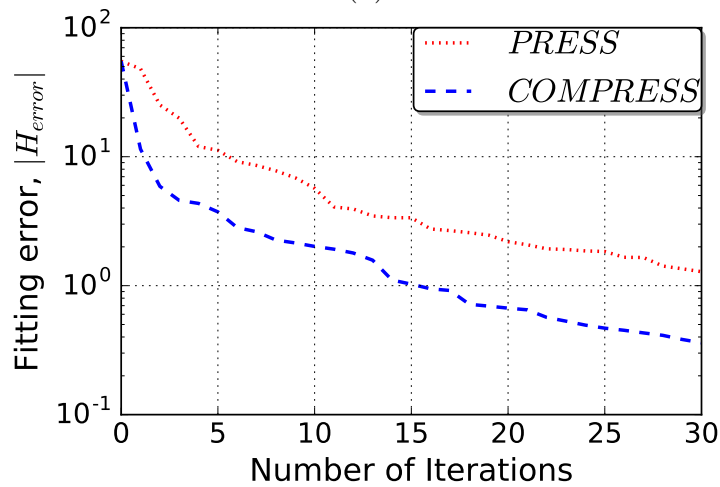
Figure 5.25: COMPRESS fitting of signal insertion loss  $S_{13}$  after 30<sup>th</sup> iteration: (a) Magnitude & (b) Phase. Permission from [7], ©2016 IEEE



(a)

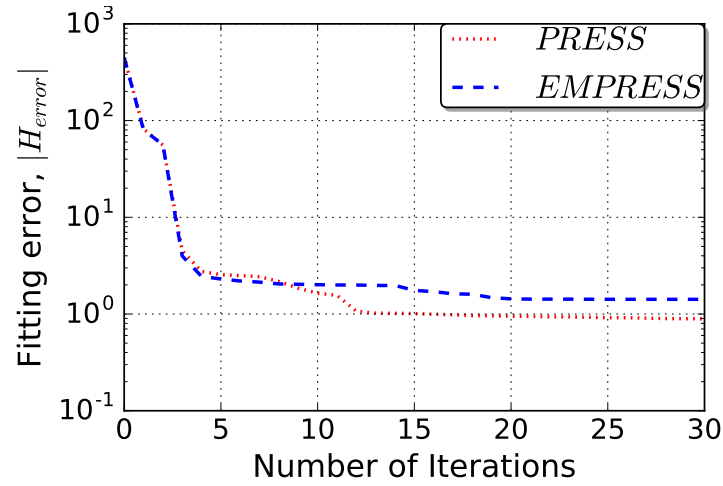


(b)

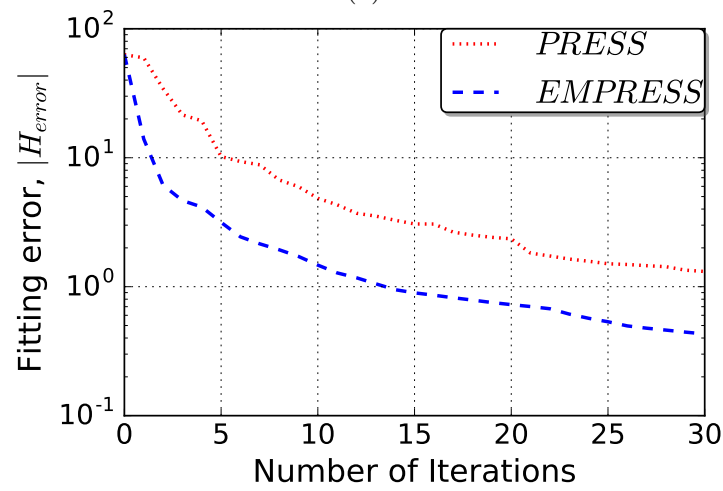


(c)

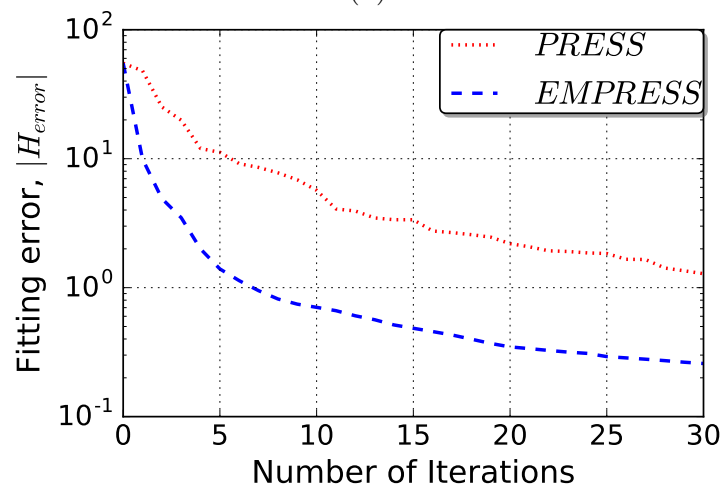
Figure 5.26: Error convergence of *PRESS* vs *COMPRESS* over 30 iterations: (a) self-admittance  $Y_{11}$ , insertion losses (b)  $S_{24}$  & (c)  $S_{13}$ . Permission from [7], ©2016 IEEE



(a)



(b)



(c)

Figure 5.27: Error convergence of *PRESS* vs *EMPRESS* over 30 iterations: (a) self-admittance  $Y_{11}$ , insertion losses (b)  $S_{24}$  & (c)  $S_{13}$

and 12 GB RAM, in seconds and milliseconds, is in Tables 5.1 and 5.2. Note that the PRESS computation time in the Table 5.2 covers only a single calculation of the three fit types.

Table 5.1: Comparison of fitting algorithms' computation time for 10 iterations.

Model size, N	$t_{PRESS}$ (s)	$t_{COPRESS}$ (s)	$t_{EMPRESS}$ (s)	$t_{OPRESS}$ (s)
100	14	25	16	13.6
200	13.9	106	18	15.5

Table 5.2: Comparison [1] of PRESS and Vector Fitting algorithms' computation time.

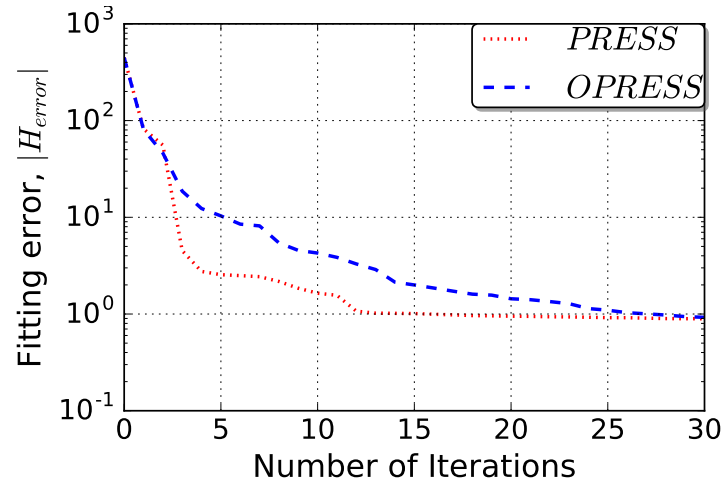
Model size, N	$t_{VF}$ (ms)	$t_{PRESS}$ (ms)
100	5	3
500	13	3
1000	16	3
5000	32	3
10000	57	3
50000	340	3

### 5.5.5 MOR by SPA

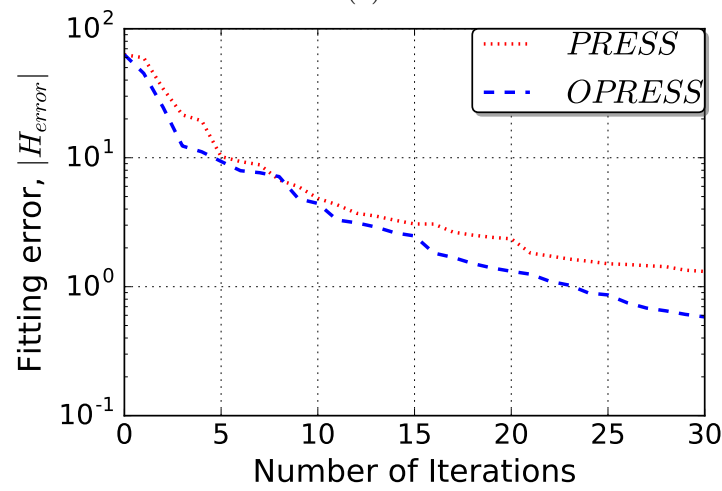
The proposed SPA based model order reduction technique is applied on the interconnect, power planes on package [6] shown in Figure 5.22. The results of PRESS [5] fitting on its self-admittance  $Y_{11}$  is shown in Figure 5.29. Based on the Hankel values in Figure 5.31, the model order is reduced [69] from 60 to 15. The performance of reduced model is compared against the original PRESS fitted model in Figure 5.32.

### 5.5.6 Validation of Indirect synthesis

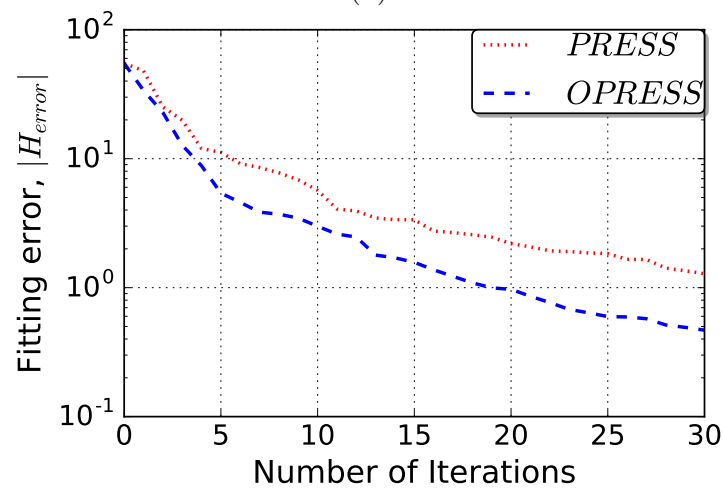
Post model order reduction, the state space is synthesized using the indirect method. Performance of the synthesized equivalent network in terms of its magnitude and phase are compared with the given response in Figure 5.33.



(a)

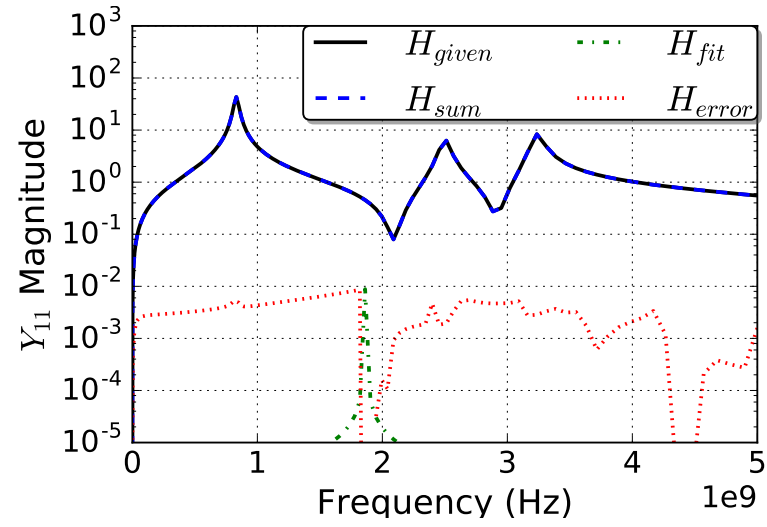


(b)

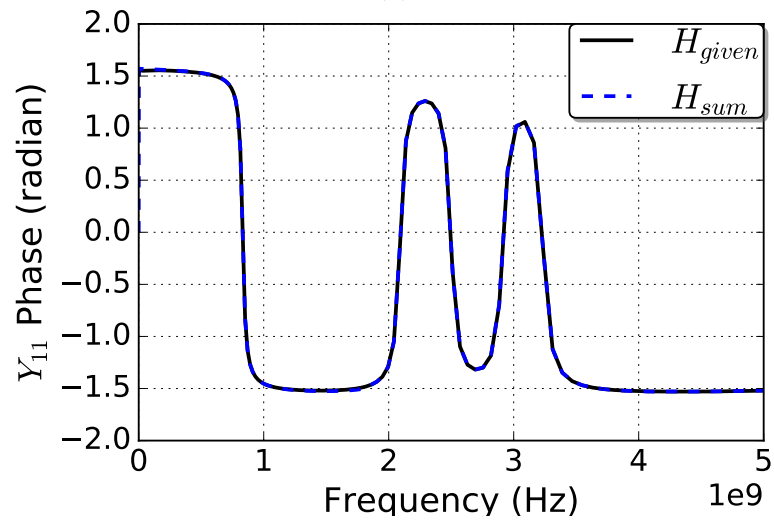


(c)

Figure 5.28: Error convergence of PRESS vs OPPRESS over 30 iterations: (a) self-admittance  $Y_{11}$ , insertion losses (b)  $S_{24}$  & (c)  $S_{13}$



(a)



(b)

Figure 5.29: Fitting of power planes admittance after 30<sup>th</sup> iteration: (a) *Magnitude* & (b) *Phase*.

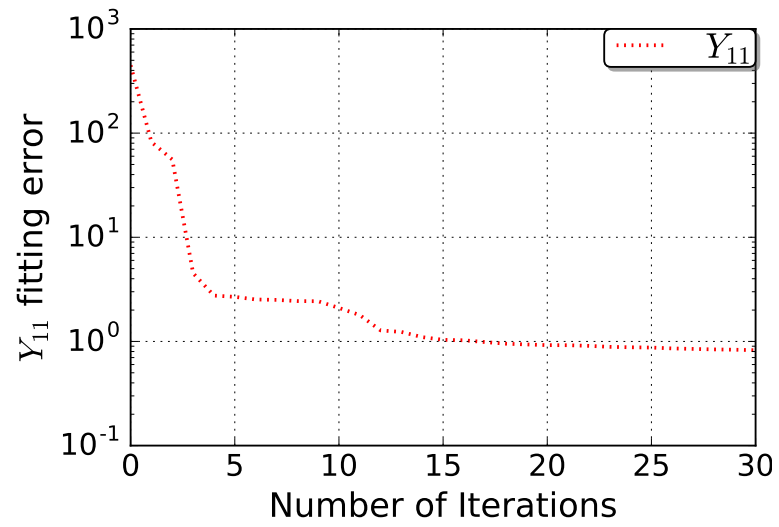


Figure 5.30: Error convergence of fit of the admittance over 30 iterations.

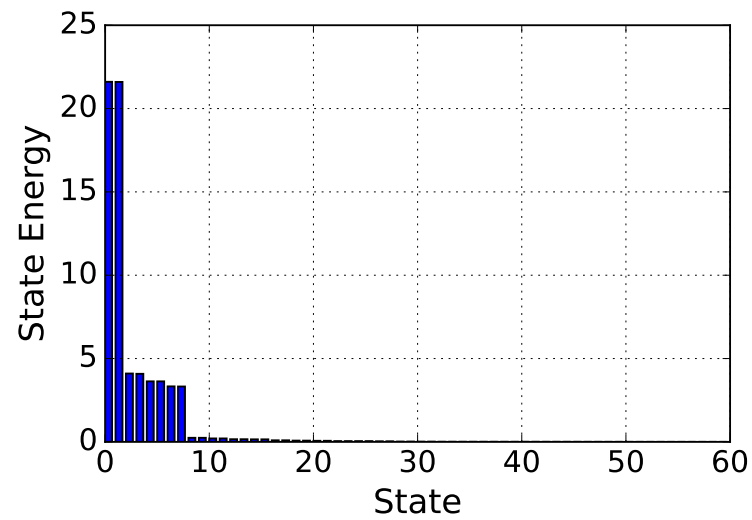
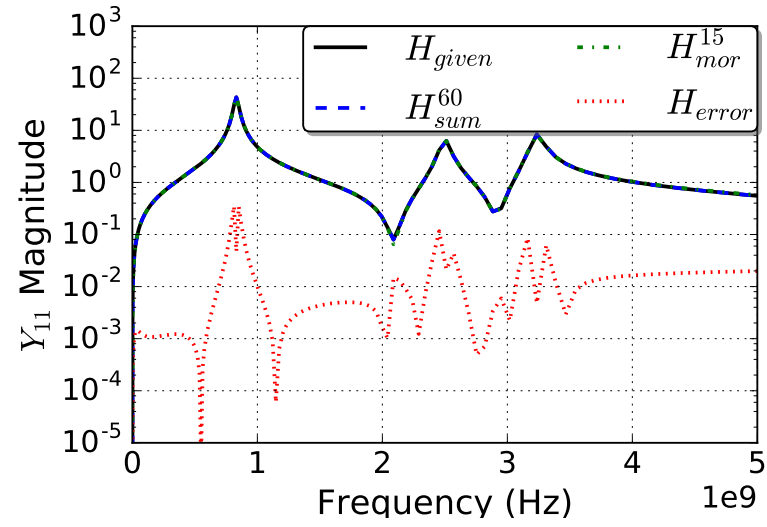
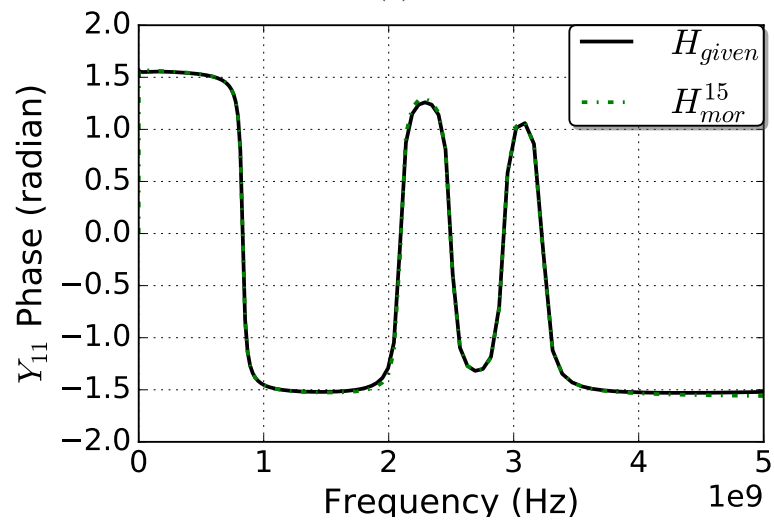


Figure 5.31: Hankel singular values of fit of the admittance over 30 iterations.

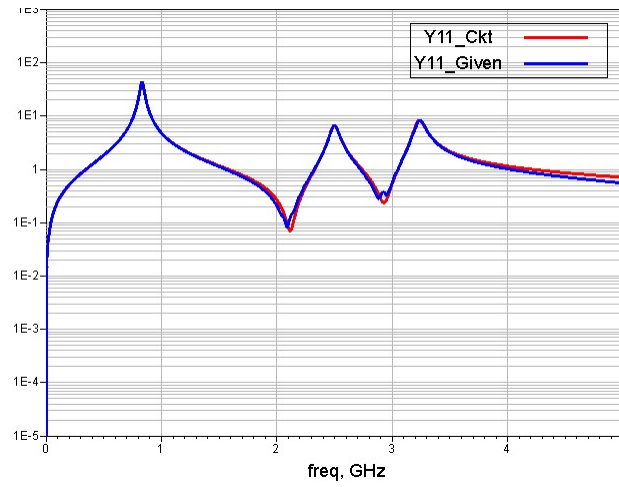


(a)

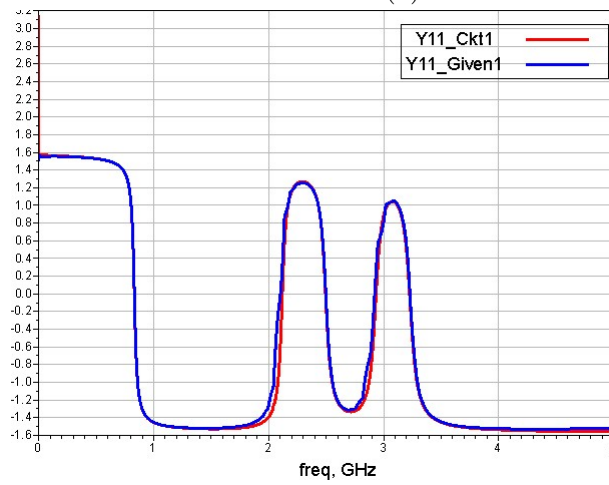


(b)

Figure 5.32: Model order reduction of fit of admittance: (a) *Magnitude* & (b) *Phase*.



(a)



(b)

Figure 5.33: Comparison of the Package power plane's return loss with that of the synthesized circuit: (a) *Magnitude* & (b) *Phase*.

## 5.6 Experiment 6: Broadband antenna

Antenna, often modeled in frequency domain, can be considered as an interconnect and co-simulated for system level analysis by using its macromodel.

### 5.6.1 Setup

The proposed algorithm is applied on a antenna test case - coax fed quarter wave patch antenna [8], a common antenna for high frequency applications, as shown in Figure 5.34.

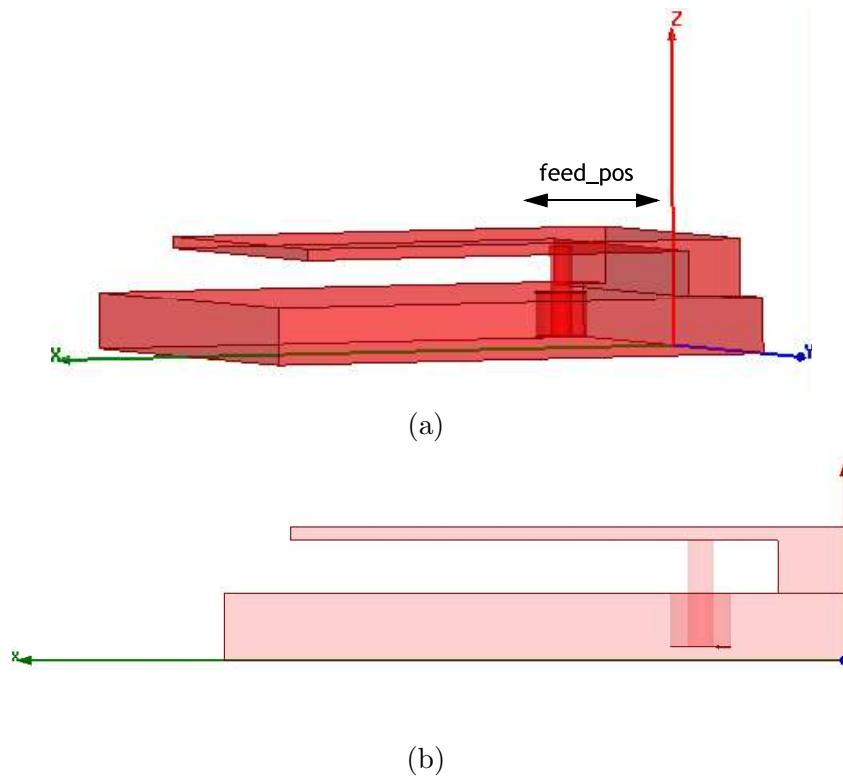
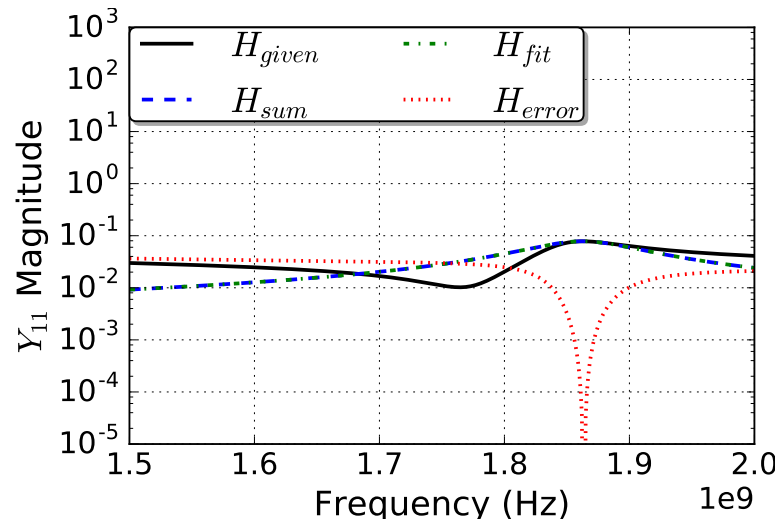


Figure 5.34: Setup - coax fed patch antenna [8]  $40 \times 30\text{mm}$  size with feed position of 10.8 mm : (a) top view (b) side view, port placement at feed

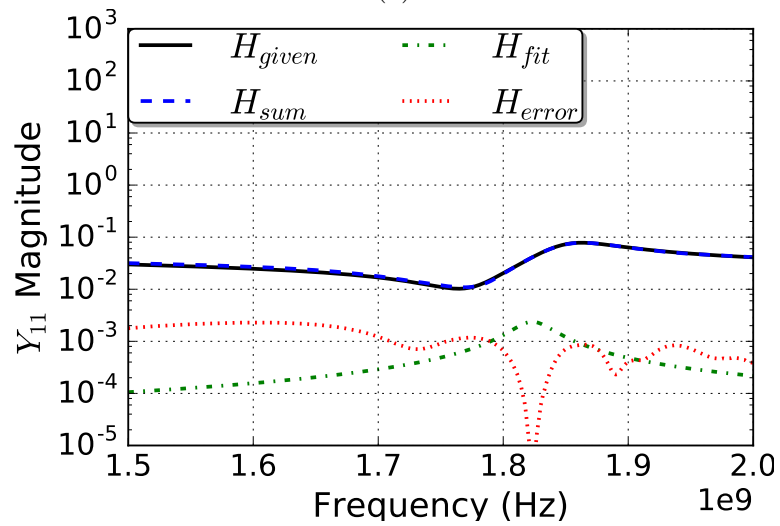
### 5.6.2 Validation of Synthesis

Fitting results of transformed admittance parameters - self admittance  $Y'_{11}$  - are shown Figures 5.35-5.36. Performance of the synthesized equivalent network is compared with the

given antenna in Figure 5.38.

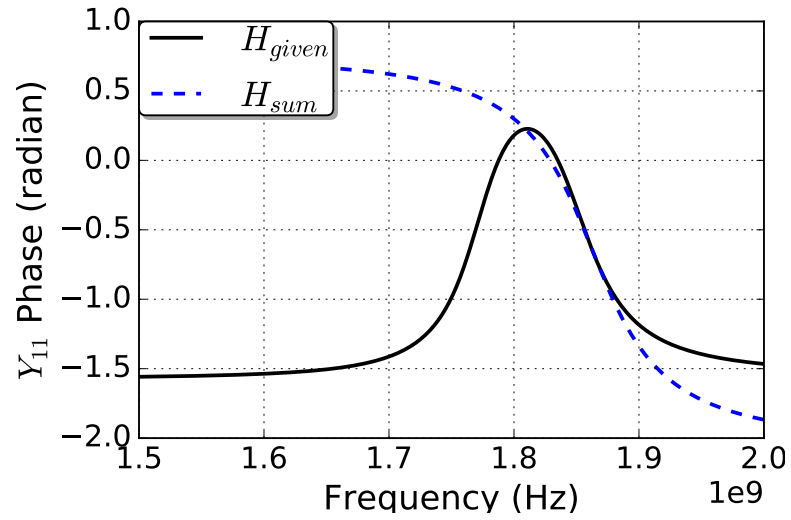


(a)

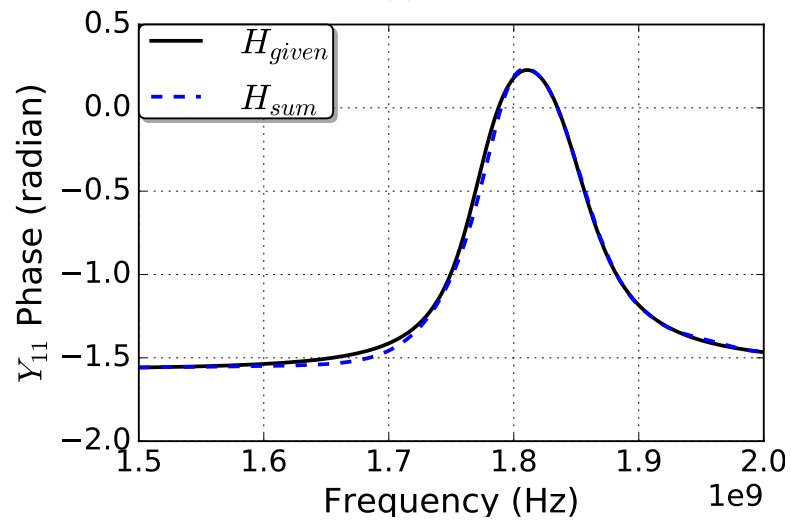


(b)

Figure 5.35: Fitting on the patch antenna  $Y'_{11}$  after iterations: (a) 1<sup>st</sup> & (b) 10<sup>th</sup> .



(a)



(b)

Figure 5.36: Fitting on the patch antenna  $Y'_{11}$  after iterations: (a) 1<sup>st</sup> & (b) 10<sup>th</sup>.

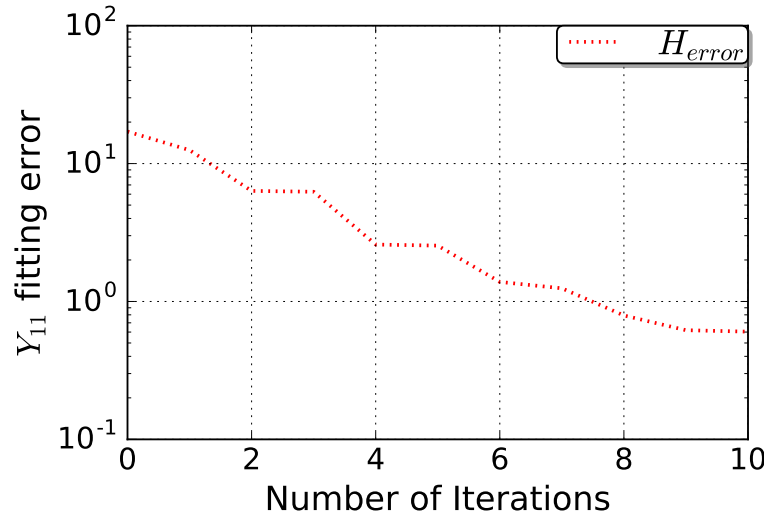


Figure 5.37: Convergence of magnitude of fitting error over 10 iterations.

## 5.7 Experiment 7: Power planes with 3 ports

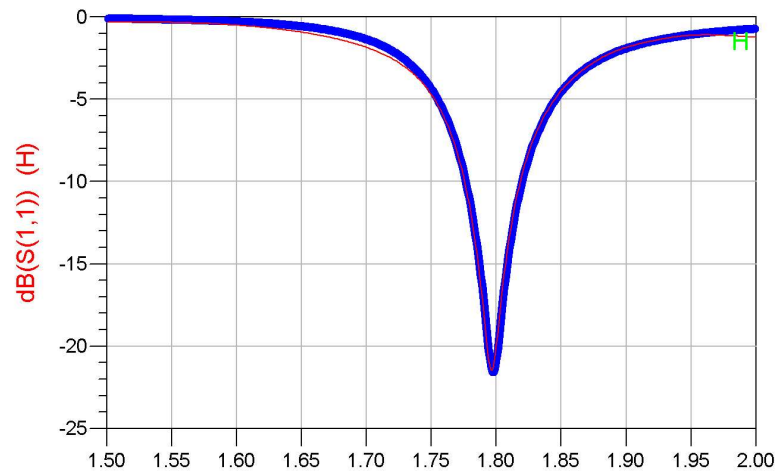
Multi-port interconnect, power planes with multiple vias, is considered in this section to validate the process of multi-port synthesis flow given in the Sections 4.1.1 and 4.1.2.

### 5.7.1 Setup

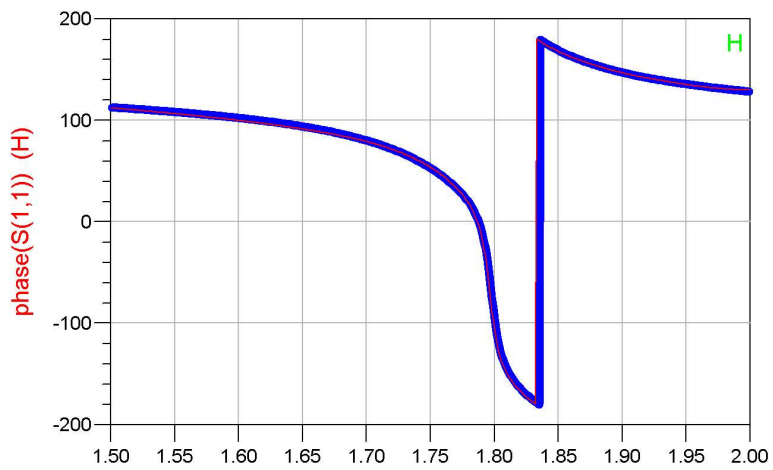
The proposed algorithm is applied on a three port test case - pair of power planes with three vias, a common power delivery interconnect, as shown in Figure 5.39.

### 5.7.2 Validation of Direct Synthesis

Fitting results of transformed admittance parameters - transfer admittance  $Y'_{32}$ ,  $Y'_{31}$  and  $Y'_{21}$ ; and self admittance  $Y'_{33}$ ,  $Y'_{22}$  and  $Y'_{11}$  respectively - are shown Figures 5.40-5.46. Performance of the synthesized equivalent network is compared with the given three port power planes in Figure 5.48.



(a)



(b)

Figure 5.38: Comparison of the antenna's return loss with that of the synthesized circuit: (a) *Magnitude* & (b) *Phase*.

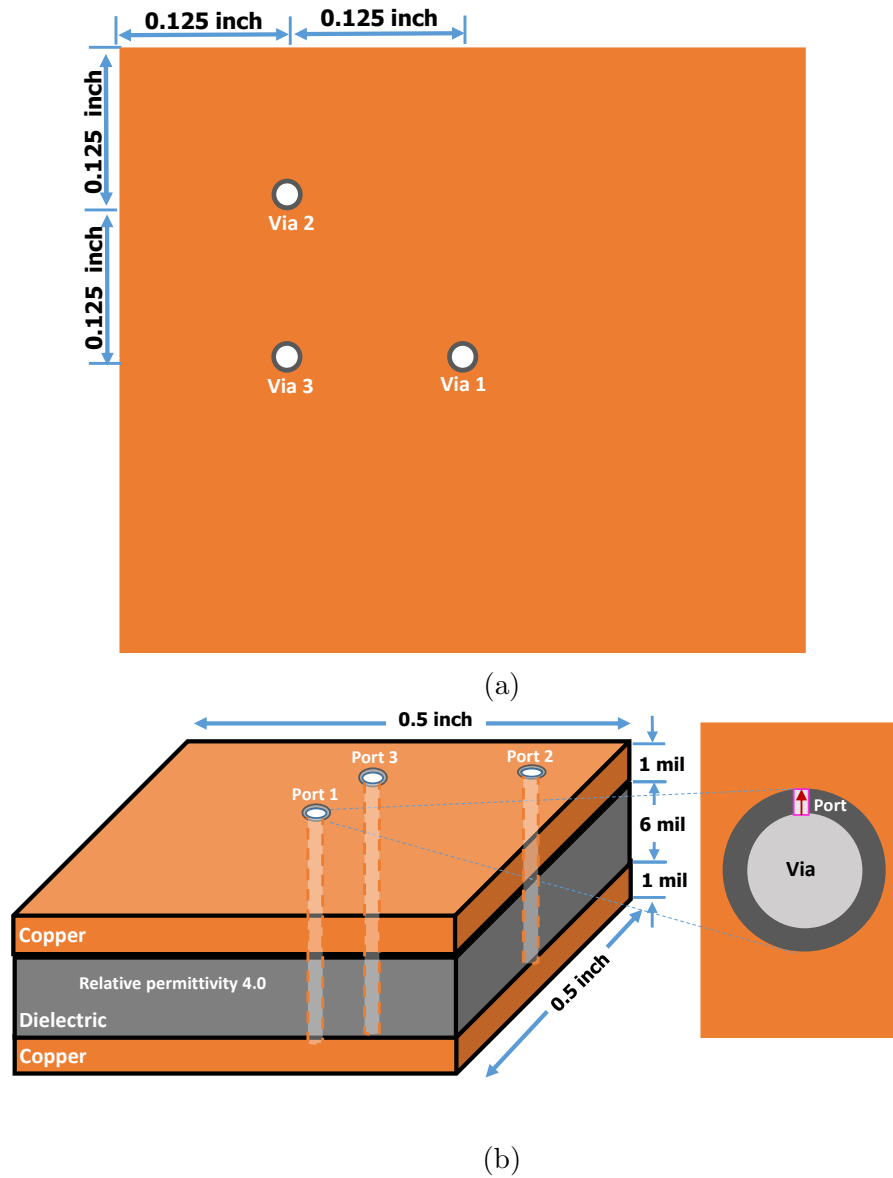
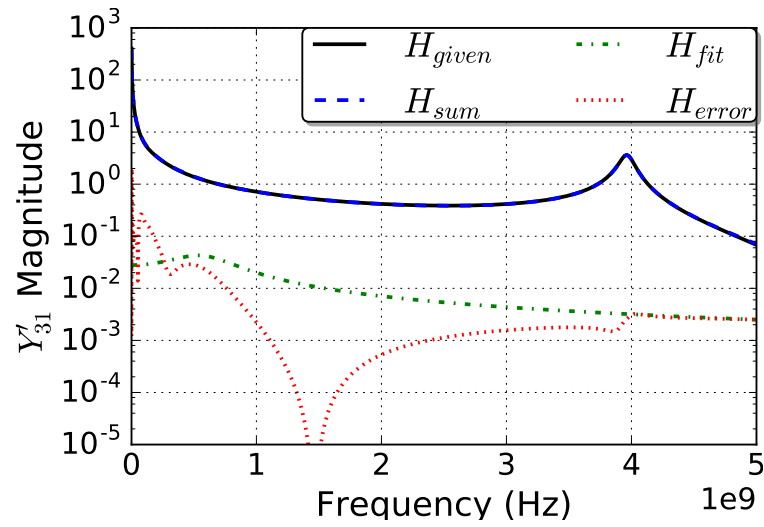
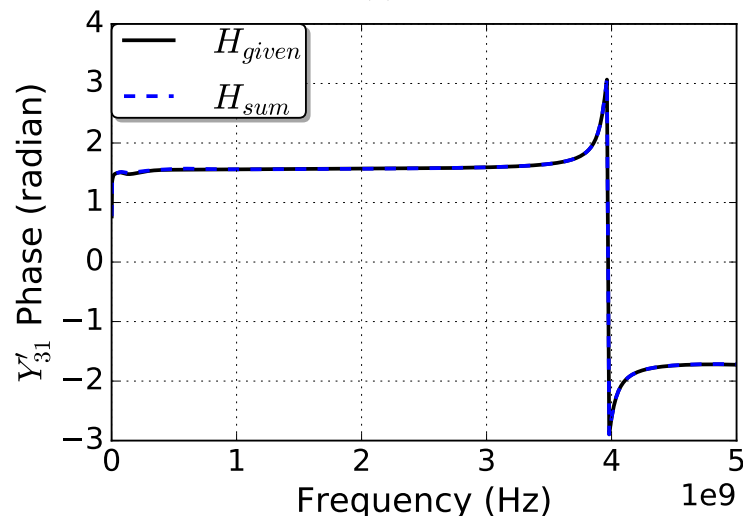


Figure 5.39: Setup - power planes  $0.5'' \times 0.5''$  size with three vias : (a) top view, vias at  $.25''$  and  $.125''$  (b) side view, port placement for each via. Permission from [2], ©2016 IEEE



(a)



(b)

Figure 5.40: Fitting of power planes  $Y'_{31}$  after  $20^{th}$  iteration: (a) *Magnitude* & (b) *Phase*.  
 Permission from [2], ©2016 IEEE

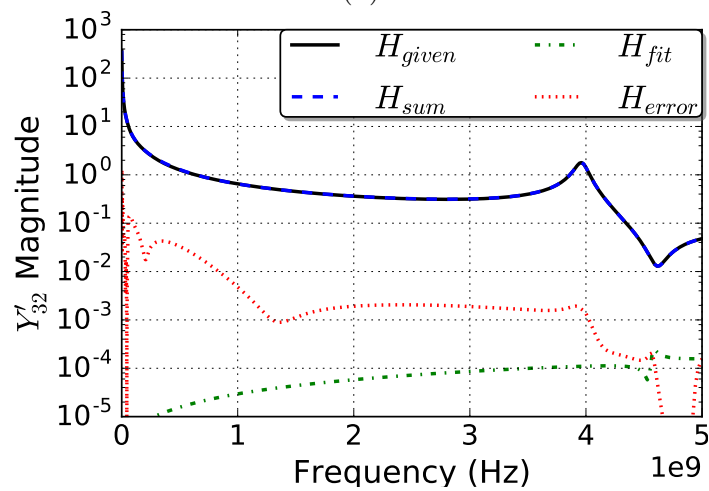
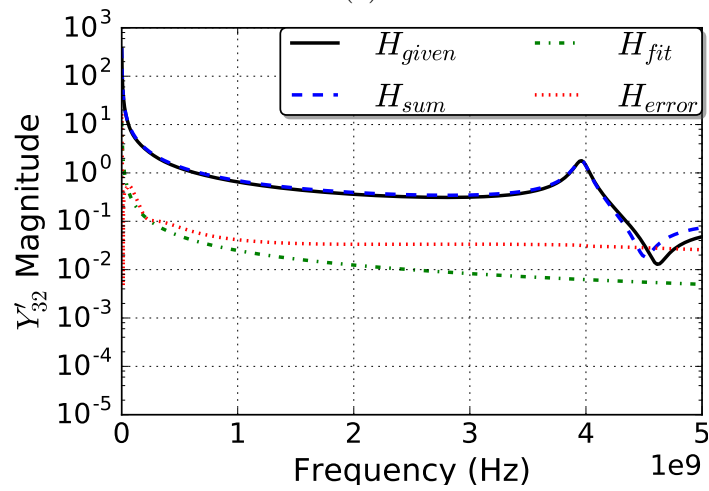
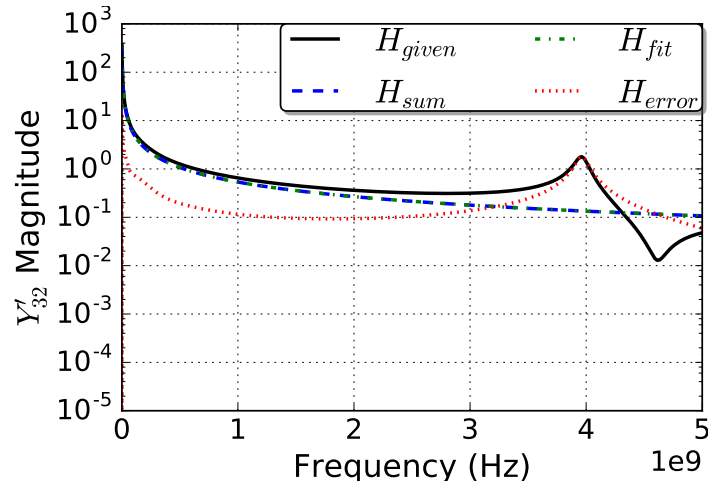
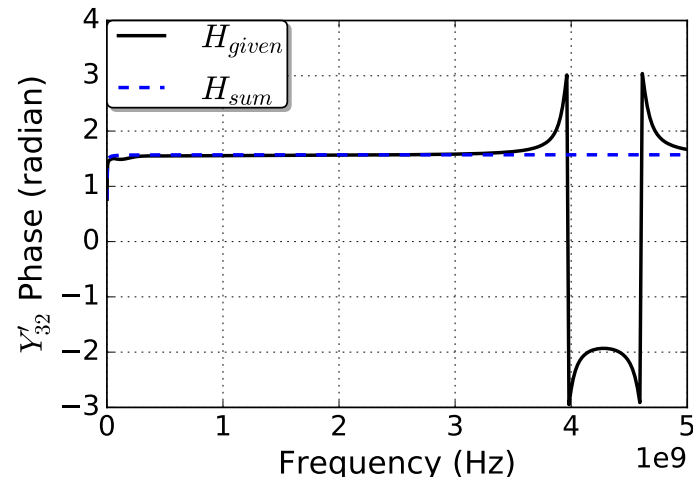
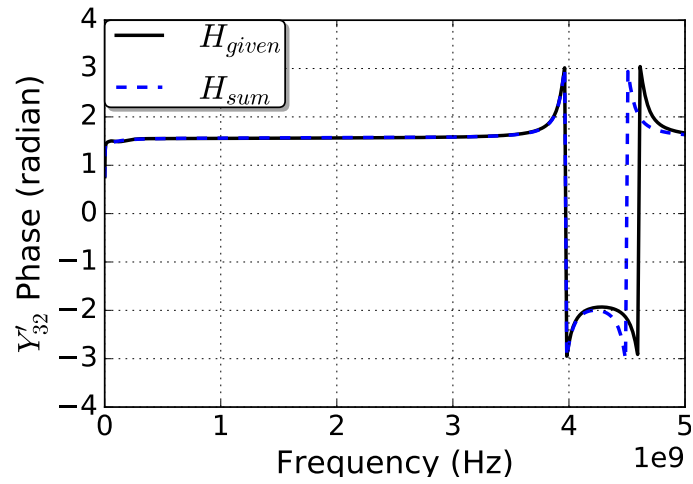


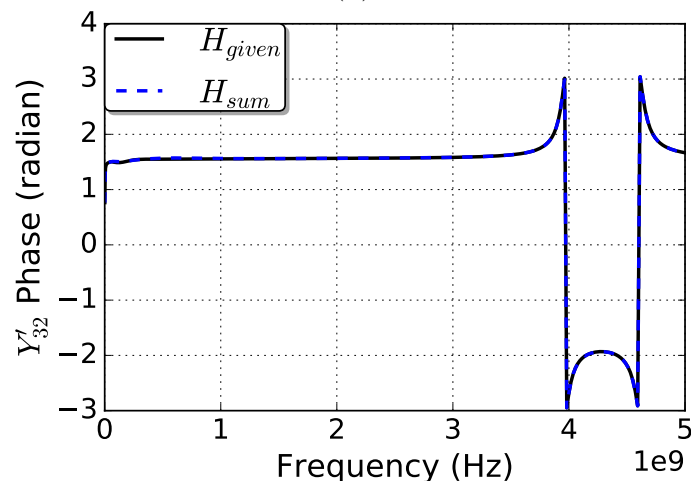
Figure 5.41: Fitting on power planes  $Y'_{32}$  after iterations: (a) 1<sup>st</sup>, (b) 5<sup>th</sup>, & (c) 20<sup>th</sup>. Permission from [2], ©2016 IEEE



(a)

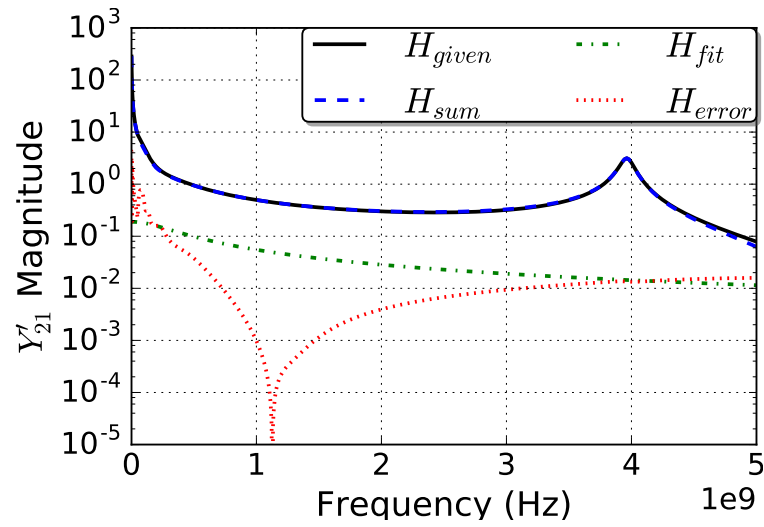


(b)

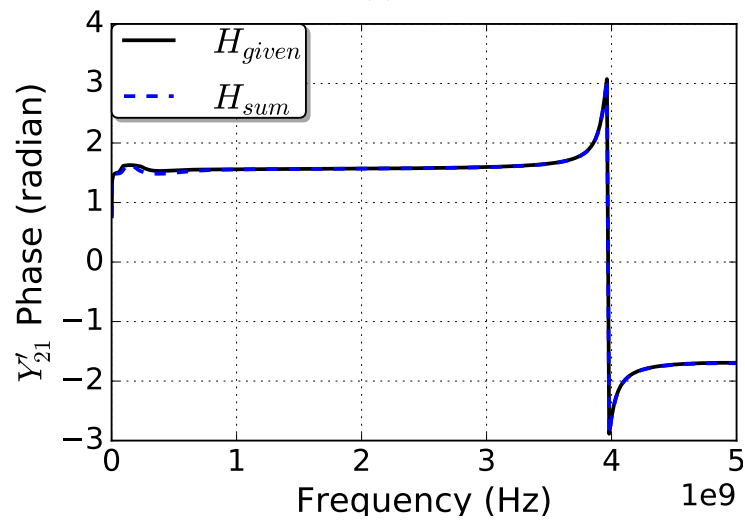


(c)

Figure 5.42: Fitting on power planes  $Y'_{32}$  after iterations: (a) 1<sup>st</sup>, (b) 5<sup>th</sup>, & (c) 20<sup>th</sup>. Permission from [2], ©2016 IEEE

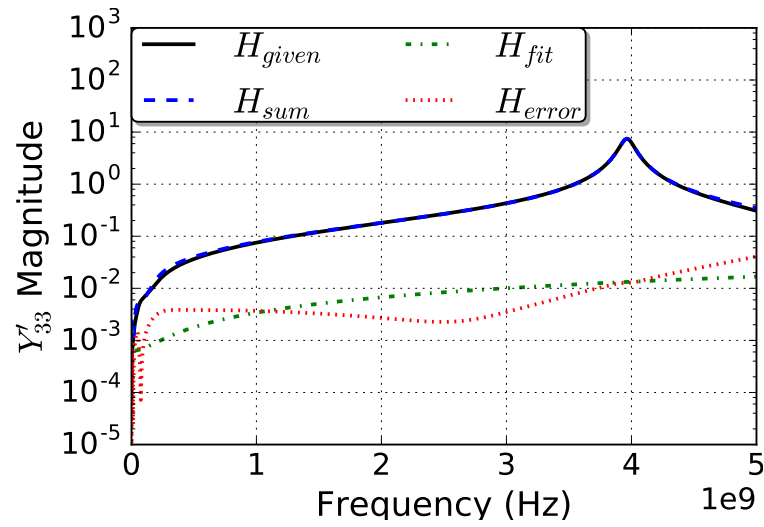


(a)

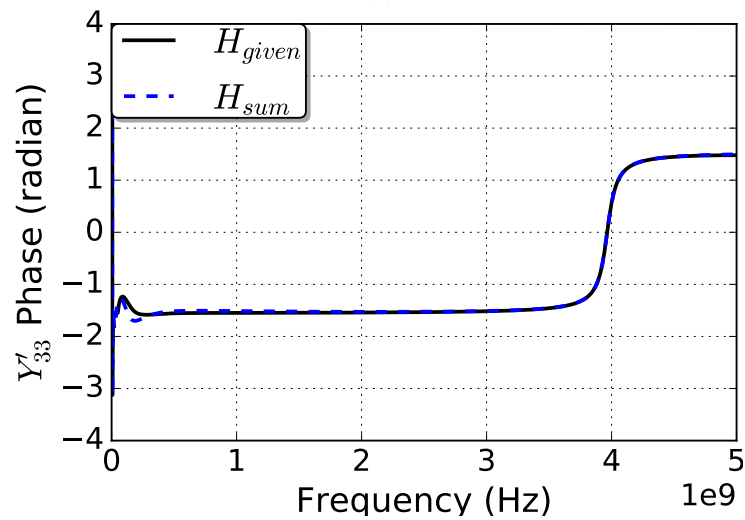


(b)

Figure 5.43: Fitting of power planes  $Y'_{21}$  after 20<sup>th</sup> iteration: (a) *Magnitude* & (b) *Phase*.  
 Permission from [2], ©2016 IEEE

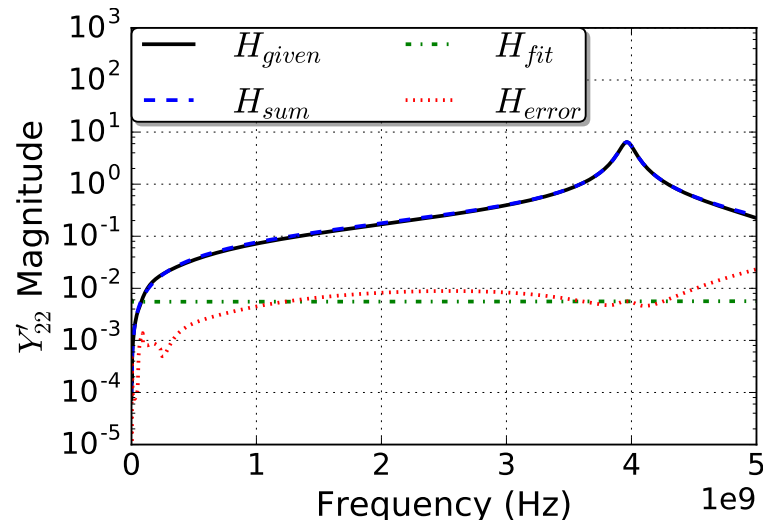


(a)

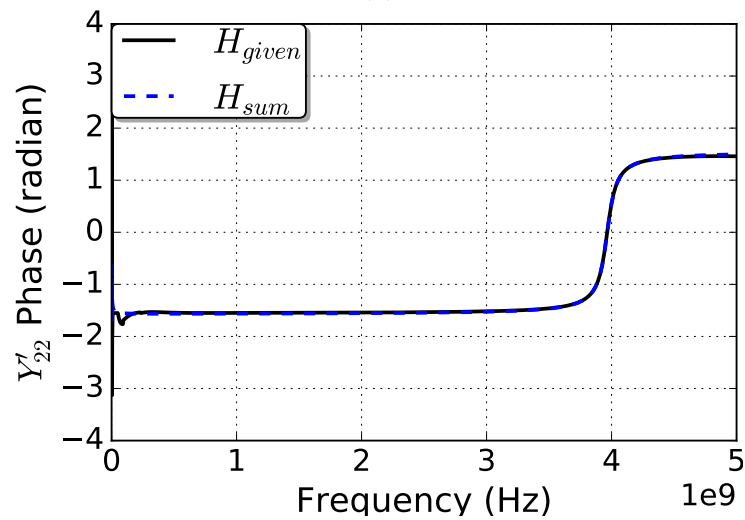


(b)

Figure 5.44: Fitting of power planes  $Y'_{33}$  after 20<sup>th</sup> iteration: (a) *Magnitude* & (b) *Phase*.  
 Permission from [2], ©2016 IEEE

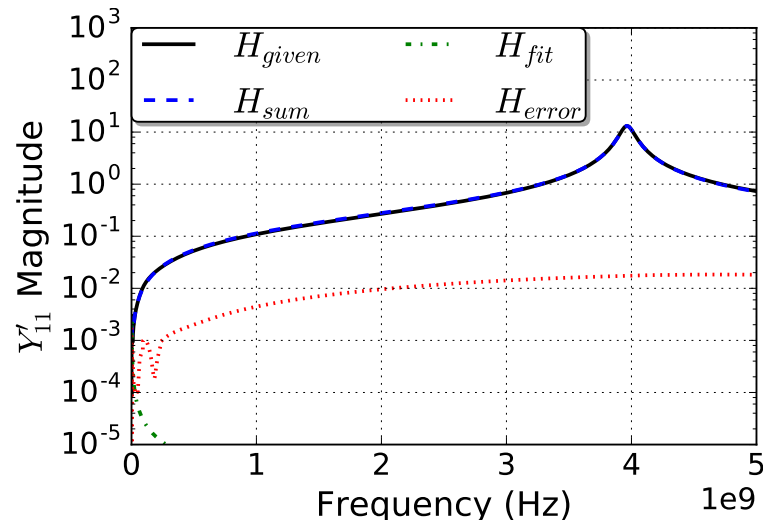


(a)

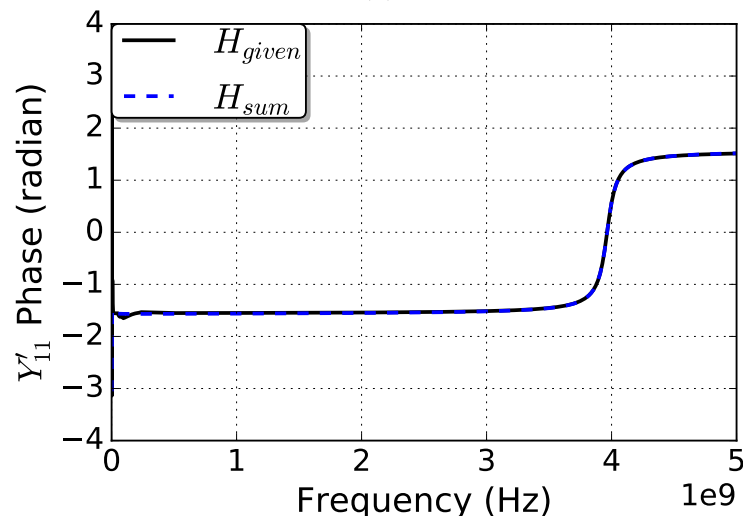


(b)

Figure 5.45: Fitting of power planes  $Y'_{22}$  after 5<sup>th</sup> iteration: (a) *Magnitude* & (b) *Phase*.  
 Permission from [2], ©2016 IEEE

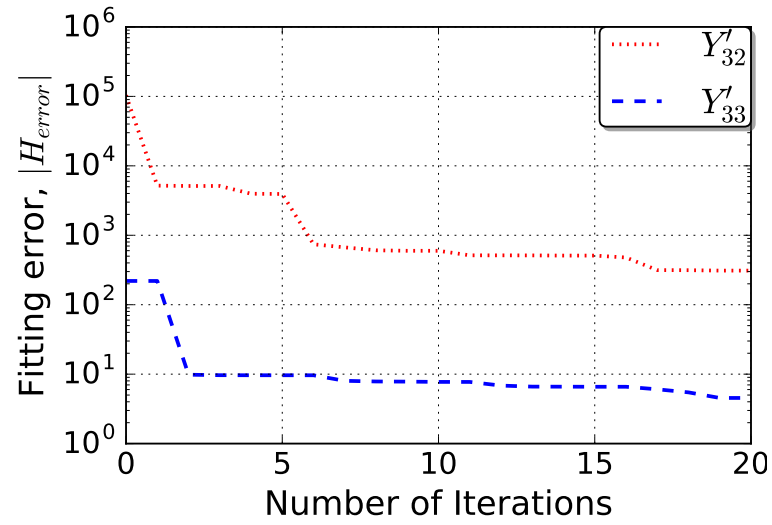


(a)

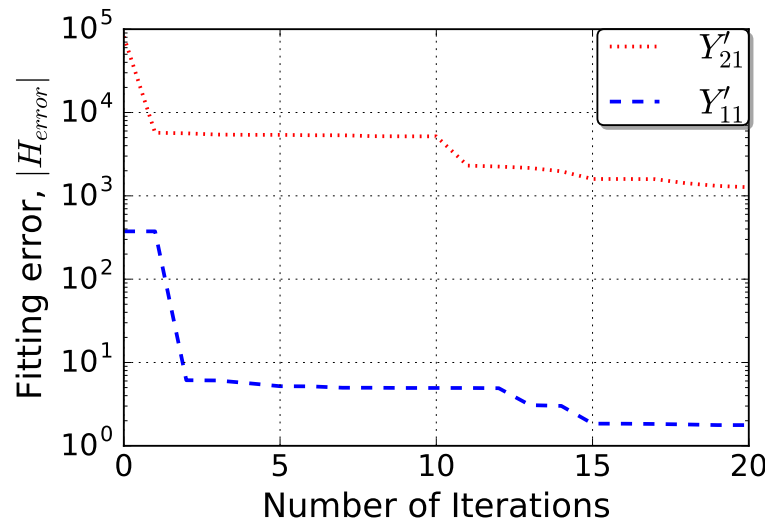


(b)

Figure 5.46: Fitting of power planes  $Y'_{11}$  after 5<sup>th</sup> iteration: (a) *Magnitude* & (b) *Phase*.  
 Permission from [2], ©2016 IEEE

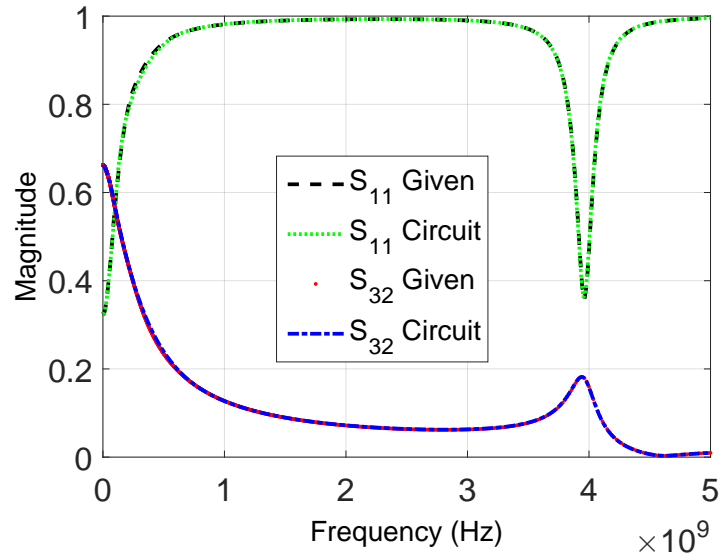


(a)

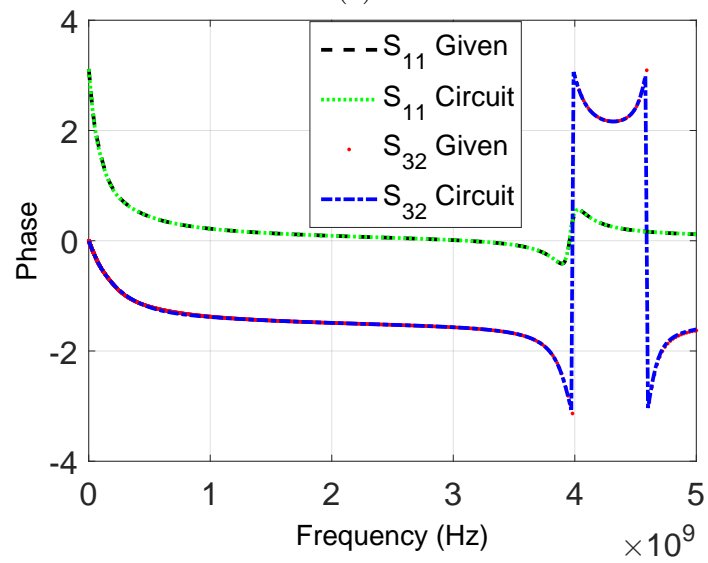


(b)

Figure 5.47: Convergence of magnitude of fitting error of admittance over 20 iterations: (a) transfer admittance  $Y'_{32}$  and self admittance  $Y'_{33}$  & (b) transfer admittance  $Y'_{21}$  and self admittance  $Y'_{11}$ . Permission from [2], ©2016 IEEE



(a)



(b)

Figure 5.48: Comparison of power planes frequency-domain model with the synthesized circuit: (a) *Magnitude* & (b) *Phase*. Permission from [2], ©2016 IEEE

## CHAPTER 6

### Discussion

Electrical performance and the computational complexity of the proposed fitting and synthesis methods, algorithms are discussed here.

### 6.1 Performance

#### 6.1.1 Fitting

#### PRESS

The proposed iterative method does an accurate fit of the frequency response of the two test cases: strip-line and four-port package. Note that with each iteration the fitting error level goes down as shown in Figures 5.3 and 5.4. The relative error level  $|H_{err}|$  compared to given response  $|H_{given}|$  has gone down from less than one order at  $10^{th}$  iteration as shown in Figure 5.3b to more than two orders at  $100^{th}$  iteration as shown in Figure 5.3c. In the case of package insertions loss, the error level gets nearly two orders lesser in just 50 iterations as shown in Figure 5.11a.

The progress of fitting the frequency responses of strip-line and package, in terms of error reduction, is shown in the Figures 5.5 and 5.12 respectively. With the fitting error following continuously downward trend as the number of iterations increase, it is clear that the proposed method successfully converges with the error magnitude  $|H_{err}|$  at approximately 2 orders of magnitude lower than given response  $|H_{given}|$  in general. In spite of the complexities in frequency response, the proposed method finds a good overall fit,  $H_{sum}$ . Even a small irregularity near 1.7 GHz of phase response, for instance, is religiously tracked and accurately fitted as shown in the Figures 5.8b, 5.9b and 5.10b.

We also observe that the rate of error reduction varies with and depends on the given frequency response data. Error convergence of fitting strip-line follows nearly exponential [1]

decay pattern while the package traces bumpy uneven curve. The progress of fitting package has sudden drops in error followed by stagnation. Near-end crosstalk  $S_{31}$ , for example, has a drop in error around iteration 9 then stagnates for nearly 5 iterations, as shown in the Figure 5.12, contrasting the progress of fitting strip-line, insertion loss  $S_{21}$  and return loss  $S_{11}$ , which has exponential [1] error reduction with increasing iterations, as shown in the Figure 5.5.

Also, usability and equivalence of the poles-resides generated by the proposed method from a given frequency response to that of vector fitting is seen from the 5.6a-5.6b. Excited by a step voltage at port 1 of the strip-line equivalent circuit, the current at port 1 and voltage at port 2 are matching closely. Moreover, the transient simulation results correlation shown in Figure 5.48 of the synthesized equivalent circuits demonstrates that the poles/residues generated by the proposed method are equivalent to that of the vector fitting [39].

But, in the case of power planes, the error level is higher at its first resonance at approximately 1.32 GHz as shown in Figure 5.20. More iterations are required to further reduce the error, where each iteration adds more terms to  $H_{sum}$ . Similarly, higher relative error observed for the case of strip-line return loss as shown in Figure 5.10a can be reduced with more iterations adding terms to  $H_{sum}$ .

Application of either the model order reduction techniques [12] as discussed in the Chapter 4 or improved PRESS algorithm - EMPRESS, COMPRESS, OPPRESS - may be needed to reduce the number of terms and computational cost for transient simulations.

## COMPRESS

Despite the complexities in the frequency responses, the phase response shown in Figure 5.25b for instance, the proposed COMPRESS fitting method successfully converged, with fitting error falling smoothly, never stagnating, as shown in the Figures 5.26a, 5.26b and 5.26c. It also has two key benefits over the PRESS method: while the fitting error of PRESS stagnates, like at iteration 12 in Figure 5.26a, the proposed method has error reduction in proportion

to the number of iterations as shown the Figures 5.26a and 5.26c ; the fitting error was lower than PRESS, by nearly an order of magnitude for the case shown in Figure 5.26c. These benefits, however, come at a cost: computational complexity, shown in the Table 5.1, is highest for the COMPRESS among the algorithms.

## **EMPRESS**

Unlike the COMPRESS algorithm, EMPRESS was not always effective in fitting than the original PRESS. Despite the complexities like in the frequency response shown in Figure 5.25b, the proposed EMPRESS fitting method successfully converged, with fitting error falling continuously as shown in the Figures 5.27a, 5.27b and 5.27c. It has a drawback: tendency to stagnate. Similar to the stagnation of fitting error of PRESS at iteration 12 in Figure 5.27a, the proposed EMPREESS method has earlier error stagnation at iteration 5 itself, thereby ending up with higher than the PRESS at the end of 30 iterations as shown the Figure 5.27a. It has two key benefits though: the fitting error was lower than PRESS, by nearly an order of magnitude for the cases shown in Figures 5.27b and 5.27c; computational complexity, shown in the Table 5.1, is much lower than the COMPRESS.

## **OPPRESS**

Like the COMPRESS algorithm, OPPRESS was effective in fitting than the original PRESS. Despite the complexities like in the frequency response shown in Figure 5.25b, the proposed EMPRESS fitting method successfully converged, with fitting error falling continuously as shown in the Figures 5.28a, 5.28b and 5.28c. It has three key benefits though: while the fitting error of PRESS stagnates, like at iteration 12 in Figure 5.26a , the proposed method has error reduction in proportion to the number of iterations as shown the Figures 5.28a, 5.28b and 5.28c; the fitting error was lower than PRESS, by nearly an order of magnitude for the cases shown in Figures 5.28b and 5.28c; computational complexity, shown in the Table 5.1, is lower than both the COMPRESS and EMPRESS and comparable to the original

PRESS.

### 6.1.2 Model order reduction

Though PRESS fitting method successfully converged with fitting error falling continuously as shown in the Figure 5.12, it begins to saturate at iteration 5. By the 30<sup>th</sup> iteration, 25 terms were type-2 and 5 terms were type-3, thus the fit has 60 states. Ordered Hankel values shown in the Figure 5.31 show that there are around 15 contributing-states and the rest corresponds to saturated iterations. As shown in Figure 5.32, the reduced-order model matches closely to the original samples.

### 6.1.3 Synthesis

#### Direct synthesis

The proposed method does well in fitting and synthesis of the one-port antenna. Its successfully converges, error continuously reducing with iterations as shown in the Figure 5.37. The fitting method works iteratively and with each iteration the total fit  $H_{sum}$  improves, as it approaches the target  $H_{given}$ . The progress of fitting  $Y'_{11}$  magnitude and phase responses can be seen from the Figures 5.35 and 5.36 respectively. In terms of magnitude, the relative error level  $|H_{err}|$  compared to given response  $|H_{given}|$  has decreased by nearly two orders of magnitude at 10<sup>th</sup> iteration as shown in Figure 5.37.

Post fitting and synthesis, the equivalent circuit's S-parameters, extracted from Keysight ADS tool [67], match closely to that of the antenna model, as shown in Figure 5.38 and the it can be further improved with more iterations adding terms to  $H_{sum}$  and corresponding circuit branches.

Similarly, the proposed method does very well in fitting and synthesis of the multi-port networks, despite complexities in its frequency responses. The fitting method works iteratively and with each iteration the total fit  $H_{sum}$  improves, as it approaches the target

$H_{given}$ . The progress of fitting  $Y'_{32}$  magnitude and phase responses can be seen from the Figures 5.41 and 5.42 respectively. In terms of magnitude, the relative error level  $|H_{err}|$  compared to given response  $|H_{given}|$  has decreased from about one order of magnitude at 5<sup>th</sup> iteration as shown in Figure 5.41b to more than two orders of magnitude at 20<sup>th</sup> iteration as shown in Figure 5.41c. In terms of phase, there are two singularities of  $H_{given}$  near 4 GHz and 4.5 GHz as shown in 5.42a. The singularity at 4 GHz is matched after 5<sup>th</sup> iteration as shown in 5.42b, while both singularities are matched after 20<sup>th</sup> iteration as shown in 5.42c. Similarly, even a small blip in the phase response of  $Y'_{21}$  and  $Y'_{33}$  near 0.1 GHz is picked up and matched as shown in Figures 5.43 and 5.44.

The ability of the proposed method to converge successfully is seen from the Figures 5.47a and 5.47b. The magnitude of fitting error generally decreases with the number of iterations. In the cases of  $Y'_{22}$  and  $Y'_{11}$ , a good fit is achieved within 5 iterations as shown in the Figures 5.45 and 5.46 respectively.

Post fitting and synthesis, the equivalent circuit's S-parameters, extracted from Keysight ADS tool [67], match closely to that of the actual power delivery network, as shown in Figure 5.48 and the it can be further improved with more iterations adding terms to  $H_{sum}$  and corresponding circuit branches.

## Indirect synthesis

Post PRESS fitting and SPA based model order reduction, the obtained state-space is synthesized; the equivalent circuit's S-parameters, extracted from Keysight ADS tool [67], match closely to that of the actual power delivery network, as shown in Figure 5.33 and the it can be further improved with either increasing the order of reduced model or choosing an efficient model order reduction technique.

## 6.2 Computational complexity

The proposed method has a benefit in scalability, which is a potential weakness [70] in the Vector fitting method. As VF relies on least-square solutions of equations involving the matrices of the size of given frequency response model consisting  $N$  samples and  $n$  number of ports, larger models have higher complexity. Its computational time complexity [70] is  $O(n^2Nr^2)$  and memory size requirement [70] is  $Nn^2 \times ((r + 1)n^2 + r)$ , where  $r$  is the order of system or the number of initial poles.

The proposed method, PRESS, on the otherhand, relies on solving atmost six equations-2.9 and 2.14 for six unknowns for each iteration. The complexity for solving  $l$  linear equations for  $l$  unknowns is well known [71] as  $O(l^3)$ . Since the equations in the proposed method are non-linear and polynomial, the upper bounds for solving such simultaneous non-linear equations can be estimated to be definitely higher, say by a positive real number  $x$ , than the linear system. For  $t$  iterations, the time complexity is  $O(t \times 6^{3+x})$  and Memory requirement is  $((t + 1) \times t)$ ; note that the proposed method's numerical complexity is independent of the given frequency model size. For larger multi-port models, the proposed method would offer a better solution of fitting poles/residues in terms of computational complexity. Accurate computational complexity of the proposed method will be covered in a future work.

In comparison, computational requirements of Vector Fitting increase exponentially in proportion to the size of the given frequency-domain model; while, the proposed method is independent of model size, as showin in the Table 5.2. Parallelization techniques would help in accelerating [70] the computations for VF. The proposed method can also be optimized by parallelization, which will be covered in a future work.

## CHAPTER 7

### Conclusion

In this thesis, a novel, simple, yet powerful algorithm, Pole Residue Equivalent System Solver (PRESS), that finds poles/residues from multi-port frequency-domain model and synthesizes them to equivalent circuits is proposed. The iterative method does multiple local fits of the given frequency response so that the sum of such local fits approximates the overall response. The method allows for a new macromodeling methodology of systems, but has a couple of drawbacks - error stagnation at higher iterations, large model order and high computational complexity of the type-3 local fit.

Improvements to the algorithm are proposed to fix these problems: Error Maxima-agnostic Pole Residue Equivalent System Solver (EMPRESS) fits at all the points of the given response, instead of doing so only at the peak as in the original PRESS method, allowing wide range of possible local fits to choose the best one from at each iteration; Coarse-to-fine Malleable Pole/Residue Equivalent System Solver (COMPRESS) supports non-consecutive points based local fits, instead of consecutive points based local fit in PRESS, allowing adaptability to the variable bandwidths of the peaks and troughs in the given numerical frequency response data; Optimized Pole/Residue Equivalent System Solver (OPPRESS) simplifies the type-3 local fit, lowering the computational complexity. Comparison of these algorithms, in terms of computation time and fitting error convergence, showed that the OPPRESS offers the optimum balance between the fitting performance and computational complexity, while COMPRESS, although gives the best fitting performance, is prohibitively computationally expensive for large models and EMPRESS tends to stagnate at higher iterations. Moreover, to reduce the model order and optimize the generated SPICE netlist, Singular perturbation approximation (SPA) based model order reduction is proposed. And multi-port network synthesis methodology, utilizing both the direct and indirect methods, is covered. The proposed macromodling flow was successfully demonstrated on various, disparate interconnect systems including a three port power delivery network and a broadband antenna example.

Due to its reliance on maximum of only 3 data points per iteration, the fitting method offers an attractive alternative for synthesis of large systems with many ports. However, the method lacks the ability to identify the poles, as possible with the well-established vector fitting method, and instead finds the equivalent poles. This needs further development and investigation, adding computational complexity to the proposed algorithm; however, parallelization of the algorithm, utilizing the GPU accelerated computing, like CUDA, would help in such implementations.

## References

- [1] Ata Zadehgol and Venkatesh Avula. A novel iterative algorithm for approximating equivalent circuits of numerical transfer functions. *International Journal of Numerical Modelling: Electronic Networks, Devices and Fields*, pages 1–14, 2016.
- [2] Venkatesh Avula and Ata Zadehgol. A novel method for equivalent circuit synthesis from frequency response of multi-port networks. In *IEEE EMC Europe 2016*, Wroclaw, Poland, September 2016.
- [3] Venkatesh Avula and Ata Zadehgol. A novel iterative method for approximating frequency response with equivalent pole/residues. In *2016 IEEE International Symposium on Electromagnetic Compatibility (EMC 2016), featuring an embedded Signal and Power Integrity Conference (SIPI 2016)*, Ottawa, Candada, July 2016.
- [4] Ansys. Package.aedt example. *ElectronicsDesktop HFSS Signal Integrity*, 2016.
- [5] Venkatesh Avula and Ata Zadehgol. Pole residue equivalent system solver (PRESS). In *20th IEEE Workshop on Signal and Power Integrity (SPI 2016)*, Turin, Italy, May 2016.
- [6] ANSYS Inc. SIwave pkg analysis.siw file. *SIwave*, 2016.
- [7] Venkatesh Avula and Ata Zadehgol. Coarse-to-fine malleable pole residue equivalent system solver (COMPRESS). In *IEEE EDAPS 2016*, Honolulu, USA, December 2016.
- [8] Ansys. tune coax fed patch.aedt example. *ElectronicsDesktop*.
- [9] L. D. Smith, R. E. Anderson, D. W. Forehand, T. J. Pelc, and T. Roy. Power distribution system design methodology and capacitor selection for modern cmos technology. *IEEE Trans. on Advanced Packaging*, 22:284–291, 1999.
- [10] S. Lin and E. S. Kuh. Transient simulation of lossy interconnects based on the recursive convolution formulation. *IEEE Trans. Circuits Syst*, 39:879–892, 1992.

- [11] S. N. Lalgudi, K. Srinivasan, G. Casinovi, R. Mandrekar, E. Engin, M. Swaminathan, and Y. Kretchmer. Causal transient simulation of systems characterized by frequency-domain data in a modified nodal analysis framework. *Topical Meeting on Electrical Performance of Electronic Packaging*, 23:123–126, 2006.
- [12] R. Achar and M. S. Nakhla. Simulation of high-speed interconnects. *Proc. IEEE*, 89:693–728, 2001.
- [13] E. Chiprout and M. Nakhla. Asymptotic waveform evaluation and moment matching for interconnect analysis. *Kluwer, Boston, MA*, 1993.
- [14] R. Achar and M. S. Nakhla. Efficient transient simulation of embedded subnetworks characterized by s - parameters in the presence of nonlinear elements. *IEEE Trans. Microw. Theory Tech.*, 46:2356–2363, 1998.
- [15] I. Ierdin, M. Nakhla, and R. Achar. Circuit analysis of electromagnetic radiations and field coupling effects for networks with embedded full - wave modules. *IEEE Trans. Electromagn. Compat.*, 42:449–460, 2000.
- [16] L. M. Silveira, I. M. Elfadel, J. K. White, M. Chilukuri, and K. S. Kundert. Efficient frequency - domain modeling and circuit simulation of transmission lines. *IEEE Trans. Comp. Packag. Manuf. Technol. B*, 17:505–513, 1994.
- [17] W. T. Beyene and J. E. Schutt Aine. Efficient transient simulation of high - speed interconnects characterized by sampled data. *IEEE Trans. Comp. Packag. Manuf. Technol. B*, 21:105–114, 1998.
- [18] R. Neumayer, F. Haslinger, A. Stelzer, and R. Wiegel. Synthesis of spice - compatible broadband electrical models from n - port scattering parameter data. In *in Proc. IEEE Symp. Electromagn. Compat.*, page 469–474, Minnesota, USA, August 2002.

- [19] M. Elzinga, K. L. Virga, and J. L. Prince. Improved global rational approximation macromodeling algorithm for networks characterized by frequency - sampled data. *IEEE Trans. Microw. Theory Tech.*, 48:1461–1468, 2000.
- [20] T. Mangold and P. Russer. Full - wave modeling and automatic equivalent - circuit generation of millimeter - wave planar and multilayer structures. *Trans. Microw. Theory Tech.*, 47:851–858, 1999.
- [21] Ata Zadehgo. An efficient approximation for arbitrary port suppression of multiport scattering parameters. *International Journal of Numerical Modelling-Electronic Networks Devices and Fields*, 27(1):164–172, 2014.
- [22] Ata Zadehgo and A. C. Cangellaris. Isotropic spatial filters for suppression of spurious noise waves in sub-gridded FDTD simulation. *IEEE Transactions on Antennas and Propagation*, 59(9):3272–3279, 2011.
- [23] Ata Zadehgo, A. C. Cangellaris, and P. L. Chapman. A model for the quantitative electromagnetic analysis of an infinitely long solenoid with a laminated core. *International Journal of Numerical Modelling-Electronic Networks Devices and Fields*, 24(3):244–256, 2011.
- [24] Ata Zadehgo. Passivity considerations for sub-gridded FDTD with discrete complex wave impedance. In *IEEE EMC Europe 2016 Wroclaw International Symposium and Exhibition on Electromagnetic Compatibility*, September 2016.
- [25] Ata Zadehgo and Andreas C. Cangellaris. Probabilistic finite-difference time-domain method through stochastic electromagnetic macro-models. In *11th IEEE International Workshop on Finite Elements for Microwave Engineering (FEM2012), Estes Park, CO, USA*, 2012.
- [26] Ata Zadehgo and Andreas C. Cangellaris. Isotropic spatial filters for suppression of spurious waves in finite difference time domain simulations with sub-gridding. In *IEEE*

*International Symposium on Antennas and Propagation and USNC-URSI National Radio Science Meeting*, June 2011.

- [27] Ata Zadehgol and Andreas C. Cangellaris. Efficient fdtd modeling of the impact of fine-feature statistical variability on the electromagnetic response of multi-scale structures. In *IEEE AP-S/URSI International Symposium on Antennas and Propagation*, 2011.
- [28] Ata Zadehgol. *Probabilistic Finite-Difference Time-Domain Simulations using Stochastic Electromagnetic Macro-Models*. PhD thesis, University of Illinois at Urbana-Champaign, Urbana, Illinois, 2011.
- [29] B. Gustavsen and A. Semlyen. Simulation of transmission line transients using vector fitting and modal decomposition. *IEEE Trans. Power Delivery*, 13:605–614, 1998.
- [30] S. B. Olivadese, P. Brenner, and S. Grivet-Talocia. Dc-compliant small-signal macro-models of non-linear circuit blocks. In *17th IEEE Workshop on Signal and Power Integrity (SPI)*, Paris, France, May 2013.
- [31] Ata Zadehgol. A frequency-independent and parallel algorithm for computing the zeros of strictly proper rational transfer functions. *Applied Mathematics and Computation*, 274:229–236, 2016.
- [32] K. Yekeh Yazdandoost and R. Kohno. Design and analysis of an antenna for ultra-wideband system. *14th IST Mobile and Wireless Communications Summit, Dresden*, 2005.
- [33] FCC. Ultra-wideband operation fcc report and order. *Technical Report US 47 CFR Part 15*, 2002.
- [34] Ata Zadehgol. Signal and power integrity of microelectronic networks through modelling and simulation of fields and devices. *International Journal of Numerical Modelling: Electronic Networks, Devices and Fields*, 29(3):544–544, 2016.

- [35] Wang Ren. Circuit modeling methodology for small uwb antenna with vector fitting technique. *Microwave and Optical Technology Letters*, 53:2116–2119, 2011.
- [36] Youngwook Kim and Hao Lin. Equivalent circuit modeling of broadband antennas using a rational function approximation. *Microwave and Optical Technology Letters*, 48:950–953, 2006.
- [37] Er-Ping Li. Electrical modeling and design for 3d system integration. *Wiley*, 2012.
- [38] Zohaib Mahmood, S. Grivet Talocia, Alessandro China, Giuseppe C. Calafiore, and Luca Daniel. Efficient localization methods for passivity enforcement of linear dynamical models. *IEEE Transactions on Computer-Aided Design of Integrated Circuits and Systems*, 33:1328 – 1341, 2014.
- [39] B. Gustavsen and A. Semlyen. Rational approximation of frequency domain responses by vector fitting. *IEEE Trans. Power Deliv.*, 14:1052–1061, 1999.
- [40] B. Gustavsen. Improving the pole relocating properties of vector fitting. *IEEE Trans. Power Deliv.*, 21:1587–1592, 2006.
- [41] A. Semlyen and B. Gustavsen. Vector fitting by pole relocation for the state equation approximation of nonrational transfer matrices. *Circuits Systems Signal Process*, 19:549–566, 2000.
- [42] D. Deschrijver, M. Mrozowski, T. Dhaene, and D. De Zutter. Macromodeling of multiport systems using a fast implementation of the vector fitting method. *IEEE Microwave and Wireless Components Letters*, 18:383–385, 2008.
- [43] P. Triverio, S. Grivet Talocia, M. S. Nakhla, F. G. Canavero, and R. Achar. Robust causality characterization via generalized dispersion relations. *IEEE Transactions on Advanced Packaging*, 31:579–593, 2008.

- [44] P. Triverio and S. Grivet-Talocia. A robust causality verification tool for tabulated frequency data. In *10th IEEE Workshop Signal Propagation Interconnects*, Berlin, Germany, May 2006.
- [45] P. Triverio and S. Grivet-Talocia. On checking causality of bandlimited sampled frequency responses. In *2nd Conf. Ph.D. Res. Microelectron. Electron. (PRIME)*, page 501504, Otranto, Italy, June 2006.
- [46] Aminul Hoque and Ata Zadehgol. On the sensitivity of causality filter parameters. In *IEEE Electrical Design of Advanced Packaging and Systems (EDAPS), Hawaii, USA*, pages 1–3, December 2016.
- [47] Matt Doyle, Rohan Mandrekar, and Jason Morsey. Techniques and considerations for verification of model causality. In *IEEE Electronic Components and Technology Conference (ECTC)*, Florida, USA, June 2011.
- [48] Er-Ping Li, En-Xiao Liu, Le-Wei Li, and Mook-Seng Leong. A coupled efficient and systematic full-wave time-domain macromodeling and circuit simulation method for signal integrity analysis of high-speed interconnects. *IEEE Transactions on Advanced Packaging*, 27:213–223, 2004.
- [49] Ata Zadehgol. An impedance transfer function formulation for reduced-order macromodels of sub-gridded regions in FDTD. *IEEE Transactions on Antennas and Propagation*, TBD(TBD):1–4, 2016.
- [50] Ata Zadehgol. Stochastic reduced-order electromagnetic macro-models in FDTD. *IEEE Transactions on Antennas and Propagation*, 46(8):3496 – 3508, 2016.
- [51] Ata Zadehgol. Deterministic reduced-order macromodels for computing the broadband radiation-field pattern of antenna arrays in FDTD. *IEEE Transactions on Antennas and Propagation*, 64(6):2418–2430, 2016.

- [52] S. Grivet Talocia. Passivity enforcement via perturbation of hamiltonian matrices. *IEEE Transactions on Circuits and Systems I*, 51:1755–1769, 2004.
- [53] S. Grivet Talocia and A. Ubolli. On the generation of large passive macromodels for complex interconnect structures. *IEEE Trans. Adv. Packag.*, 29:39–54, 2006.
- [54] S. Grivet Talocia. An adaptive sampling technique for passivity characterization and enforcement of large interconnect macromodels. *IEEE Trans. Adv. Packag.*, 30:226–237, 2007.
- [55] B. Gustavsen and A. Semlyen. Fast passivity assessment for s - parameter rational models via a half - size test matrix. *IEEE Trans. Microw. Theory Tech.*, 56:2701–2708, 2008.
- [56] D. Deschrijver and T. Dhaene. Modified half - size test matrix for robust passivity assessment of s - parameter macromodels. *IEEE Microw. Wireless Compon. Lett.*, 19:263–265, 2009.
- [57] D. Deschrijver and T. Dhaene. Fast passivity enforcement of s - parameter macromodels by pole perturbation. *IEEE Trans. Microw. Theory Tech.*, 57:620–626, 2009.
- [58] B. Gustavsen. Fast passivity enforcement for s - parameter models by perturbation of residue matrix eigenvalues. *IEEE Trans. Adv. Packag.*, 33:257–265, 2010.
- [59] A. Zadehgo. A semi-analytic and cellular approach to rational system characterization through equivalent circuits. *International Journal of Numerical Modelling: Electronic Networks, Devices and Fields*, 2015.
- [60] Nuzhat Yamin and Ata Zadehgo. Verification and enforcement of passivity through direct minimal modification of equivalent circuits. In *IEEE EMC Europe 2016 Wroclaw International Symposium and Exhibition on Electromagnetic Compatibility*, September 2016.

- [61] Y. Liu and B. D. O. Anderson. Singular perturbation approximation of balanced systems. In *28th IEEE Conference on Decision and Control*, Tampa, Florida, December 1989.
- [62] A.J. Laub, M.T. Heath, C.C. Paige, and R.C. Ward. Computation of system balancing transformations and other applications of simultaneous diagonalization algorithms. *IEEE Trans. Auto. Contr.*, AC-32:115–122, 1987.
- [63] R. Samar, I. Postlethwaite, and Da-Wei Gu. Applications of the singular perturbation approximation of balanced systems. In *3rd IEEE Conference on Control Applications*, 1994.
- [64] B. Gustavsen and A. Semlyen. Enforcing passivity for admittance matrices approximated by rational functions. *IEEE Trans. Power Syst.*, 16:97–104, 2001.
- [65] A. S. Morched, J. H. Ottevangers, and L. Marti. Multi-port frequency dependent network equivalents for the EMTP. *IEEE Trans. Power Deliv.*, 8:1402–1412, 1993.
- [66] The Vector Fitting Web Site. [www.sintef.no/projectweb/vectfit/downloads/vfut3](http://www.sintef.no/projectweb/vectfit/downloads/vfut3). *sintef*, 2016.
- [67] Keysight Technologies. Advanced Design System. [www.keysight.com](http://www.keysight.com).
- [68] Myoung Joon Choi, Vishram S. Pandit, and Woong Hwan Ryu. Controllable parameters identification for high speed channel through signal-power integrity combined analysis. In *58th Electronic Components and Technology Conference*, Florida, USA, May 2008.
- [69] GNU Octave with CACSD. Computer-aided control system design tool. <http://octave.sourceforge.net/control/overview.html>.
- [70] Alessandro Chinaea and Stefano Grivet-Talocia. On the parallelization of vector fitting algorithms. *IEEE Transactions on Components, Packaging and Manufacturing Technology*, 1:1761–1773, 2011.

- [71] G.H. Golub and C.F. Van Loan. Matrix computations. *3rd ed., Johns Hopkins University Press, Baltimore, MD, 1996.*